Thermal measurement and degradation quantification of teeming ladle refractories and the effects on the process

Swansea University
Prifysgol Abertawe

Liam Cotton

Materials and Manufacturing Academy

College of Engineering

Swansea University

Submitted to Swansea University in fulfilment of the requirements for the Degree of Doctor of Engineering

September 2020

Abstract

The key objective of the thesis was to quantify the heat loss caused to the liquid steel due to the cooling effect of the teeming ladle refractories. It was previously hypothesised that the in-situ degradation of insulation layer would increase this cooling effect. To determine the cooling effect of the degraded insulation material it was first thermally characterised with in-situ thermocouple measurements. Post-mortem samples were recovered from the teeming ladles used for the thermocouple measurements during their regular production cycles in a BOS plant. The post-mortem samples were then tested for their thermophysical properties. From this it was possible to determine the density increased from $260kg/m^3$ to 759.6 kg/m^3, the thermal conductivity increased from $0.039W/m.K$ to $0.15W/m.K$ and the specific heat capacity decreased by 40% compared to its original state. These findings were then used to calculate the increased heat loss rate of the refractory material in the teeming ladle, which then in turn causes increased heat loss to the steel transported by the ladle. A thermal model was used to determine the heat flux stored in a fully saturated ladle and then different time periods of cooling with and without a lid. The effect of teeming ladle lids reduced the heat losses by up to 11°C per cycle compared to a ladle without a lid. Whereas the heat loss due to the insulative layer degradation was calculated to be <1°C for the initial heats before the ladle reached production temperatures and, therefore, had minimal effect. However, the degradation did show an increase in teeming ladle shell temperatures, which needs to be taken into account for service temperature monitoring. The thermal profiles of the modelled scenarios showed that if an accurate hot face measurement could be achieved it would be possible to accurately predict the cooling effect of each teeming ladle in production. This study was able to accurately measure the refractories and slag taken from a teeming and utilise the geometry of the ladle to reduce the error from thermal imaging. Previously predictions were used that could cause errors up to ±175°C when taking thermal images of the teeming ladle hot face. Through the method adopted in this study it was possible to take accurate measurements of the hot face within ±5°C. This can now be utilised by a thermal model to make accurate real time predictions of the heat loss caused by teeming ladle refractories. Thereby reducing the reheating required and improving the quality of steel produced.
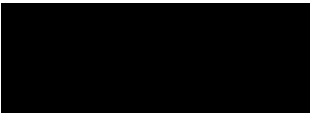
Declarations and Statements

This work has not previously been accepted in substance for any degree and is not being concurrently submitted in candidature for any degree.
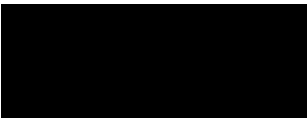
Signed: _____ ███████████████ _____

Date: _____26/6/21_____

This thesis is the result of my own investigations, except where otherwise stated. Other sources are acknowledged by footnotes giving explicit references.   A bibliography is appended.
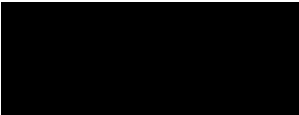
Signed: _____ ███████████████ _____

Date: _____26/6/21_____

I hereby give consent for my thesis, if accepted, to be available for photocopying and for inter-library loan, and for the title and summary to be made available to outside organisations.

Signed: _____ ███████████████ _____

Date: _____26/6/21_____

The University's ethical procedures have been followed and, where appropriate, that ethical approval has been granted.

Signed: _____ ███████████████ _____

Date: _____26/6/21_____

Contents

This thesis is dedicated to Kobe Cotton, who taught me to stay present and enjoy the

small things.

"Nothing worth having comes easy" — *Theodore Roosevelt*

Acknowledgements

Lastly to Frances Lyndale without our final conversation I may not have had the courage to take on this challenge.

Figures

Tables

Equations

Nomenclature

α	Thermal diffusivity (m^2/s)
A	Area (m^2)
c_2	Planks second radiation constant (1.4388×10^{-2} m.K)
C_p	Specific heat capacity (J/(kg.K))
ε_{bb}	Enhanced emissivity
ε_s	Spectral emissivity
h_c	Thermal contact conductance (W/(m^2.K)
K	Change in temperature (°C)
k	Thermal conductivity (W/(m.K))
L	Length of cavity (m)
λ	Mean effective wavelength (m)
ρ	Density (kg/m^3)
q	Heat flux (W/m^2)
R_{aper}	Radius of aperture (m)
T	Temperature (°K)
x	Distance (m)
BOF	Basic Oxygen Furnace
BOS	Basic Oxygen Steelmaking
CAD	Computer Aided Design
CC	Continuous Casters
CFD	Computational Fluid Dynamics
DSC	Differential Scanning Calorimetry

DSLR	Digital Single-lens Reflex
EAF	Electric Arc Furnace
FEA	Finite Element Analysis
FBG	Fibre Bragg Grating
H#	Hypothesis number from novel research questions
LFA	Laser Flash Analysis
LWIR	Long-wavelength Infrared
MWIR	Mid-wavelength Infrared
PM	Post-mortem
PTFE	Polytetrafluoroethylene
Q#	Novel research question number
RFID	Radio Frequency Identification
RGB	Red Green Blue
SEM	Scanning Electron Microscopy
XCT	X-Ray Computed Tomography
XRD	X-Ray Diffraction

Chapter 1 – Introduction

Teeming ladles are used to transport liquid steel and provide a vessel for the final stage of refinement to meet the steel grade specification. The teeming ladles are lined with refractory materials which reduce the temperature the ladle shell is exposed to. This is required to reduce the temperature of the liquid steel ~1600°C to lower than the service temperature of the ladle shell ~350°C. The thickness of the ladle shell is determined by the temperature and stresses it is subjected to (1). Therefore, the greater the insulation effect of the refractories the thinner and lighter the shell can be and less of the crane's weight limit is from the shell. Higher volume ladles can therefore be used, which increases the amount of steel produced per cycle. The most efficient layer of the refractory linings for reducing this temperature is the insulation layer (2). Microporous materials are now commonly used in steel ladles which have a very low thermal conductivity when installed. The insulation layer produces the largest drop in temperature, but it typically accounts for less than 5% of the refractory thickness. Because of this, the insulation layer is essential for maintaining the ladle shell integrity during production. If this layer is removed Gupta et al. (2004) calculated that 60% of the temperature lost from the steel would come from the ladle barrel (3). It was unclear if the microporous insulation retained its Green properties during production and was suggested that degradation would increase the temperature lost (2). The work performed in this thesis investigated the production effects on the insulation via in-situ measurements and post-mortem analysis. The results were then compared to the literature as an attempt to confirm the theories presented.

In order to select ladles that are at the correct temperature for production, or understand how changes in the lining will impact the thermal efficiency, thermal models are used to predict the temperature of the refractory layers (4). These models use signals from the steel plant to indicate what state the ladle is in and plot an increase or decrease in the refractory lining temperature. It was noted from the literature review that there is a gap between the data produced on plant and the thermal models tracking ladles for production. There is an element of separation, because current models attempt to simulate the ladle based on its location and state but do not have a calibration point to adjust for errors. Boone et al. (2018) were able to quantify the error in temperature measurements when the emissivity of an object is estimated incorrectly (5). The accuracy of emissivity is rarely within 0.2, which Boone et al. (2018) calculated would

cause an error of ±140°C. The large inaccuracies in measurements need to be investigated if radiometers were to be used to provide accurate hot face data. Geometry enhancement provides an opportunity to reduce the emissivity error (6). If the geometry enhancement could then enable accurate radiometer data it would provide an opportunity to calibrate a thermal model based on the refractory hot face measurement. This would improve the accuracy of the model and enable the possibility of accurately predicting the cooling effect of the teeming ladle refractories thus improving production efficiency, quality of the steel and providing a large saving for the steel manufacturer.

The key objective of the thesis was to quantify the heat loss caused to the liquid steel due to the cooling effect of the teeming ladle refractories. Previous literature had stated that the insulation layer was a key component in the cooling effect of the teeming ladle refractories . Therefore, Chapter 3 focuses on the recovery of post-mortem samples of the insulation material. It also describes the in-situ thermal characterisation experiments performed via thermocouple measurements in the teeming ladle during production. Chapter 4 then discusses the experimental procedures and findings from thermophysical characterisation of the recovered post-mortem insulation samples. In Chapter 5, the properties from Chapter 4, are used to improve the accuracy of a thermal model prediction of the thermal profile of the teeming ladle refractories. Chapter 5 also quantified the increased thermal losses caused by the insulation degradation. From these assessments it was determined that accurate hot face measurements are required to accurately predict the cooling effect of the teeming ladle refractories. Chapter 6 details the experiments performed and data collected to improve the accuracy of thermal imaging of the teeming ladle hot face to utilise the cooling effect predictions from Chapter 5. The accuracy improvement was achieved by the correct utilisation of the spectral response at the teeming ladle hot face temperatures, the increased accuracy of the emissivity values of teeming ladle slag and refractories and the utilisation of teeming ladle geometry to reduce the variation of emissivity values.

Chapter 2 – Literature review

2.1 Introduction

Teeming ladles transport molten steel from a Basic Oxygen Furnace (BOF) or Electric Arc Furnace (EAF) to the Continuous Casters (CC). Figure 1 shows the production process of steel of hot iron arriving from the blast furnace to slabs produced by the CC. It is essential to manage the ladle fleet efficiently to maintain the CC production rate. To ensure the product quality is maintained the steel needs to be supplied to the CC at the correct time and temperature. To ensure the teeming ladles arrive on time at the correct temperature they need be managed on three aspects. Firstly, refractory integrity, to ensure operator safety by containing the steel in the ladle. Secondly, location, to ensure the ladle follows the correct production route and reaches the CC. An example of the BOS plant layout can be seen in Figure 2. Finally, temperature, so the steel does not freeze in the ladle at the CC (or is not heated to a point where slag reversion takes place). This literature review will first give an overview of the currently available methods used to manage these aspects of a teeming ladle fleet. It will critique the key data acquisition approaches required to improve the management of the fleet. The effectiveness of the materials employed that minimise thermal losses through the process was assessed. Any potential for novel improvement is identified throughout to help guide the scope of work for the research project.
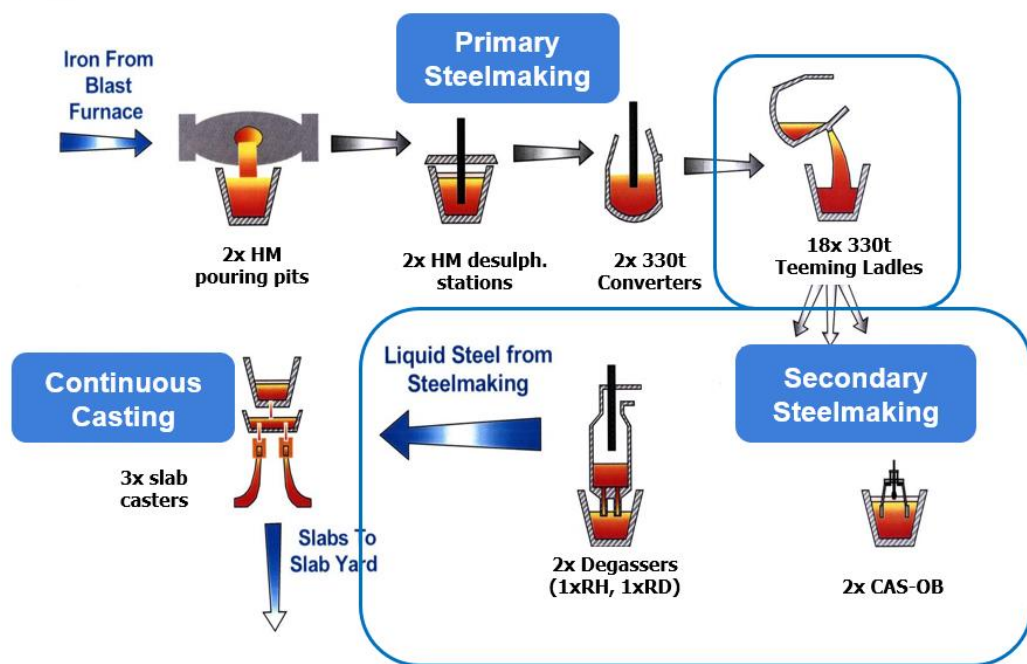
Figure 1: Steel production stages with teeming ladle processes circled.

3
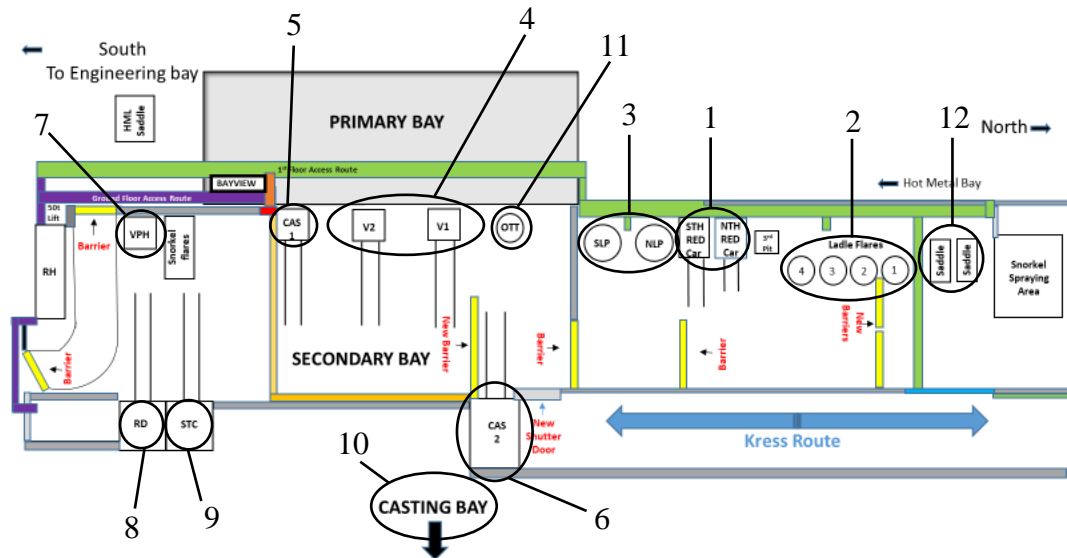
Figure 2: BOS plant layout. A larger version of this can be found in the appendices (provided by Lee Bowen – Secondary production manager).

Figure 2 shows an example of a BOS plant layout which is connected to the CC plant indicated by the casting bay at point 10. Figure 2 has been annotated to show the key areas of the teeming ladle cycle and how it moves around the plant via crane lift movement. These are described here to help explain the ladle cycle from cradle to grave:

1. The refractories are built inside the ladle ensuring the suppliers expansion allowance is met to reduce the stresses applied to the teeming ladle shell.

2. The ladle is then transported to the ladle flares where a natural gas or coke oven gas flame is used to preheat the ladle refractories. The preheat is required to expand the refractories and close the gaps between the individual bricks to ensure steel does not penetrate between these gaps. These are also used when the ladle is taken out of production for intermediate repairs that require it to cool down to be worked on.

3. Once the bricks have expanded sufficiently that the ladle can be rotated on its side it is taken to the ladle pits where the porous plug and well block are installed. The porous plug allows for argon to be blown into the bottom of the teeming ladle during production to help mix in the alloying elements and keep the steel homogenous. The well block is used to teem the steel out of the bottom of the ladle at the CC. After these have been installed the teeming ladle returns to the flares at 2 for the final stage of preheating. The ladle is then

returned to the ladle pit to fill the well block with sand, which ensures the steel can be teemed out of the ladle at the casters, the ladle is then ready for production.

4. Steel is tapped into the teeming ladle from the converters before being sent to the secondary steelmaking units for the final stage of refinement. Temperature measurements are taken to determine if any additional heat is required at the secondary steelmaking stage and gauge the temperature loss from the tap and teeming ladle refractories.

5. CAS unit of secondary steel making that is used to produce the steel grades by adding the necessary alloying elements and bringing the steel up to the correct superheat for the grade and to ensure it does not freeze during casting.

6. CAS unit as above

7. Degasser unit some steel grades require a vacuum system to remove higher amounts of carbon from the steel. To do this a degasser unit is required and is also used to add the alloying elements and reheat required for the grade.

8. Degasser unit as above

9. Once the secondary steelmaking refinement has been completed the teeming ladle is transported to the casting bay via a transfer car and cranes

10. In the casting bay the steel is teemed out of the ladle into a tundish where it is then cast into slabs via a continuous casting unit of moulds. Once the ladle is empty the remaining slag in the bottom of the ladle is poured into a slag pot and the ladle is then sent back to the transfer car (9)

11. Once bay in the secondary bay the ladle is thermally scanned to ensure the steel shell is not increasing beyond its service temperature. The ladle is then taken to the ladle pits (3) to have the steel and slag that has sintered in the well block removed and refilled with sand. This then completes 1 cycle of the ladle and takes typically 2 hours but can take up to 8 hours for specific grades, which are commonly referred to as lives or heats in industry.

12. The teeming ladle then follows stages 4 – 11 until the porous plug and well block need to be replaced at around 50 and 100 cycles. When the ladle reaches the predetermined life cap (typically around 150 cycles) the refractories are then removed at the ladle saddles. The process then restarts again at stage 1.

Teeming ladle refractories consist of multiple layers (typically three or four) designed to reduce the temperature that steel shell is subjected to and resist the wear mechanisms of steel and slag attack (7). Figure 3 shows an example of a teeming ladle refractory build.

Figure 3: Cross section of a teeming ladle showing an example of a refractory build.

In the example above the bottom of the ladle consists of three layers. A more detailed view of the layers can be seen in Figure 4, consisting of the precast bottom first, which is designed to insulate the shell and channel the steel towards the well block to reduce steel retention at the CC. Precast bottoms are typically made from alumina based refractories. Then secondly, a safety lining made of fired alumina is used to provide additional insulation and assist with removal of the refractory wear lining. The final layer is the wear lining that can withstand the impact of the tapping stream from either the BOF or EAF and the interactions with the steel most commonly used are alumina mag carbon bricks (AMC).

6

Figure 4: Detailed view of the three refractory layers in the teeming ladle bottom (area Y from Figure 3).

Figure 5 shows a detailed view of a typical three-layer refractory build on the ladle barrel. The wear lining is a higher density refractory designed to resist the consistent interaction with steel and slag. MgC bricks are typically used for the barrel wear lining, however, with the drive to reduce ladle shell temperatures and reduce heat losses fired spinel and AMC bricks are now also commonly used. The fired alumina safety lining (or linings in a 4 layer refractory design) is designed to reduce the temperature the insulation is exposed to, ensuring it is below its working limit. It is also able to survive one cycle of steel production as a last line of safety against losses of containment. It is generally understood this is not something that should be relied on regularly. If the safety lining does not remain intact it causes catastrophic failure of the shell and a loss of containment (8). The insulation layer consist of an amorphous silica board or panel and is the final layer of refractory that is designed to ensure the ladle shell is not subjected to temperatures above its designed service temperature, typically 350°C. The most common form of insulation used is microporous pyrogenic silica, which is contained in a fiberglass bag and pressed to give a flexible board.
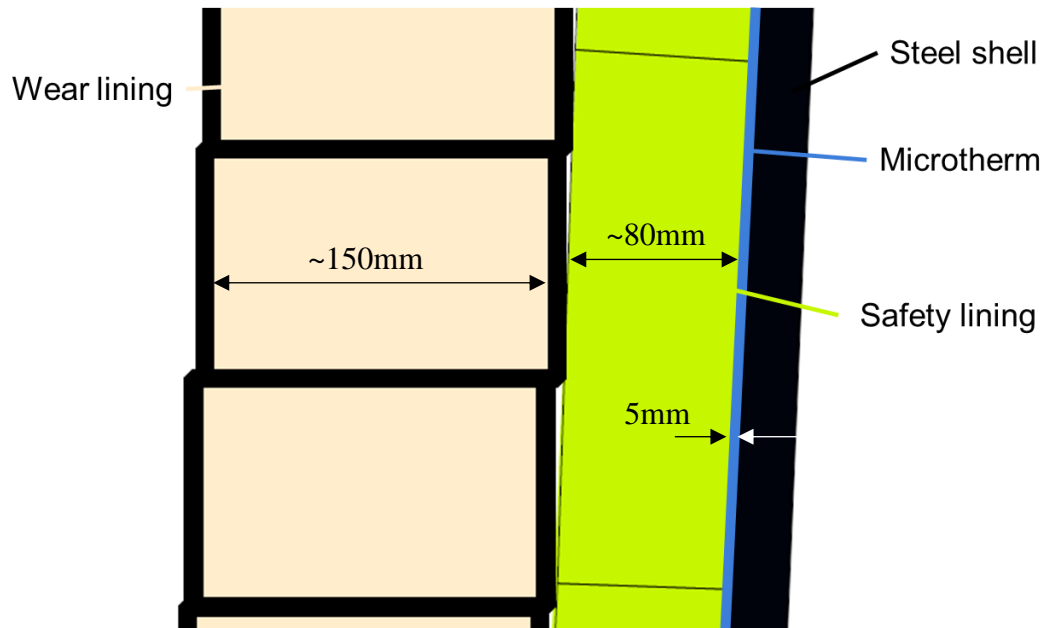
Figure 5: Three-layer teeming ladle refractory design of the barrel (area X from Figure 3).

2.2 Approaches to ladle management

As previously stated, the efficient management of teeming ladles is an essential element of their function. This section of the literature review will focus on approaches to the three key elements of ladle management: refractory integrity, location and temperature, with the intention to identify areas of improvement therein.

2.2.1 Refractory integrity

Monitoring of wear lining refractory integrity generally relies on laser scanning and experienced workers to verify any erroneous scans or damage during maintenance (9). This is due to the risks involved with pushing a refractory past its limit and causing a loss of containment of the steel. Most steel plants will have a set of rules that limits the refractory lining to a number of cycles or contact time, based on previous data and the scans. This is generally conservative as losses of containment can cause injury of the workforce and, in the most extreme of cases, loss of life. Because of this these events are very rare and losses of containment are taken very seriously. Laser scanners are common in nearly all steel plants at the time of writing and there is limited novelty in exploring refractory integrity.

2.2.2 Location

There are several methods used to track the location of teeming ladles within a steel plant. The original method used was to rely on operators to track the ladles as they arrived and left the various locations of the plant. This relied on the communication of

operators to understand where ladles were required and had significant drawbacks in terms of errors in data recorded and subsequent data integrity. Due to the lack of traceability, and human error, many steel plants have looked to automate their tracking systems. This has also increased the quality of data available, which can be analysed to improve the processes. Several solutions have been found to automate the tracking of ladle locations. These include, but are not limited to; resistors, Radio Frequency Identification (RFID) tags, thermal imaging and visual recognition cameras. RFID tags have been successfully used in industry to improve the ladle processes in plants that have adopted this technology (10). Jun (2014) used RFID tags to increase accuracy and knowledge of locations and time required at the secondary steelmaking stage (11). This reduced the temperature loss in the ladle and was able to reduce the tapping temperatures of the BOF by 11.2°C (11). The reduction in tap temperatures provided a large cost saving and it prolonged the refractory life in the BOF and provided quality benefits through improved refinement in the converter. The study did not quantify the cost benefits but if benefit were converted to secondary reheating costs it would equate to ~£2mil/annum. This emphasises the importance of correct steel ladle management because it benefits or detriments the whole production process. A number of companies have set up ladle tracking systems, which they sell to steel plants as a third-party, based around RFID tags (12,13). This validated the maturity of the technology of RFID tags and has already been successfully implemented. The ladle state can be tracked but there is no available literature that states a system exists that automatically tracks whether a ladle is lidded or not. Using ladle lids was shown to have a large effect on the cooling curve and is essential data for an accurate thermal model (14,15). However, the ladle cannot be constantly lidded as the ladle needs to be tapped into and the secondary units need access to the steel. More accurate quantification of the cooling effects of the steel without lids is required to put more emphasis on the production operators to prioritise ladle lidding. The operator is still relied on to manually input the data of whether a ladle is lidded or not. If RFID tags or another system could be developed that was able to track when a ladle is lidded it would provide commercial benefits.

2.2.3 Temperature

Tracking the temperature profile of the refractory material is essential for ensuring the ladle shell is kept below the temperature limits stated in the standards (1,16,17). It is

also important to monitor the thermal state of the refractories to ensure they are not subjected to excessive thermal shocking. This is also detrimental to the process as it causes a cooling effect on the steel which results in excess reheating, quality detriments (through excess alumina in the steel or potential slag reversion) and increased costs for production. Due to the number of ladles used in a steel plant thermal models are used to track the thermal state of the refractory lining. There are two groups of thermal models in the literature, most commonly separated by the definitions of "online" and "offline" models (18). Online models can calculate the changes in refractory state at a rate that allows them to track the changes with production. Offline models are commonly used to improve refractory performance and thermal profiles of refractories due to changes. They can also be used to verify new working procedures and determine where temperature savings can be utilised from plant data (11). Without the need to keep up with production they can utilise simulation methods that are more time consuming and accurate. Discussions of the various online and offline models from the literature can be seen in the next sections.

2.2.3.1 Online models

Online models tend to be 1D models that use average values of the refractory lining to give a validated estimate of the rate of change in temperature due to a change in state. These assumptions and reductions of a ladle to a 1D structure are due to the limitations in computing power and time that is required to simulate 2D or 3D models. There are two key types of online model, empirical models and finite difference models (19). Empirical models rely on experimental data and formulate equations that are then able to match the data recorded (19,20). Finite difference models utilise fundamental equations and changes in ladle state to predict the future temperature of the refractory lining (4,21,22). Both these methods are sensitive to location data and emphasise the importance of correct data to produce accurate predictions. These models are the most commonly used in steel plants because they are the only models that current computing power can maintain at the same rate as production at the time of writing. Often a number of assumptions are associated with the numerical based models to simplify them further (19). Each assumption reduces the accuracy of the model and removes its ability to adapt to every scenario the ladle is subjected to (21,22). Samuelsson (2007) also came to the conclusion that "the off-line applications are generally more complex than models intended for on-line applications" because

10

offline models are not limited to keeping up with production rates (19). The lack of literature surrounding online models is due to the benefits they have to companies and they are often kept as trade secrets. An observation from the author is that these models rely on the location and state to track the temperature of the ladle, but a calibration point is not present. If a ladle model has a signal error and starts to drift from the actual ladle scenario there is nothing to bring the accuracy back on the model. Samuelsson (2007) and Du Sichen (2012) concluded that the complexity levels of thermal models increased with each level added to the model (4,19). This is the common trade off with modelling, that the on-line models which adapt to production speeds are less accurate than the Computational Fluid Dynamic (CFD) models. Samuelsson (2007) suggests that the models should be combined to bring the benefits of the CFD accuracy to the speed of the online models. Through discussions with industry experts, and gaining an understanding of the physical measurements that are recorded from the steel plant, the author suggests that a model with a more selective data set be used. Models attempt to use a state system with a simplification of each state to make the modelling less taxing. However, there are datasets commonly collected for production support. If these were utilised by an online model, they would provide a more robust monitor of the refractory thermal state. If the temperature measurements that are taken to ensure the steel super heat were used with the model a higher degree of accuracy could be achieved. The preheating gas flow is commonly used by the operators to determine if the preheaters are functioning correctly. Adding this data to a ladle thermal model increases the robustness of the model to interpret the preheating states. Laser scanners are common practise in most steel plants now, which give the thickness of the refractory layers. With an understanding of which thicknesses are most related to the model and production these can be used instead of predicted wear scenarios.

2.2.3.2 Offline models

2.2.3.2.1 Computational Fluid Dynamic (CFD) models

CFD models utilise the Navier-Stokes fundamental equations of fluid dynamics developed in the 19th century (23). CFD models are the most accurate method for simulating liquids. This directly translates to teeming ladles with the molten steel interface with the refractory material and the slag. This in turn allows the convective heat transfer when the ladle is full of steel and also when the ladle is empty causing the refractories to interact with air (24). The downside to CFD modelling, and the

reason it is less commonly adopted in steel plants, is the amount of computer power required to run the simulations. Each simulation can take a number of days to run and therefore is unable to keep up with the rapid changes in production (19). CFD models have been used to verify numerical models in a cost effective way, without the time and financial investment of physical temperature measurements of the ladle (19). This creates an issue as the knock-on effect of errors is carried over from the CFD model and the verification step via measurement of the ladle is not directly related to the new model. To ensure a thermal model is accurately measuring the temperatures of the ladle a validation via plant data is essential. A model will only ever be accurate within an acceptable tolerance, a build-up of tolerances leads to an increase in temperatures produced.

2.2.3.2.2 Finite Element Analysis (FEA) models

FEA was originally developed to model problems in solid mechanics. However, it has since been utilised to model thermal changes in materials with the use of Fourier's law of heat flow. With adjustments to the thermal properties it has been possible to successfully model liquid interactions with solids (19,25–30). By increasing the thermal conductivity it is possible to model the liquid steel via FEA because the heat transfer between liquid steel and refractory is higher than the simulated solid steel and refractory. Because FEA models the interaction between two solids this increase in thermal conductivity accounts for the difference in the simulation (30). Therefore, FEA models have been successfully used to simulate scenarios in a teeming ladle. When the teeming ladle is in a certain state the model then predicts the change in temperature of the lining. With the benefit of being an offline model it is possible to use historical plant data to track the changes in state. However, like CFD models the processing time is unable to keep up with the rate of production. FEA models are more commonly used due to the reduced simulation times and the reduced computer capacity requirements, with simulations taking several hours as opposed to days with CFD (19,25–29). This gives companies a difficult choice between accuracy and cost - from an accuracy point of view the CFD models would be the best choice. However, because any model will still need verification via physical measurement which is a large investment, the business decision is often to use FEA.

2.2.3.3 Model verification

For thermal models to be reliable for production they must first be validated. Moreover, their intrinsic accuracy and performance must be understood before deploying, to support decision-making within the manufacturing process. This is achieved by taking data from a ladle whilst it is in production. The two common methods of verification are thermocouple measurements and thermal imaging of the hot and cold face (2,24,29). The thermal imaging method will only provide two points of verification - the cold face of the ladle shell and the hot face of the refractory. This allows the model to have inaccuracies in the areas of the model between these two points. Heat is stored in the refractory linings and the amount thermal storage is suggested to have a significant effect on the steel temperature loss during transportation (31). Wu (2012) has created a simulation that shows a 250t ladle will lose 10°C from the steel to the refractory lining on the initial cycle after preheating, and the second and third heat will lose 5-7°C (32). This study used twelve thermocouples to verify the model. This highlights the importance of measuring the internal temperatures of the ladle lining. As the literature suggests these temperatures have a significant effect on the steel temperature. It is important to know if the model is accurately predicting the internal temperature of the refractory lining, as this has a large effect on the thermal storage and rate of temperature loss (31). As there is generally a lack of understanding of the correct setup for a thermal imaging camera it creates errors in the validation stage. Therefore, to rely only on thermal imaging to verify a model does not supply enough data to determine if that model is adequate for production. The amount of thermal energy that can be stored in the lining is determined by the density, thermal conductivity and specific heat capacity of the materials employed (33,34). As the ladle does not maintain steady state during production it is not accurate to use steady state equations. Therefore, thermal diffusivity equations are applied to the ladle lining. Equation 1 shows the relationship of thermal conductivity with density and specific heat capacity. This is why the thermal conductivity of refractory layers can have such a large effect on the thermal efficiency of the ladle (35).

$$\alpha = \frac{k}{C_p \rho}$$

Equation 1:Thermal diffusivity equation.

Thermal models are heavily dependent on reliable material properties of the refractory and Bakker (2001) verifies this when he states "thermal analysis is heavily dependent on material parameters" (36). However, the lack of reproducibility of thermal conductivity measurements leads also to the risk of inaccuracies in models. Gupta (2004) calculated that when a ladle is full 55-60% of the heat lost from steel into the ladle is through its barrel; 15-20% is lost through the bottom; and the remaining 25-30% is lost through the slag lining (3). This suggests the most improvements that can be made to the ladle thermal efficiency would be in the ladle barrel refractory lining. When a ladle is empty, however, the heat loss is primarily through the top of the ladle. Van Beurden (2014) was able to show that this has an increased cooling effect of 3°C on the steel compared to when the ladle was lidded (30).

2.2.4 Thermal conductivity measurements

2.2.4.1.1 Wear lining bricks

The thermal conductivity of wear lining bricks has been shown to have a large effect on the thermal efficiency of the ladle lining (31). The reduced thermal conductivity increases the thermal storage behind the hot face and reduces subsurface cooling. This in turn then reduces the cooling effect on the steel. Wear lining bricks also have an important role to play in the thermal efficiency of the teeming ladles as they balance the location of the freeze point in the lining. It is common practise to keep the freeze temperature of the steel in the wear lining, i.e. the temperature at the cold face of the wear lining brick needs to be below 1538°C. By increasing the amount of insulation in the ladle the freeze point can move closer to the steel shell. This causes a safety issue due to steel penetration of the wear lining and then the subsequent freezing and expansion of the steel when the ladle is dropped out of production. The expansion of the steel can reduce the integrity of the wear lining and cause a safety risk. Therefore, to increase the insulation and improve the thermal efficiency of the ladle this must be balanced with a reduced thermal conductivity wear lining.

2.2.4.1.2 Ladle insulation

To fully understand the thermal efficiency of a ladle in production it is essential to know the benefits of the insulation layer and whether the insulation integrity is reduced during a ladle campaign. This can be done by measuring the insulation temperatures during production and recovering a sample of the insulation after it has been removed from the ladle. As discussed in the introduction to this chapter, the thermal efficiency of a teeming ladle is heavily influenced by the thermal conductivity of the insulation materials (2,3,25–27). Gupta (2004) concluded that 55-60% of the heat lost from a full ladle is via heat transfer through the barrel when an insulation layer is not present (3). Because this assessment was made in multiple studies it is interesting to note that there are minimal studies that investigate the post-mortem properties of microporous pyrogenic silica insulation (2,3,25–27). By conducting a study on the post-mortem insulation it would be possible to determine how much the insulation degraded and the heat loss caused by the in-situ insulation properties. The only study publicly available was by Buhr (1998), which found an increase in the thermal conductivity but wasn't able to quantify these changes for the insulation production temperatures (37). The study determined that there was an increase in carbon due to the dolomite lining, which diffuses into the microporous insulation and created a higher thermal conductivity. However, the thermal conductivity of the insulation panel was determined by stacking the insulation either side of the sample and noting the difference to the Green properties. This method was only able to produce data up to 300°C and there is the need to determine the properties of post-mortem insulation above this temperature. Therefore, as refractory linings have moved away from dolomite linings and there is no other literature available for post-mortem microporous insulation, there is an opportunity to bring new information into this area with great novelty. From discussions with specialists in industry there is a common assumption that insulation materials are degraded from the production process. Another common assumption is, due to the movement of the ladle, the insulation is dislodged and is not present in some areas. If a full panel of the material could be recovered from the ladle this could either prove or disprove this hypothesis. This would also expand on Buhr's study, which was able to successfully recover a sample of used insulation but not a full panel (37).

15

Gongfa (2015) presents a study on nanometer adiabatic material as an option for the insulation layer (38). The material is verified using FEA to determine the performance of the ladle during preheating but there is no trial of the material in the ladle. The nanometer material also requires a steel protective layer to prevent compression of the material, which is simple to simulate but, on a practical level, very difficult to install with the desired performance.

Thermal models rely heavily on the thermal conductivity of a material to track the heat transfer through materials by their thermal diffusivity. Lian et al. (2016) were able to quantify the thermal conductivity of a porous thermal insulation material using the thermal diffusivity relationship (39). Using the laser flash method, they were able to get the thermal diffusivity of the porous insulation material. They then performed differential scanning calorimetry measurements on the material to quantify the specific heat capacity. By then measuring the density they were able to rearrange Equation 1 to make thermal conductivity the subject and calculate it from their findings. Lian et al. (2016) were therefore able to prove the concept of using the laser flash method to calculate the thermal conductivity of porous insulation material with Green properties. If a sample of the insulation material could be recovered from the ladle after production this methodology could be used to determine the same for a post-mortem sample.

Another principle of heat transfer that is often utilised in ladle insulation is Fourier's law of thermal contact conductance. This is more heavily utilised in a four-layer ladle refractory designs as the total thermal energy stored in one material cannot be fully transferred to another material. This is the theory adopted for the inclusion of two insulation materials to be more effective than simply using one. Equation 2 is Fourier's law which quantifies the heat flux (q) between bodies with a thermal conductivity of (k), cross sectional area (A) and temperature gradient in the direction of flow (dT/dx). It is important to note the common factor between the thermal diffusivity and thermal contact conductance is the thermal conductivity. This provides more emphasis for the work to try and reduce the current lack of understanding of this value for in-situ microporous insulation materials.

$$q = -kA\frac{dT}{dx}$$

Equation 2: Fourier's law of heat flow between bodies equation.

Equation 3 expands Fourier's law to show the relationship between two materials with different start temperatures and thermal conductivities. It uses the material surface temperatures that are not in contact (T_1 & T_3), the thermal conductivities of the bodies in contact (k_A & k_B), the contact area A and the thermal contact resistance ($1/h_c$), which is the inverse of the thermal conductance coefficient.

$$q = \frac{T_1 - T_3}{\Delta x_A/(k_A A) + 1/(h_c A) + \Delta x_B/(k_B A)}$$

Equation 3: Expanding Fourier's law to give the heat flow between two bodies in contact.

It is understood that thermal contact resistance is only applied to highly conductive material systems. Therefore, it is commonly ignored in ladle thermal models for the layers associated with insulation materials. However, it is commonly accounted for when designing building envelopes. Because a large portion of building envelopes are bricks and mortar (refractories) it suggests that this needs to be factored in for modelling teeming ladle refractories (40).

Gopal et al. (2013) use Fourier's law to create Equation 4, which is the relationship between thermal contact conductance (h_c), average axial heat flux across the contacting surfaces (q_{avg}) and the difference in temperature of the two surfaces (41). They (2013) demonstrated this effect by loading and unloading stainless steel washers with various surface finishes (41). They found large variations in temperature transfer of 58.3°C for lapped washers with surface finishes of 7µm. This produced a variation of 8.7% in thermal conductivity between the washers that had been prepared to be "identical" with a very high tolerance. This results in a thermal contact conductance variation of 85% and demonstrates that if the variance of thermal conductivity with temperature is ignored it can produce significant errors (41). Currently thermal models for teeming ladle refractories often use a set figure for thermal conductivity. The heterogeneous nature of refractory bricks will cause much rougher surfaces and variation in the contact surface properties due to the mix of grains and matrixes in refractories.

$$h_c = \frac{q_{avg}}{\Delta T}$$

Equation 4: Thermal contact conductance from Fourier's law.

2.2.4.1.3 Ladle slag

Ladle slag analysis was conducted most extensively by Glaser (2012) with a high degree of repeatability (42). The testing facilities used for this study were also very specialised and not easily accessible. The tested slags can be seen in Table 1 and were recorded to have thermal conductivities ranging from 0.025W/m.k at 1700°C to 0.179W/m.k at 1500°C (43).

Analysed Composition of the Al2O3/CaO/SiO2/MgO System
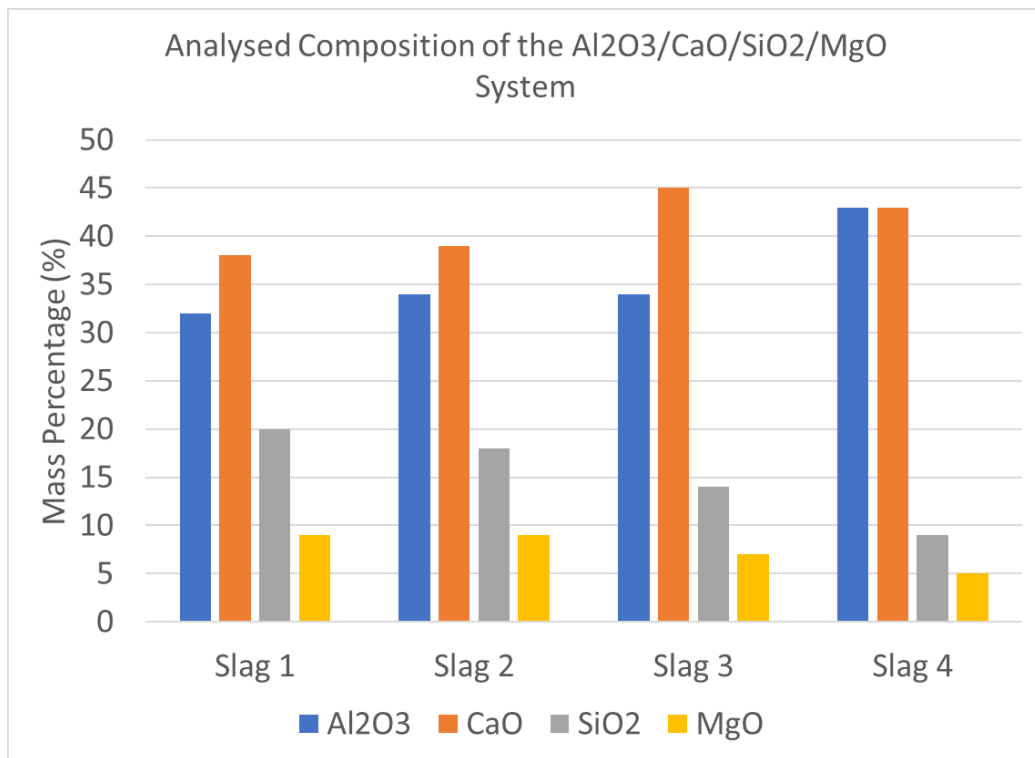
Table 1: Ladle slag chemistries tested by Glaser (2012) (42).

Due to the extensive testing required, and the limited differences in thermal conductivity found due to the large differences in chemistry, the literature already has a concise answer for ladle slag thermal conductivity. Therefore, it was deemed by the author that this thesis would not attempt to expand on this element of ladle thermal efficiency.

2.3 Temperature measurement

For thermal models to be relied on to support production they must first be verified. This is achieved by taking data from a ladle whilst it is in production. The two common

methods of verification are thermocouple measurements and thermal imaging of the hot and cold face (2,24,29).

2.3.1 Thermocouples

To record subsurface temperatures of the refractory layers there were three-options thermocouples, Fibre Bragg Grating sensors (FBG) or thermo-acoustic sensors. At the time of writing FBG sensors were only able to measure temperatures up to 400°C (44,45) and thermo-acoustic sensors were still a theoretical measurement technique. Therefore, thermocouples are the most tried and tested method for this application. The challenges of using thermocouples on a teeming ladle are the mobility of the datalogger and protecting the datalogger from the shell temperatures of the ladle. This was needed for consideration for any in-situ thermocouple experiments performed during this study.

2.3.2 Thermal imaging

Thermal imaging is highly dependent on two key parameters, the spectral response of the camera and the emissivity of the object at the wavelength recorded.

2.3.2.1 Spectral response

The spectral response is well understood within the radiometry sector but is not often used correctly when measuring temperatures in industry with thermal imaging cameras. Planks law of radiation shows a spectral radiance peak for different temperatures at different wavelengths as shown in Figure 6. The changes in spectral radiance intensity enable thermal imaging cameras to determine the temperature of an object when wavelength and emissivity of the object is known (46). To get the most accurate readings the spectral radiance needs to have a high degree of change with temperature. Therefore, when measuring the temperature of an object it is essential to select a wavelength that is closest to the peak of the spectral response at the corresponding temperature (5,47). This is then the challenge of thermal imaging – a basic understanding of the temperature needs to be known before an accurate measurement can be made.
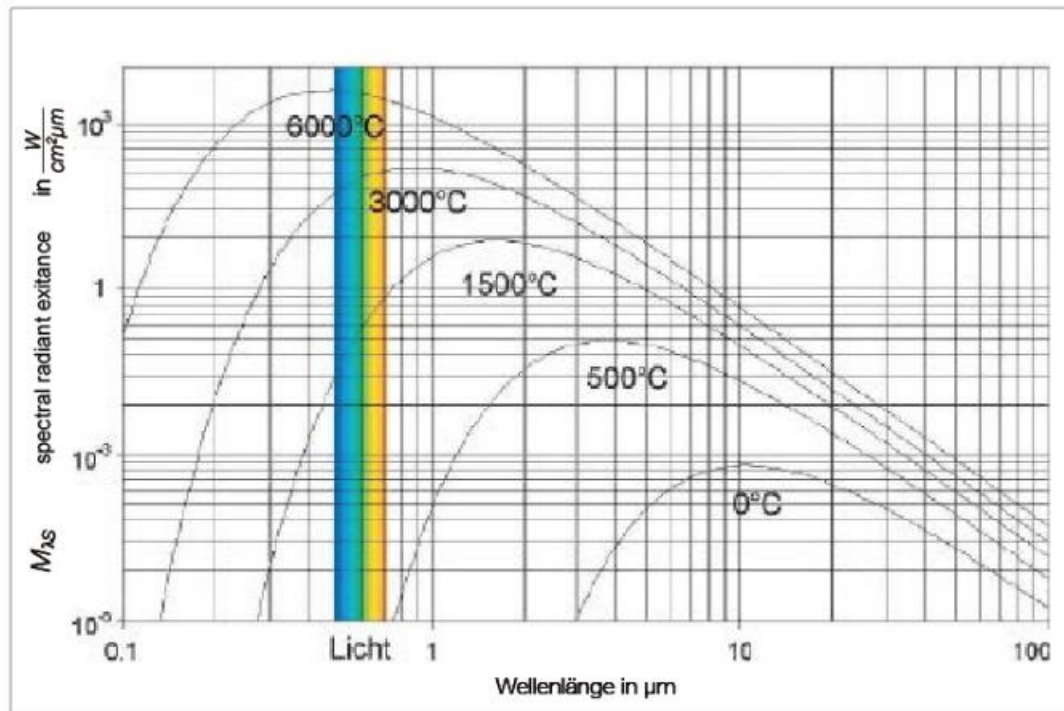
Figure 6: Wavelength against spectral radiance from (47).

The emissivity of an object also changes with wavelength, as seen in Figure 7 which is taken from a study conducted by Honnerova et al. (2014) (48). In this study Honnerova et al. (2014) quantified the spectral emissivity of coatings in the spectral range from 1.38µm to 26µm. During the study they were able to demonstrate conclusively that there are large differences in the emissivity values when measuring at different wavelengths. The results from the study can be seen in Figure 7 with the difference from the maximum and minimum recorded to be 0.4. This highlights the importance of conducting emissivity studies at the wavelength used to measure the object.
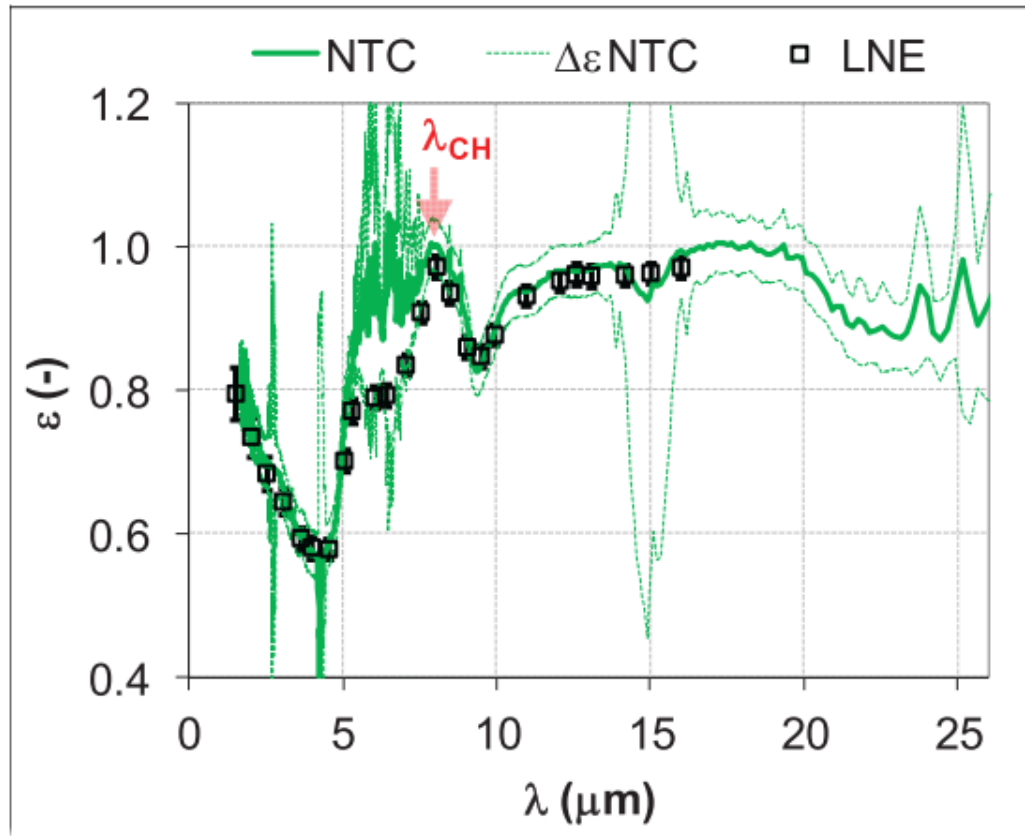
Figure 7: Wavelength against emissivity performed by various research centres taken from Honnerova et al. (2014) (48). NTC = New Technologies Research centre, LNE = Laboratoire National d`Essais

2.3.2.2 Emissivity

2.3.2.2.1 Historical methods for emissivity measurement and their relevance to refractories

Bauer (1990) conducted experiments on refractories to determine the emissivity at different temperatures at a set wavelength and variable wavelengths at 750°C (49). Bauer (1999) repeated the study but with a shielding glass and under vacuum (50). The refractories tested can be seen in Figure 8, Figure 9 and Figure 10. The refractories tested in both Bauer's studies are very pure refractories with only one and two components. The refractories installed in teeming ladles are a mix and often coated in slags which are also not tested in Bauer's studies. There are no materials containing carbon in Bauer's studies – black refractories have a higher emissivity so even visibly they can appear to glow brighter. The results from Bauer's studies suggest that the refractories have an emissivity close to 1, the theoretical maximum, as shown in Figure 8, Figure 9 and Figure 10. The idea that a refractory without carbon would have a spectral emissivity so close to the theoretical maximum is unlikely, especially when

21

compared to the findings in more recent studies (24,51). This casts doubt on the values calculated in these studies.
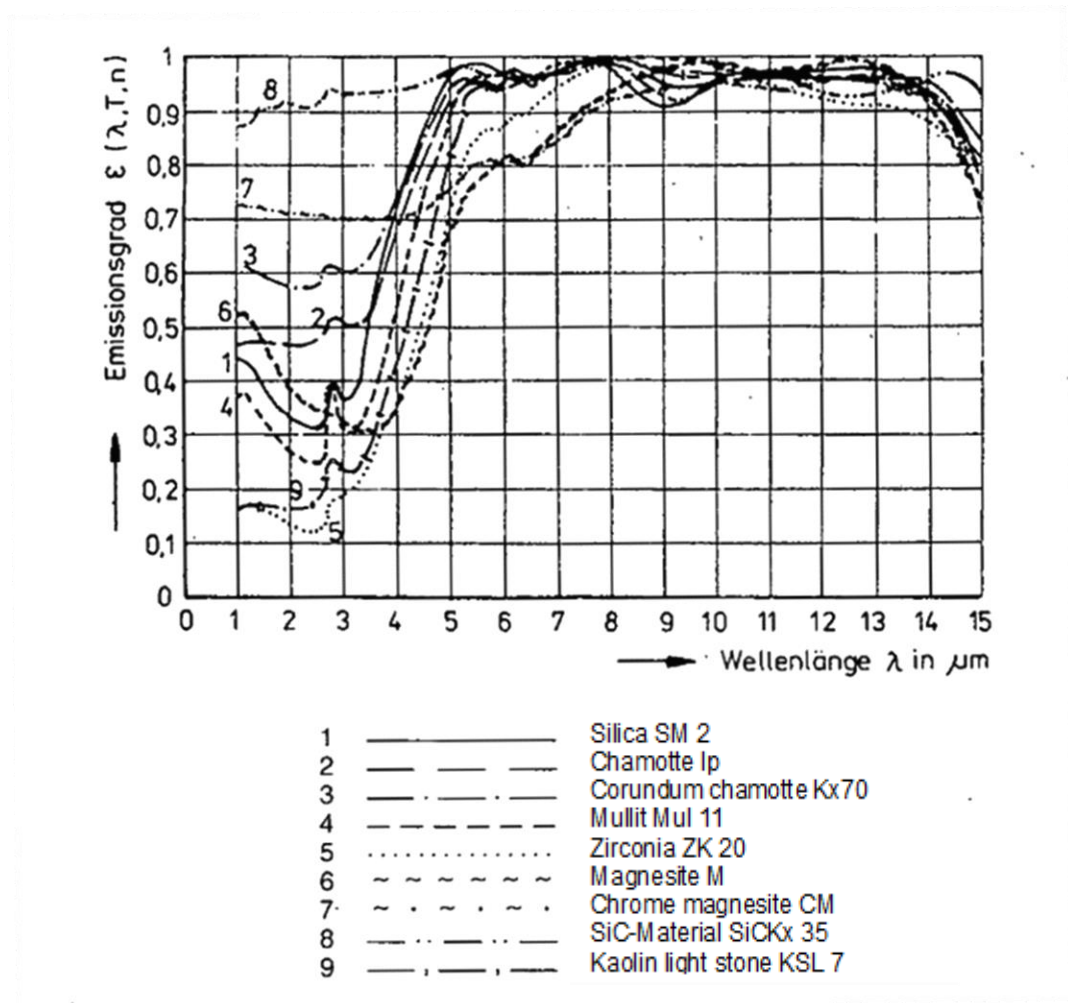
Figure 8: Emissivity table from Bauer (1990) of emissivities at various wavelengths for different refractories at 750°C (49).
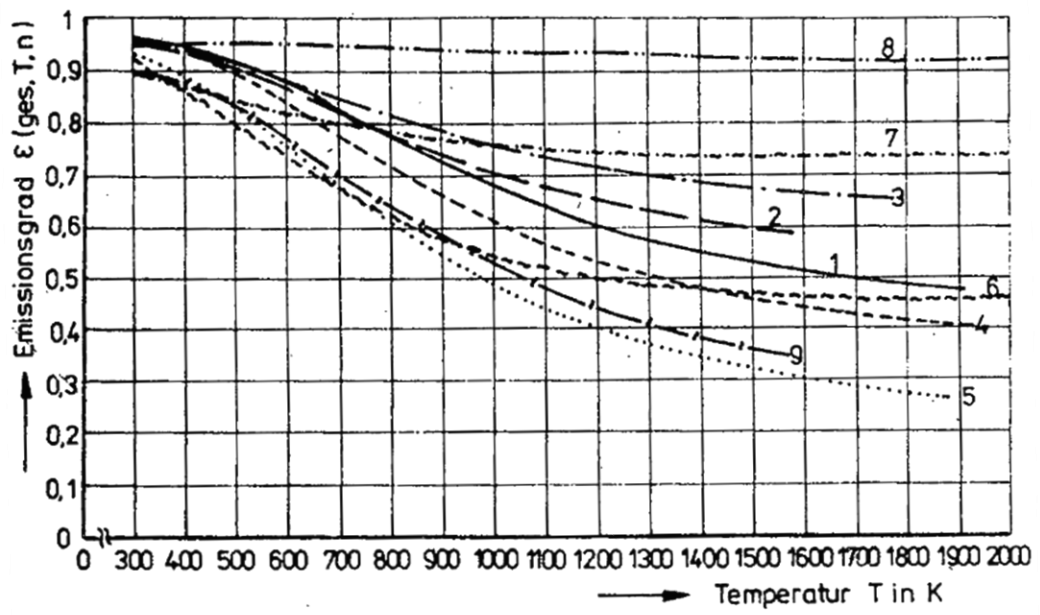
1	———————	Silica SM 2
2	— — —	Chamotte Ip
3	— · — · —	Corundum chamotte Kx70
4	— — — — —	Mullit Mul 11
5	· · · · · · · · ·	Zirconia ZK 20
6	~ ~ ~ ~ ~	Magnesite M
7	~ · ~ · ~ ·	Chrome magnesite CM
8	— ·· — ·· —	SiC-Material SiCKx 35
9	— , — , —	Kaolin light stone KSL 7

Figure 9: Emissivity variation with temperature from Bauer (1990) (49).
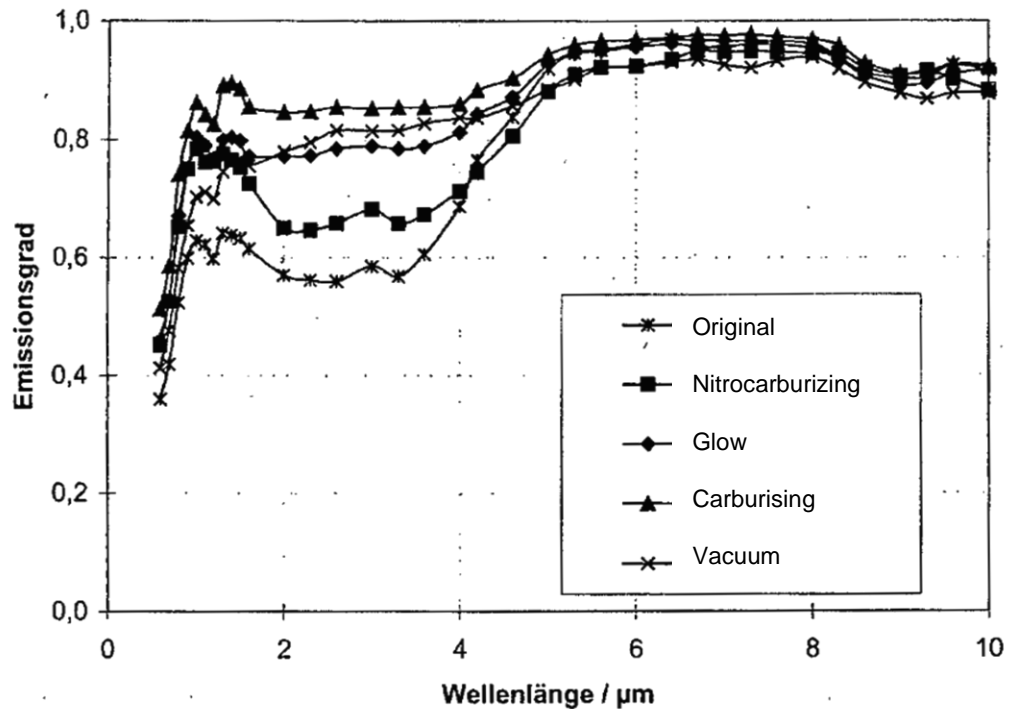
Figure 10: Emissivity of Sillimanite in various atmospheres Bauer (1999) (50).

Wall (1992) measures the emissivity of pure molybdenum, ruthenium and tungsten alloys for their application in thermionic energy conversion of heat to electricity (52). The method used is a vacuum tube with a blackbody cavity and sample measured in sync. The materials measured in this study are not used in teeming ladle refractories due to their high price and volume required.

Rulison (1994) proposes a technique for measuring refractory material by supercooling a melt to determine the radial emissivity and specific heat of a material (53). This technique measures the emissivity of the sample with a pyrometer with a spot diameter of 1mm of a sample that is 2.5mm in diameter and a purity level of 99.95%. This is not representative of the slags and refractories found in teeming ladles. The materials are also heated to 2300°K and the emissivity is assumed to be independent of temperature at this point (53). This is not shown to be the case in both Glaser's (2011) and Jain's (2015) studies and consequently this method is not applicable to the measurements required for accurate teeming ladle measurements (24,51).

Elich (1995) presents a study of the refractories used in a glass melting furnace and measures the reflectivity of these refractories using the integrated sphere method, which is then used to calculate the emissivity (54). The tested refractories in Elich's

(1995) study are silica and zirconium-based and therefore do not relate to the materials tested in Glaser's (2011) or Jain's (2015) studies. Elich's (1995) study found that the initial heating of the refractories had a large effect on the materials tested and was attributed to water evaporation from the materials. The differences found from this initial heating amounted to 20% error in the calculated emissivity. However, the temperature range of the equipment is 500-700°C and the accuracy of the temperature of the sample is "about 50 and 100°C" (54). The measured results, including a room temperature measurement, are used to extrapolate to temperatures from 327°C up to 1827°C. Within this extrapolation the emissivity values are found to be between 0.9 and 0.45. The error in temperature accuracy would have a contribution to the emissivity error and the extrapolation from a small data set would then account for the error that adds up to Elich's (1995) 20%. This study was conducted in 1995 and the accuracy of equipment has since increased. As such this method will not be used for the measurement of refractory and slag emissivity.

Otsuka (2005) presents a study for obtaining the hemispherical emissivity of 304 stainless steel and molybdenum with an oxide layer (55). The method used heats the materials in a bell jar under vacuum and the samples are heated by passing a DC current through the metals. This method is not possible to use with slags or refractory materials due to the sample thinness needing to be 0.5mm.

Ohlhorst (2007) measures refractory coatings for jet engine rotor blades in search for a high emissivity coating to transfer the heat away from the blade (56). The experimental setup uses a vacuum chamber and conduction coil to heat zirconium based refractory coatings. The equipment is based in the NASA Johnson Space Center and therefore unavailable for this study. Even with availability this method would not be applicable to the refractory slags and refractories due to the heating mechanism and can therefore be discarded for this study.

Wiecek (2010) uses the emissivity difference of liquid steel and slag to track the slag transferred from a converter during the tapping process (57). This is an example of the understanding of a difference in emissivity but an attempt to use the difference rather than an exact value in the application. Wiecek (2010) does not state in the paper a value used for emissivity, so it is unclear whether the value is representative or not. MWIR and LWIR cameras are used for correlation of the readings to increase the

accuracy and provide more information for the neural network implemented. This study helps to demonstrate the lack of understanding when using thermal imaging cameras and emissivity. The spectral range adopted is better suited for applications below 500°C. However, in this study it is used for tapping of steel which would be above 1500°C.

Mourao (2015) conducted a review of the NASA studies and patents on high emissivity coatings and their potential application to industrial furnaces (58). The emissivity values contained in this review are therefore of coatings and not refractory materials that are associated with teeming ladles. The application of high emissivity coatings could be applicable to accelerating the initial drying time of the wear lining after installation but gives no extra insight to refractory or slag emissivity.

2.3.2.3 Currently relevant studies on refractory emissivity

There have been two key studies into the emissivity of refractories and ladle slags in recent years. Both studies heated a refractory brick in a furnace and used a thermocouple to calibrate the radiometer by adjusting the emissivity setting until the temperatures recorded matched. Glaser (2011) published a paper on his findings of refractories and slag coated refractories where he used a FLIR ThermaCAM P65 to measure temperatures from 397-1000°C (24). This camera uses a spectral range of 7.5-13µm and will be very sensitive to emissivity changes at temperatures above 500°C as discussed (59). In his summary he states "more investigations are needed to determine the emissivities of the inner wall" (24) which he adds to in his thesis stating that "studies on the emissivity of the different textures need to be carried out" (42). This acknowledges that the surface of a material affects the emissivity and estimates will need to be used for the full hot face of the teeming ladle refractory/slag. The refractories in Glaser's study are not specified but it is stated that the materials were heated in a furnace for "more than one hour" at 400°C before being elevated to measurement temperature (24). From the table of thermal properties in Glaser's paper it can be concluded that these refractories contain carbon. Because of this the refractories are susceptible to decarburisation. By heating them in a furnace in this manner, and opening the door to the furnace it introduces oxygen. This in turn decarburises the refractories at the higher temperatures measured in this study (24). Therefore, the measurements Glaser is making is of decarburised refractory, when it is not coated in slag, and will not be a true representation of the emissivity at

production temperatures. Also, if the emissivity at the wavelengths measured by Glaser were used in a thermal model to represent the radiation heat loss they would be inaccurate, as the emissivity measured is not at the peak of the spectral radiance for an object at 1000°C. Glaser has tested used bricks coated in slag to eliminate the errors caused by the decarburised refractory. However, this waiting period due to the sample face being "approximately 30 cm^2" (24) will cause a drop in temperature of the surface by being exposed to the atmospheric temperatures. As Glaser is measuring the surface to be able to match the temperature to the thermocouple there will be an overestimate of the emissivity in achieving this. The overestimate of the emissivity values is assumed but with sound logic. If the thermocouple was measuring higher than the thermal imaging camera the emissivity would be reduced to correlate. As the hot face temperature will be lower than the subsurface temperatures then the emissivity would need to be increased to correlate with the thermocouple. Therefore, it can be said with confidence that the emissivity values are an overprediction.

Jain's (2015) study uses a similar testing method to Glaser's but the furnace used to heat the samples has been adapted so the door represents the refractory build of a teeming ladle (51). The sample size in Jain's study is 50mm x 30mm x 10mm and the pyrometer used is a Chino IR-AHS which has a spectral response of 0.96µm (60). The pyrometer was setup with 1.25m between the sample and the pyrometer. The diameter of the measured area by the pyrometer is calculated by the formula given in the IR-AHS instruction manual as D = L/100(ø, mm) which gives a measured diameter of 12.5mm, which is just under half the size of the 50x30mm face measured (60). The spot size is important for accurate measurement with a pyrometer. As stated by Gruner (2003) the target should be double the spot size for accurate readings (46). These initial setup conditions, therefore, provide a better scenario to record more accurate data than the Glaser study, as the correct wavelength for the temperatures is used. However, the door to the furnace still needs to be opened to measure the emissivity of the sample. This introduces oxygen to the refractory sample and, due to its size, would decarburise in a short period of time. Jain makes reference to this in the body of the paper stating "emissivity of the magnesia–carbon refractory material, as it appears, decreases with increase in temperature due to continuous oxidation of carbon and the resultant increase in the porosity of the refractory surface due to prolonged heating." (51). This shows that the emissivity measurements in this study have an error factor that was not

considered. The repeatability is shown to be strong, but the accuracy is not accounted for.

A study needs to be conducted in an inert atmosphere that will reduce the decarburisation to a minimum throughout the testing at each temperature interval. The author has graphed the values from the Glaser and Jain studies and clear differences can be seen up to 0.15 in the emissivity values measured. This information can be seen in Figure 11. The differences in spectral response are demonstrated and it is important to note the differences in emissivity results. Neither Glaser nor Jain quantify the errors in their studies. The author has produced error bars based on the differences in their results.
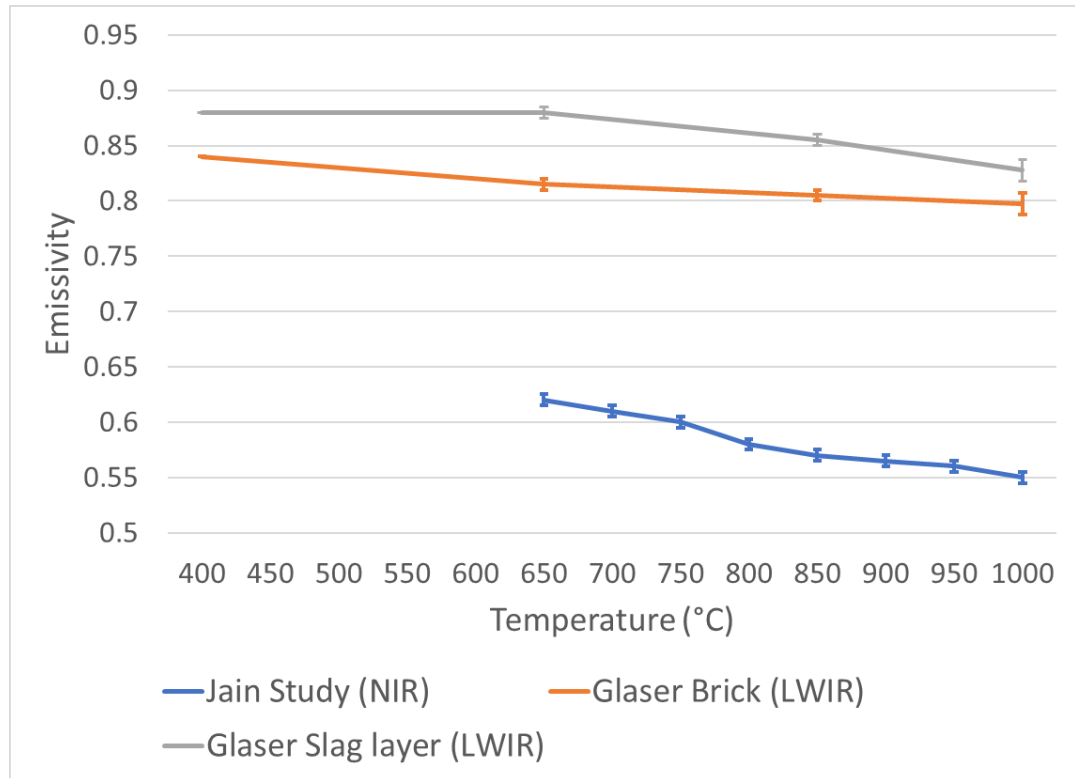
Figure 11: Emissivity values from Glaser and Jain studies plotted on same graph with error bars calculated from variance in data published.

Boone et al. (2018) use a thermal imaging camera to accurately record electron beam melting and quantify the errors caused by emissivity. The equation from Boone's paper provides an estimate of the error for different spectral responses for a pyrometer or thermal imaging camera and is given in Equation 5, where %/K is change in signal per Kelvin, c_2 is Planks second radiation constant ($1.4388 \times 10-2$ m. K), T is the blackbody temperature in Kelvin and λ is the mean effective wavelength of the focal plane array (5).

$$\frac{\%}{K} = 100 \; x \; \frac{c_2}{\lambda T^2}$$

Equation 5: Boone's equation for temperature error from emissivity errors (5).

Boone et al. (2018) use Equation 5 to populate the values in Table 2 which can then be linked to the pyrometer and thermal imaging cameras used in Glaser's and Jain's studies. Glaser uses a LWIR thermal imaging camera, which with an emissivity error of 0.15 would give an error of 154°C, and Jain's pyrometer would have an error of 14°C. This highlights the importance of using the correct spectral response with a radiometer.

Wavelength (µm)	% Change in Signal per K	Error in K from emissivity incorrect by 0.01
1 (Silicon NIR)	1.43	0.70
4 (InSb MWIR)	0.36	2.78
10.75 (Microbolometer LWIR)	0.13	7.70

Table 2: Errors caused by emissivity error of 0.01 for different spectral responses of pyrometers and thermal imaging cameras from (5).

With these errors the use of a spectral response pyrometer or thermal imaging camera with around 1µm would appear to provide an adequate measurement of the ladle hot face. However, neither Glaser's nor Jain's studies consider the geometry enhancement of the ladle or the decarburisation of the refractories. Therefore, it is uncertain as to whether the error of the emissivity for these studies is 0.15 or larger. To solve the challenge of decarburisation a study by Zhu (2019) was found which measures the emissivity of materials in controlled atmospheric conditions (61). The study uses nitrogen and compressed air to control the oxidation of the tested samples. This reduced oxygen environment could be used to reduce the decarburisation of the refractory material found in Jain's study (51). The author utilised Zhu's testing procedure and applied it to samples of teeming ladle refractories and slags, these results are in Chapter 6.

The MSL guide provides several equations for emissivity enhancement when producing blackbody cavities for calibration of non-contact thermometry (6). The equation for a "flat-bottom tube cavity" matches the geometry of a teeming ladle and can therefore be used to calculate the emissivity enhancement of the teeming ladle (6). The flat-bottom tube equation is shown in Equation 6 where ε_{bb} is the calculated

enhanced emissivity, ε_s is the measured spectral emissivity, R_{aper} is the radius of the aperture (radius of the ladle) and L is the length of the cavity (or height of the ladle).

$$\varepsilon_{bb} \approx 1 - (1 - \varepsilon_s)\left(\frac{R_{aper}}{L}\right)^2$$

Equation 6: Emissivity enhancement from MSL guide (6).

Utilising the geometry enhancement of Equation 6 and applying it to the findings in Glaser's and Jain's studies Figure 12 was produced by the author. The enhanced emissivity values reduce the gap from the different wavelengths from 0.15 to 0.06. However, this increases the errors in the study as each of the values is consistently 0.15 higher than the measured values of Glaser's study and around 0.3 for Jain's study.
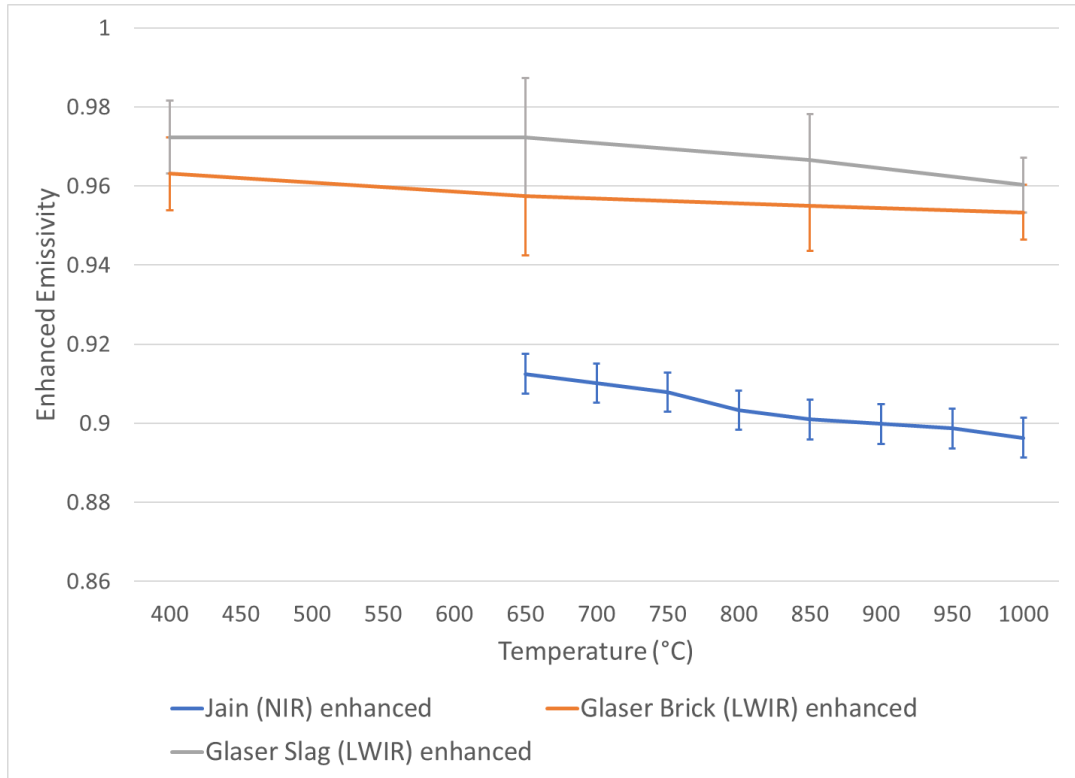
Figure 12: Enhanced emissivity values produced using Equation 6 and measurements in Glaser's and Jain's studies.

With the use of Zhu's testing method to limit the decarburisation of the refractory material, and taking into account the geometry of the ladle, the novelty for expanding the understanding of refractory emissivity in-situ in a ladle is worthy of inclusion in this study (6,61). Samples tested by Zhu's method are 25mm in diameter, which is a good representation of the refractory bricks and accounts for covering the various grains and matrixes that refractory bricks consist of. From reviewing the literature on

emissivity there is reason to conduct a research study on ladle refractory bricks and slags utilising Zhu's equipment and method.

2.4 Conclusions of the literature review

After an extensive look into the literature surrounding ladle temperature management there are some key conclusions that can be made.

1. There are many commercial offerings for ladle tracking and the success of these methods varies. However, due to the various methods there are limited technologies that can currently be used, and they have all been extensively tested. Therefore, there is little novelty available for research into this area to generate a broad solution.

2. The models rely heavily on a good understanding of the thermal properties of the refractory layers. It is mentioned in numerous papers that the properties of the highly insulative layer has the largest effect on the thermal profile of the ladle. It is understood that there is a change in the thermal properties of the insulation but there is not a good understanding of these changes. This thesis will look to perform thermophysical testing on a post-mortem sample of insulation to measure its in-situ properties.

3. The validation stages of the thermal models use thermal imaging cameras (24,42). Glaser (2012) states that the emissivity values for ladle refractories and slags are not fully understood and more work needs to be done in this area to gain more accurate measurements from thermal imaging (42). The author was not able to find any reliable research that attempted to categorise and relate the emissivity of refractories and slags because the system errors were not calculated in the studies found. Qualitative descriptions of refractories are generally referenced in thermal imaging handbooks and there is some information on specific refractories but little on ladle slags (49,50). Therefore, there would be novelty if an extensive understanding of the errors caused by the variance in refractory emissivities could be quantified or if emissivity independent measurements could be achieved. The geometry enhancement looks to be able to do this and a study into the emissivity of slag and refractory will be performed using Zhu's testing method, to get accurate spectral values and in turn enhanced emissivity values (61).

4. Thermal models currently rely on few data points to produce results. Therefore, errors accumulate until the ladle comes out of production for repair or at the end of its campaign. A model that has a calibration point via a thermal imaging measurement would be novel and provide a self-fixing model from knock-on effects of inaccuracies.

2.5 Novel research questions

From the conclusions above the following questions will attempt to be answered in this thesis, as these stand out as areas of opportunity for novel progression:

Q1 Can the insulation panels in a ladle be accurately thermally characterised and recovered from a ladle during the wrecking process (Chapters 3 and 4)?

Q2 Are the in-situ thermophysical properties of the insulation significantly different and do they cause excessive cooling of the steel during transport (Chapters 4 and 5)?

Q3 Do the cooling curves allow for the hot face to be an accurate enough prediction of the cooling effect of the ladle on the steel (Chapter 5)?

Q4 What is the effect of refractory and slag emissivity differences and can the ladle geometry be used to provide accurate radiometer data of the ladle hot face (Chapter 6)?

Q5 Can accurate temperature measurements be used with a thermal model to act as a calibration point for the model (Chapter 6)?

Chapter 3 – In-situ temperature measurement of ladle insulation

3.1 Introduction

This chapter will attempt to answer the first question from the literature review (Q1) and disprove the hypothesis (H1): it is not possible thermally characterise and recover an in-situ sample of teeming ladle insulation for thermophysical characterisation.

The insulation layer of the teeming ladle refractory layers has been found to be the largest contributor to the thermal efficiency of the refractory lining. Glaser et al. (2011) concluded that "the highly insulating layer had foremost impact on the heat loss" when a ladle is full (2). And Gupta et al. (2004) observed that 55-60% of the heat lost from a full ladle is lost through the barrel (3). Glaser et al. (2011) also concluded that "a doubled conductivity of this layer (insulation) would result in considerable increase in the ladle heat loss" (2). Therefore, there is the need to thermally characterise the insulation in-situ and recover a sample of the insulation. This can then verify if a thermal conductivity change has occurred in the insulation.

In order to thermally characterise the in-situ ladle insulation it was essential to use a method of measurement that could withstand the predicted temperatures of ~1000°C at the hot face and 300°C at the cold face (30). There are many methods of temperature measurement currently available including, but not limited to; pyrometers, thermal imaging cameras (TIC), Fibre Bragg Grating sensors (FBG), thermo-acoustic sensors and thermocouples. Of these measurement methods it became clear that only thermocouples were fit for the purpose of measuring the insulation effects, which has been shown from the literature to be the most influential refractory layer for thermal efficiency (31,35,37,38). Pyrometers and TICs could record the surface temperatures in this range but were unable to measure subsurface. FBG sensors were commercially limited at the time of this thesis to 400°C and therefore unable to measure the peak temperatures (44,45). Thermo-acoustic sensors were an unproven technology and still in the implementation stage with a patent being approved for them in 2014 (62,63). This left thermocouples as the logical choice and the reason they were the chosen technology for the thermal characterisation of the insulation. The planning required to conduct a thermocouple study in-situ in a BOS plant and the results of these trials are presented in this chapter.

3.2 Equipment location on ladle barrel

The first challenge of recording thermocouple measurements in the teeming ladle was to find a safe location on the steel shell for the equipment. The teeming ladle is transported to various locations within the BOS and CC plants and travels around 1km for each cycle of production. It was essential the equipment could be attached to the ladle and then left to record the data. This meant the datalogger that records the thermocouple temperatures needed a portable power supply. As the datalogger would need to be attached to the ladle it would then need to be protected from the steel shell temperatures that were simulated to peak around 350°C. This posed two key challenges; protecting the datalogger from the shell temperatures of the ladle and finding a safe location on the ladle that was safe from mechanical damage of crane hooks.

The solution to the temperature challenge was to design and have manufactured a refractory insulated water reservoir that the datalogger could be placed into, protecting it from the shell temperatures. An engineering drawing of the insulation box can be seen in Appendix 11.2. This box would keep the datalogger below 100°C, as the water was converted to steam. This solution came at the expense of an increased footprint required on the ladle. To check potential locations were safe from mechanical damage, dummy boxes were manufactured and attached in two selected locations. The ladle already had electrical connections housed in a "doll's house". As these doll's houses are attached to each ladle (indicated in Figure 13) and have remained safe for many years, it was logical to benefit from this tested location and use them as a reference point.

It is important to understand the severity of the safety concerns of installing 70kg of equipment onto an active steelmaking ladle that contains a large amount of water. Not only would it be a financial loss in the investment of the equipment, but if the box were to be damaged the water could escape. The water would then become a super-heated steam due to the ladle temperatures being around 300-400°C and have the potential to injure operators. If the box were to fall into liquid steel at the CC the pressures could increase beyond the designed limits and again create a hazard to operators nearby. Water has been used in previous applications and proven that it is able to keep equipment below the required temperatures and without causing harm to

operators. Therefore, it was essential to know with certainty that the equipment could be installed in a location that was free from mechanical damage.

Figure 13: Teeming ladle with doll's house circled.

The two selected locations were the same height from the base of the ladle as the doll's house but rotated 90° and 180° around the barrel. Both the dummy boxes remained damage free for seven weeks whilst the ladle was used for production and cycled around the steel plant. However, the box that was 180° from the doll's house position was damaged when the ladle was placed on the wrecking saddle, which is used to remove the refractory linings. This was vital information because, to measure a complete campaign of the insulation, the equipment would have to safely go through this process without getting damaged. Conversely, the 90° location, shown in Figure 14, remained on the ladle for eight months undamaged. This gave enough certainty that this location was safe for the equipment and was utilised when the equipment was installed on the ladle.

Figure 14: Teeming ladle with dummy box 90° around ladle from doll's house (circled).

3.3 Ladle shell integrity

To install the thermocouples into the refractory lining of the ladle it is necessary to drill holes into the ladle shell. These holes are used to attach the equipment and provide an entry point for the thermocouple sensors. The teeming ladles are fabricated with weep holes to allow any volatiles from the refractory to be burnt off. In this case it was not possible to use these exclusively and new holes were still required. Ladle shell failures in the worst-case scenario can cause a breakout of a full ladle. This poses a substantial safety and operational risk. FEA was performed in ANSYS by members of the Tata Steel modelling team. They were able to demonstrate that stress concentrations did not increase beyond the hoop stresses already found on the surface of the shell (64). Figure 15 shows the boundary conditions applied to the simulation the red arrows on the figure show the ferro static pressure caused by the weight of the transported steel (340t). This creates hoop stresses on the teeming ladle shell that if too large can cause failure. Because of the weep holes used to allow volatiles out

during cooling are positioned far enough away that stress concentrations did not occur and increase the hoop stresses to a point of failure. Figure 16 shows the mesh concentration, which focussed primarily on the areas around the holes in the shell. The concern was that the additional holes could cause a stress concentration that could cause a breakout. Therefore, to ensure the stresses did not increase to the point of failure the mesh concentrated on the areas surrounding the holes.
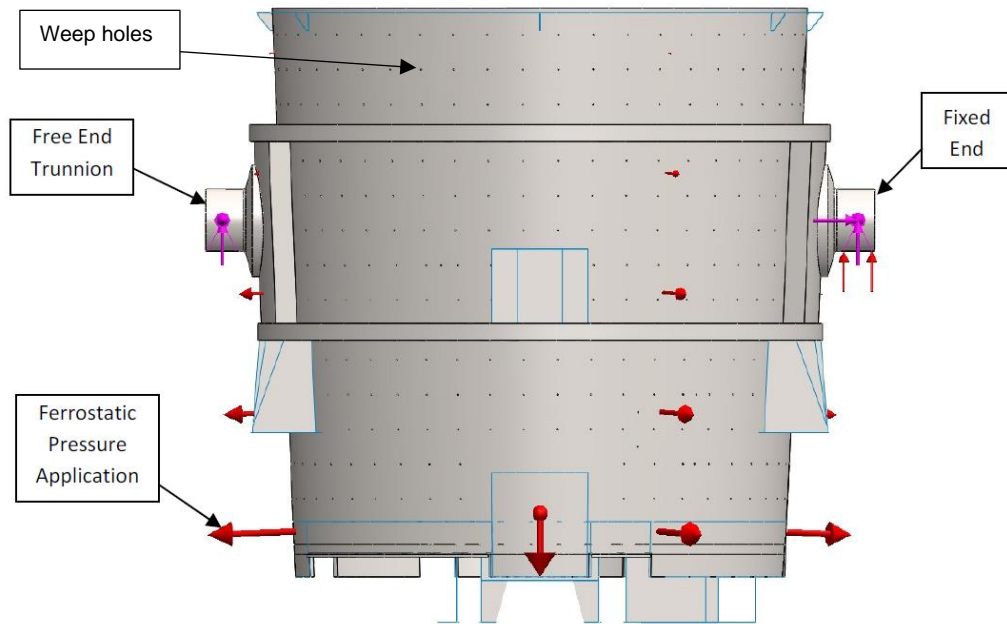
Figure 15: Boundary conditions for FEA of teeming ladle with extra thermocouple holes.
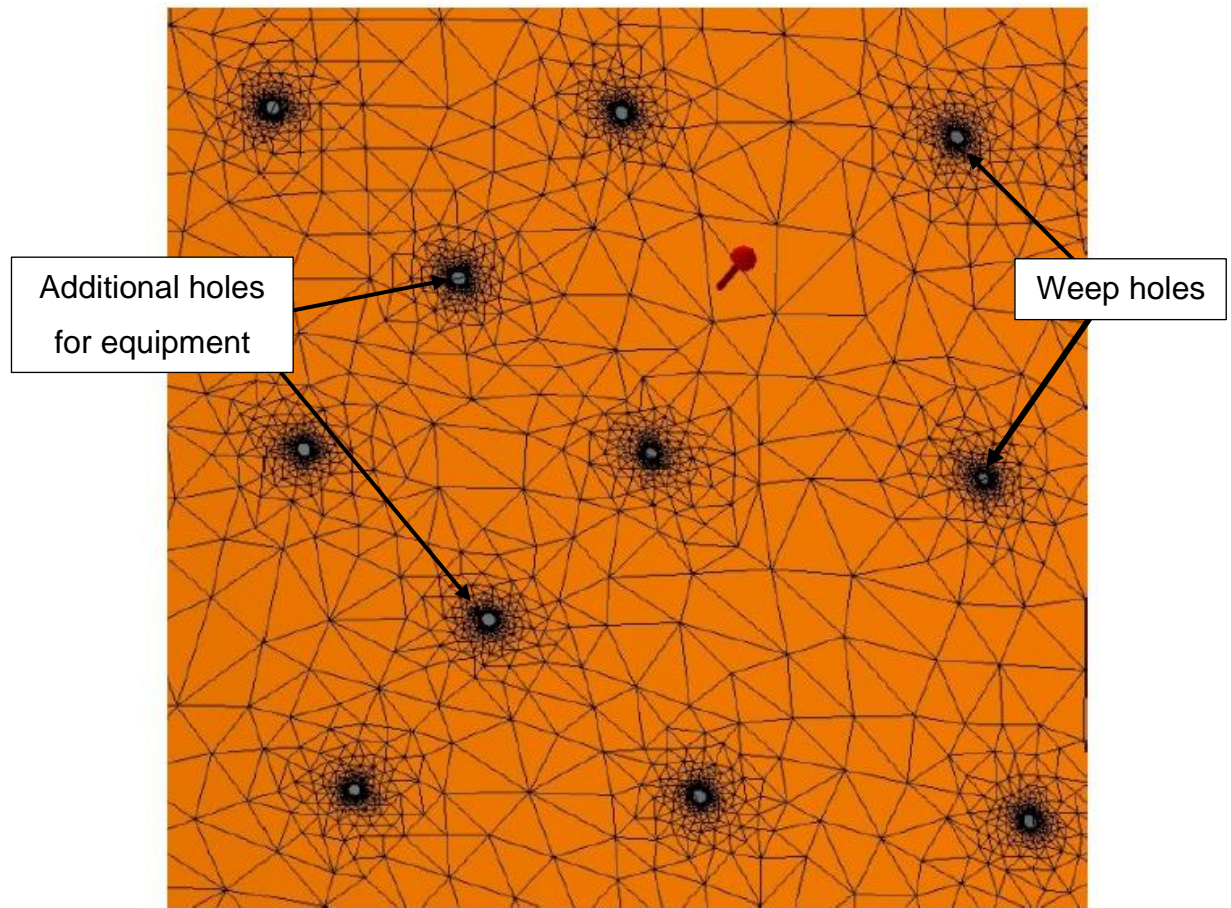
Figure 16: Mesh for FEA of teeming ladle, with increased density around holes.

3.4 Thermocouple trial #1

3.4.1 Installation method and housing design

The mechanical bay was used to gain correct access to the ladle to install the equipment and thermocouples, indicated in the plant layout in the Appendix 11.1. The first six holes were drilled and tapped (four of which were existing weep holes) for the datalogger equipment to be attached. A pre-made mount was required to attach the insulation box to the ladle. That also created an air gap between the box and the ladle shell, increasing the insulation of the datalogger from the shell temperatures. The mounting plate was also designed with a roof to protect the equipment from falling debris and was angled to deflect and reduce the chance of damage from any impacts. Figure 17 shows a CAD render of the mounting plate and an engineering drawing of this can be seen in the appendices.
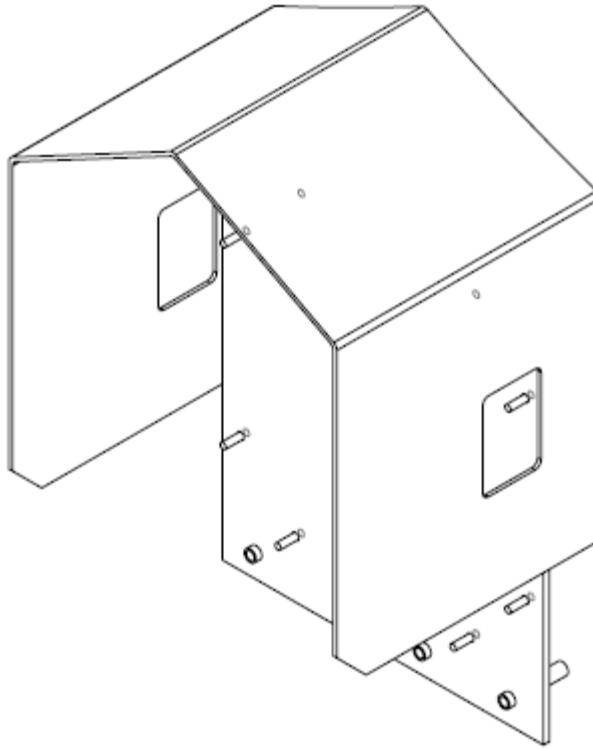
Figure 17: Mounting plate used to attach insulation box to ladle.

Threaded bars were then fixed into the holes and the mount's design allowed for tubes to pass over the threaded bars and were bolted in place. Two bolts were used to lock the mount to the ladle and reduce any chance of the bolts coming loose. Figure 18 shows the installed equipment on the ladle.
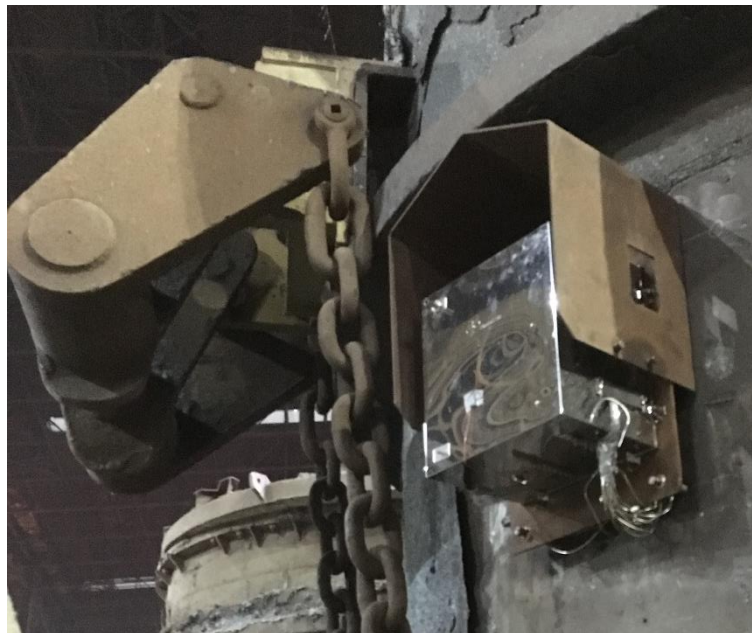
Figure 18: Insulation box and mount attached to ladle.

Once the equipment was attached the thermocouple holes were drilled ensuring they were separated by at least 10cm and were not within 10cm of any weep holes that were already on the shell (as recommended by the FEA). The thermocouples were then inserted into the ladle shell through the access holes. The thermocouples' labels were checked inside the ladle to ensure they had not been damaged whilst passing through the access holes. At this point the thermocouples were protected inside the shell for transport to the refractory installation area of the plant. During the refractory build it was important to track the locations of the thermocouples for future reference, to understand which thermocouple corresponded to the locations within the refractory build. It was also essential to track where the thermocouples' cables were, from the access holes in the shell to the measurement point. By doing so it was then possible to place the subsequent thermocouples without overlapping the cables, which would have then cause damage once the lining expanded and the ladle was filled with steel. Figure 19 shows a schematic of the thermocouples installed either side of the insulation (indicated by red lines).
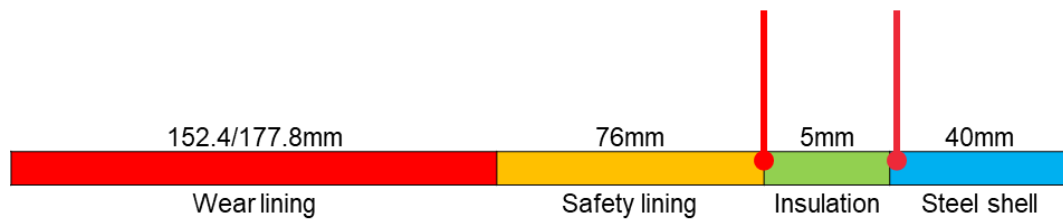
Figure 19: Refractory layers and thermocouple locations in ladle barrel, indicated either side of insulation.

Thermocouples were also installed in the bottom layers of the refractory between the safety lining and the precast bottom as shown in Figure 4. A schematic of the refractory layers in the bottom of the ladle and the location of where the thermocouples were installed can be seen in Figure 20. The thermocouples were placed in this location to provide information of the preheating cycle and the amount of time required for the ladle bottom to heat up for production. This was then used to verify if the online thermal tracking model, the Ladle Watcher, was tracking the same trend in temperature in this location. Ladle Watcher is a tool used by production to track the thermal profiles of the ladle fleet. It is a finite difference model that uses Equation 1 to calculate the increases and decreases of the refractory thermal profile. The weight changes and RFID tags on the cranes are used to understand the state of the ladle (full, empty with or without a lid and preheating on flare) based on the location of the crane in the BOS. Ladle Watcher then calculates and increase or decrease in temperature of

the hot face and a prediction of the effect on the refractory thermal profile in its current state and the next 8 hours. The production teams use this information to determine when a ladle has been preheated enough for production on the ladle flares and how long the ladle can be empty and still be used. As the thermal profiles are calculated without a physical temperature input, they are subject to errors. If an accurate hot face measurement could be achieved and used as a calibration point it would heavily reduce this error and is the subject of Chapter 5 and 6.
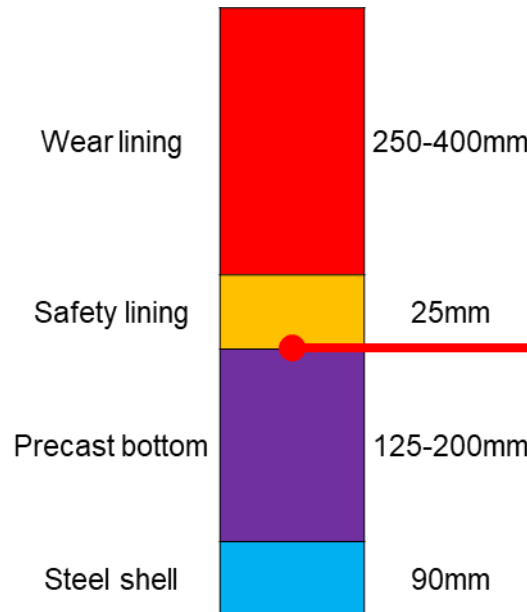
Figure 20:Refractory layers and thermocouple locations in ladle bottom, indicated between safety lining and precast bottom.

The thermocouples' locations and cables were tracked and held in place using duct tape and a marker pen. This provided a simple and effective way to prevent overlapping the thermocouples, which could cause damage and temporarily keep the thermocouple measuring points in the correct locations. Figure 21 shows an image during the thermocouple installation from inside the ladle. In Figure 21 it is possible to see the thermocouple cables have been drawn and tracked by the marker pen on the insulation pads. Once the safety lining was built to the height of the thermocouples they were then fixed in place and movement reduced as best possible during transport to the preheating stage. Once the lining had been heated to operation temperatures it was then assumed the thermocouples were fully locked in place. This assumption was justified by the known expansion of the wear lining and safety lining that locks the lining in place. When a ladle is first built it must be treated with care to prevent the bricks from loosening but once the ladle is at production temperatures it can then be

fully inverted without concern of the lining falling out. The forces required for this were significant and provided the contact forces necessary to give accurate readings and prevent large movements of the thermocouples from the installed location.
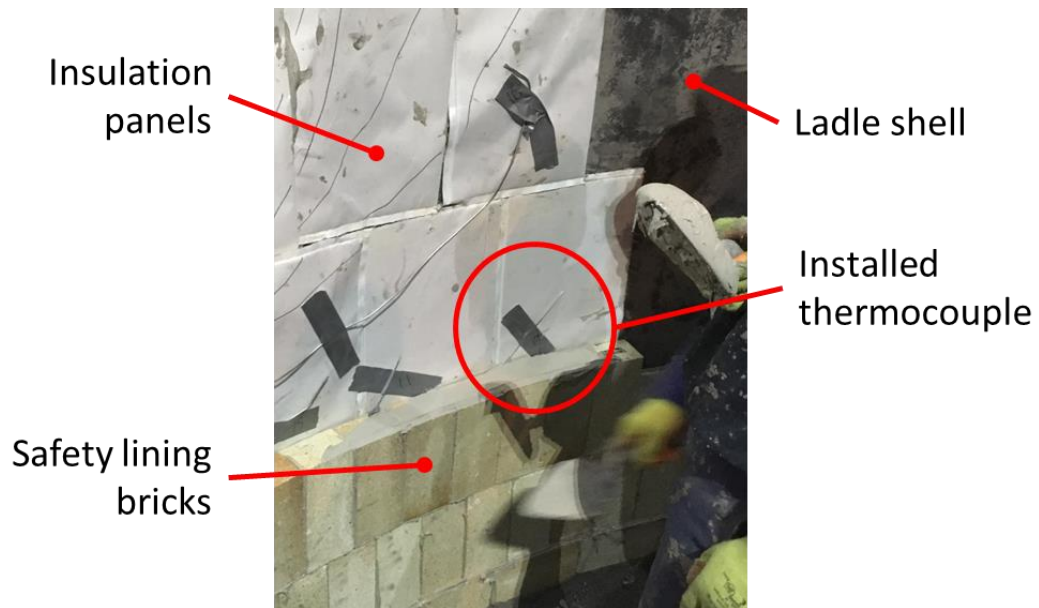
Figure 21: Thermocouple cables tracked with marker pen and held in place with duct tape until secured by safety lining.

3.4.2 Data analysis and findings

The thermocouple data was analysed and compared to the Ladle Watcher model in this section. The thermocouples were able to successfully record the initial heating of the lining on the preheaters and the first 15 cycles of production. At this point the ladle failed to open and the steel needed to be recycled into another ladle. This caused heat damage to the thermocouple wires that were not in the insulation box. This will be discussed in more detail in the following section. Ladle Watcher was used to support production and inform the ladle co-ordinator which ladles were hot enough for production. It is also used to determine how long a ladle can be left empty and still be hot enough for production or if it required reheating. Ladle Watcher influences production so it is important that it be accurate. Therefore, if there are any discrepancies between the thermocouple measurements and the Ladle Watcher outputs it is important to understand why these occurred.

3.4.2.1 Thermocouples in ladle bottom

The thermocouples in the bottom of the ladle highlighted an error in Ladle Watcher predictions. Ladle Watcher had received an error in the interpretation of the ladle location and plotted the ladle as being on a preheater when the refractory lining was

still being built on the RED car, shown in the plant layout in the appendices. This created a large discrepancy with the predicted temperatures from Ladle Watcher and the temperatures of the refractory recorded by the thermocouples in the same location. The temperatures predicted by Ladle Watcher and the recorded temperatures from the thermocouples can be seen in Figure 22. The difference peaked at 800°C and there was still a difference of 100°C in this location when the ladle was first used in production. This 100°C difference in the safety lining cold face may not transfer to the same temperature discrepancy from Ladle Watcher vs the real temperatures of the wear lining when preheated. However, the heat storage in the back layers of the lining is essential when the ladle is taken into production. This acts as heat storage for the wear lining and reduces the refractory cooling rate (31). This is also the case when the steel is tapped into the ladle, with insufficient heating of the layers behind the working lining. More heat is transferred from the steel which then has to be replaced by reheating, causing an increase in production costs and carbon footprint (31). In Chapter 5 this cooling effect is quantified.
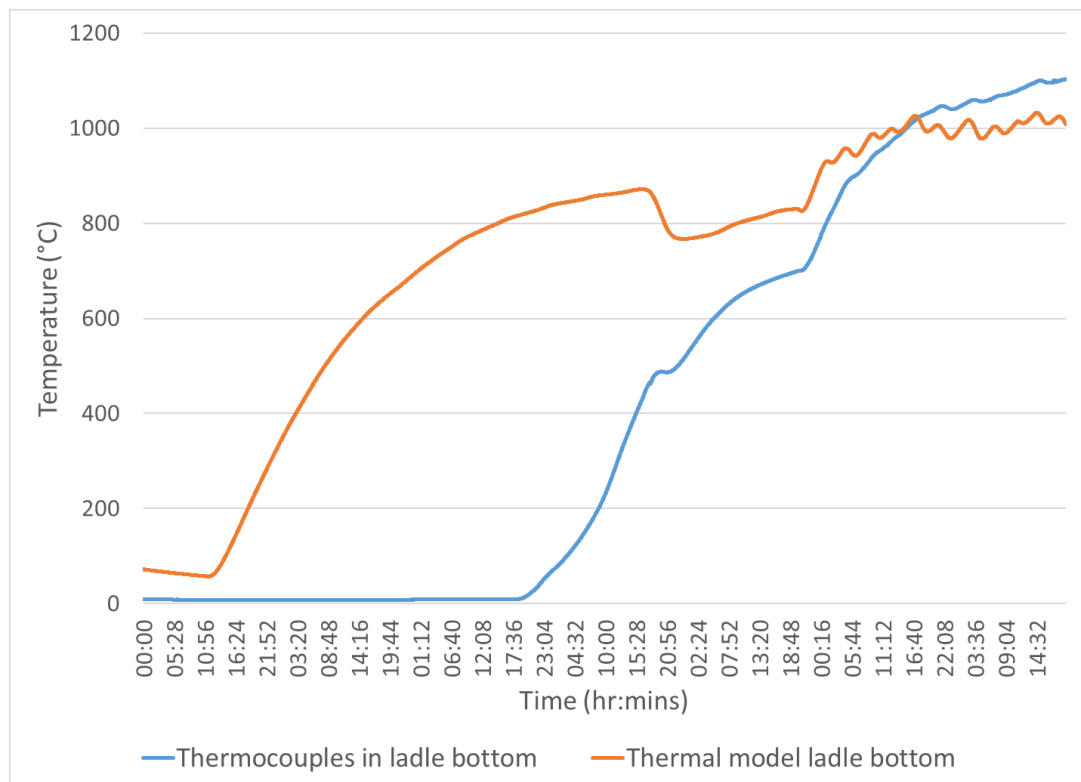
Figure 22: Ladle Watcher outputs and thermocouple measurements.

After five cycles of production the thermocouples showed there was an increase in temperature above the predicted temperatures from Ladle Watcher. The underprediction of the temperature could be attributed to the location and state error

43

produced from preheating. There was also an error in the cooling rate in ladle watcher due to the refractory removal at higher temperature before the thermocouples were installed. This meant Ladle Watcher started higher than the thermocouples, which were reading close to 0°C due to the tests being performed in winter. However, the overprediction indicated there was an error in the setup of the refractory lining in Ladle Watcher and was a one off error that is now resolved. The precast bottom is created with a slope to assist drainage of the ladle at the casters and reduce steel retention in the ladle. Ladle Watcher's setup only allows for a single measurement of the precast bottom. Because of this an average of the thickness is used in Ladle Watcher. The thermocouples were positioned on the opposite side to where the steel is drained from the ladle, thus they were above the thickest area of the precast bottom. Therefore, in this location the thermocouples would have been insulated more by the precast bottom than the Ladle Watcher predictions. This explains the higher temperature measured by the thermocouples during this period and why there is a discrepancy between Ladle Watcher and the thermocouple measurements. This is verified in Chapter 5.

It then follows that a decision was required as to which values should be used for Ladle Watcher. The refractories at the thickest point would be more beneficial to model for the preheating stage. However, they would also cool at a slower rate than the thinner sections. If the Ladle Watcher modelled the thickest section of the precast bottom the ladle bottom could be colder than the model predicts. This discrepancy was modelled, and the details of the outcome can be found in Chapter 5. The findings showed that the refractories in the bottom of the ladle are insulated by the heat contained in the ladle. This meant that there were minor cooling effects of the refractories on the steel, which explains the lack of focus for this. However, the temperature profile across the bottom can be seen to be significant and this will have a thermal shocking effect on the refractories. This scenario also highlights the challenges of oversimplifying a model for such a large vessel and the variations in thickness of the refractories caused discrepancies of up to 100°C when comparing the modelled average to the measured thickest point.

3.4.2.2 Thermocouples installed in ladle barrel

Figure 23 shows the output data of two thermocouples that were positioned on the hot and cold face of the ladle. The vertical lines on Figure 23 denote a change in the ladle state from being full or empty. The numbers on the x-axis denote the time in that state

i.e. the first number on the x-axis "1:26" denotes the ladle was empty for 1 hour and 26 minutes then the next number "2:00" shows the ladle was full for 2 hours. It is interesting to note that during the time the ladle was empty the thermocouple temperatures were increasing rather than decreasing. This was shown to be accurate and demonstrated similar findings from the studies produced by Van Beurden et al. (2015) and Buhr et al. (2016) (31,65). The temperatures increased due to the thermal storage of the wear lining and safety lining discussed in the studies. Van Beurden et al. attributed the shell temperature delay with state to a thermal wave passing though the refractory lining to the ladle shell (65). The crossing of the hot and cold face in Figure 23 are due to the thermal wave passing through the refractories and verified this theory. This also highlighted the potential safety concern for teeming ladles. It is common practise to measure the cold face of the ladle with a thermal imaging camera to determine if the insulation has degraded, to verify accuracy of thermal models and check if the shell is being overheated (2,29,31,37,42). Temperature increases can be seen up to 10°C depending on the time after the ladle was empty and the temperature was measured. Even though this was relatively small it would still be enough to take a ladle from a safe temperature of 380°C to 390°C which would have required attention from production.
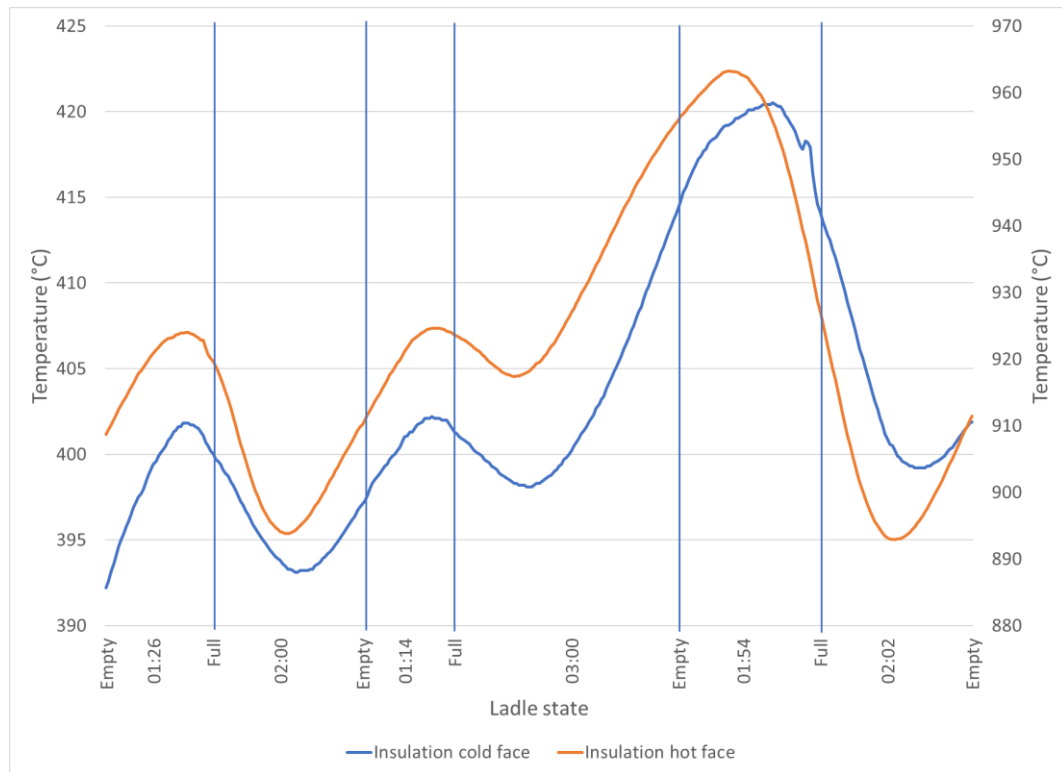
Figure 23: Thermocouple data from insulation hot and cold face plotted on same graph but on different vertical axes (cold face left hot face right) to show heat wave delay flowing through ladle lining.

Figure 24 shows the measurements from the thermocouples installed on the barrel. It shows the outputs from Ladle Watcher and the thermocouple measurements from three cycles of production. There was a strong correlation between the thermocouples and Ladle Watcher outputs, with the largest difference of 20°C equating to a difference of 2.2% of the measured and modelled value. For a predicted model over a period of 12 hours this was highly accurate. With such a small discrepancy more value can be found in investigating other areas of the modelling process.
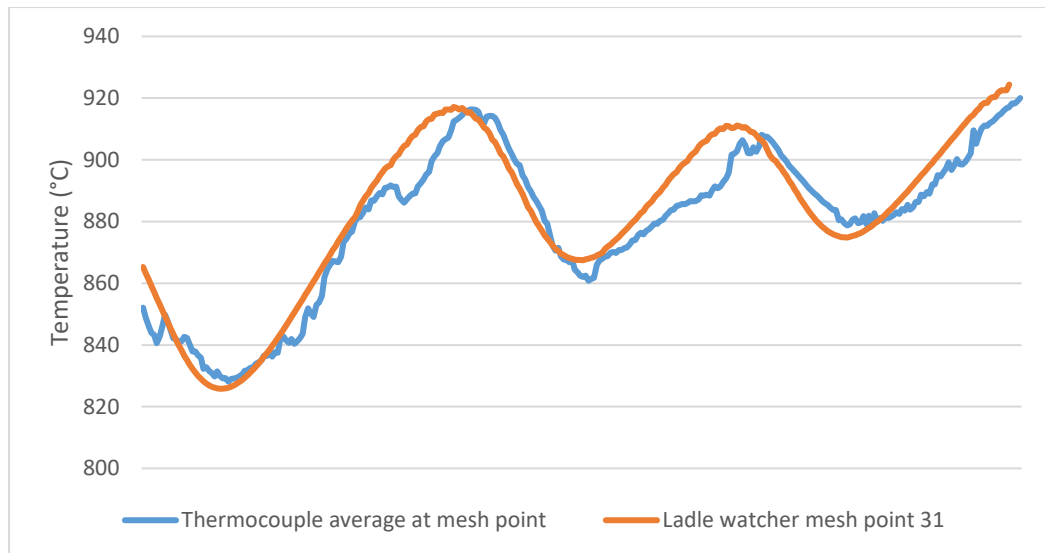
Figure 25 shows the recorded data from the thermocouples installed on the insulation hot face. It can be observed that the temperature recorded by five thermocouples regularly peaked at and above 900°C and that one of the thermocouples peaked above 1000°C on three occasions, with the highest temperature recorded of 1036°C. This information is important for thermally characterising the insulation samples recovered from the ladle at the end of the wear lining campaign. Using differential scanning calorimetry (DSC) it was possible to verify the temperatures recorded in Figure 25. More information on the DSC measurements can be found in Chapter 4.
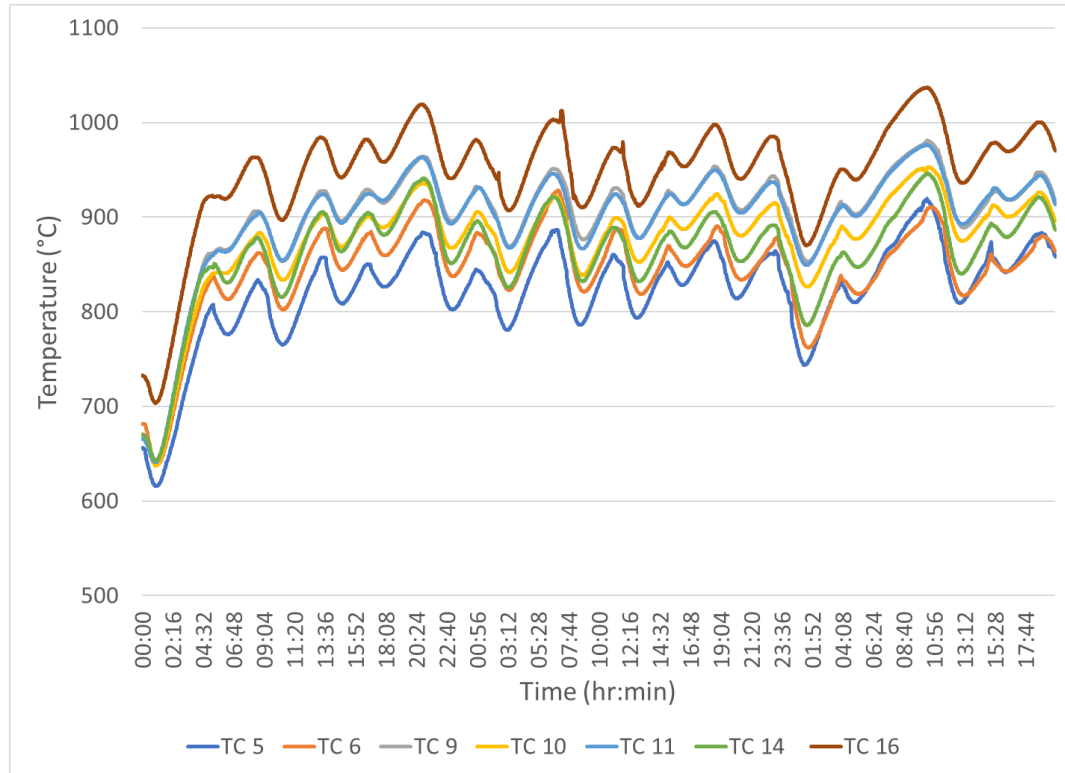
Figure 25: Thermocouple output of insulation hot face during steel production.

For ease of layout for the legend in Figure 25 the thermocouple numbers have been used, details of the reference numbers can be found in Table 3.

Thermocouple number	Area of ladle	Layer of refractory	Height from ladle bottom (mm)	Around barrel from lifting gear (mm)	Location on microtherm	Max temperature recorded (°C)
5	Barrel	SL-Microtherm	600	1900	Centre	919.2
6	Barrel	SL-Microtherm	700	1600	Edge	928.1
9	Barrel	SL-Microtherm	600	0	Centre	980.8
10	Barrel	SL-Microtherm	600	500	Edge	953
11	Barrel	SL-Microtherm	600	300	Edge	976.4
14	Barrel	SL-Microtherm	1000	1600	Centre	946.5
16	Barrel	SL-Microtherm	1100	0	Centre	1036.9

Table 3: Thermocouple locations for relation to Figure 25.

It was not possible to accurately compare the shell temperatures from the thermocouples to Ladle Watcher because there was a time step issue at the time of recording the thermocouple data. This caused Ladle Watcher to be unstable in this location and created large fluctuations in temperatures between outputs. This can be seen in Figure 26. There were moments of stability in Ladle Watcher where it was possible to see it was overpredicting the temperatures in comparison to the thermocouple measurements. It was found that Ladle Watcher was using figures for the insulation that had been increased to fit the temperatures measured during the verification stage. This would then suggest that there was an overprediction in the insulation degradation and there was less of an effect on the insulation from production

48

than when previously tested. These figures will be compared to the measured values in Chapter 4 and the differences will be determined in Chapter 5.

The Green insulation material observed during installation appeared to have very low mechanical properties. From discussions with BOS plant personnel there was an understanding that there was a reduction in cross sectional thickness of the insulation layer. This is also shown in Buhr's (1998) study (37). The insulation was installed in the ladle with a thickness of 6mm but once the ladle was in production the thickness was unknown. Thus, it was essential to recover some of the insulation material after it had been in a ladle during production. This was achieved, the degradation was measured and more detail of this can be found in Chapter 4.
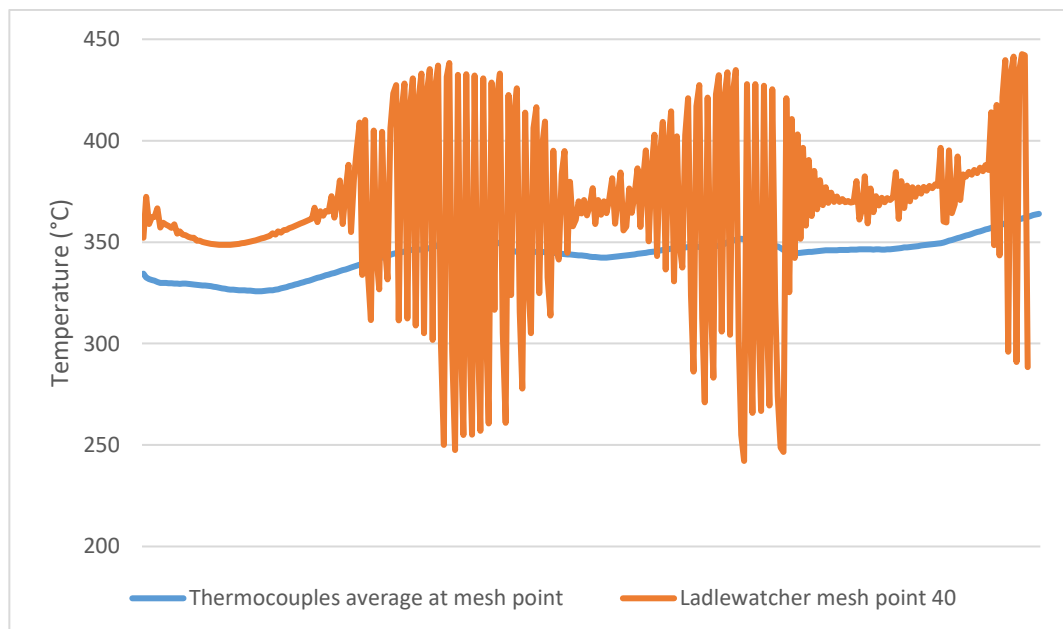
Figure 26: Ladle Watcher instability and thermocouple measurements.

3.4.3 Mode of experimental failure

For ease of access to the datalogger PTFE tails were used on the thermocouples that were unprotected by the insulation box. The flexibility of the PTFE tails allowed the removal and replacement of the datalogger for collection of the thermocouple data. However, the melting point of the PTFE was exceeded when the ladle failed to open at the CC plant, so the steel could not be teemed out of the ladle. Therefore, the steel needed to be recycled into another ladle. When steel was poured from the trial ladle the temperatures outside of the insulation box exceeded the melting temperature of the PTFE. This then removed the PTFE insulation, which prevents the thermocouple wires from short circuiting before the hot junction. This caused the thermocouples to

measure the ambient temperature outside of the ladle and they could no longer be used to gather data. Because the thermocouples failed in this manner it was important to learn from this and adapt the equipment so that the thermocouples would last longer on the second trial. Although the thermocouples failed from overheating the PTFE, it demonstrated that the insulation box was able to protect the datalogger and cables inside, even with these increased temperatures. This was confirmed when the datalogger was interrogated, and the internal temperature peaked at 93.4°C. It can be seen from Figure 27 that there was a clear line on the PTFE cables where the section of the cables that were inside the box were free from damage. Because of this it was determined the insert and thermocouple junctions needed to be adapted.

Figure 27: Thermocouple PTFE cables with heat damage and clear melt line where cables inside insulation box were protected.

3.4.4 Conclusions from first thermocouple trial

The findings from the first thermocouple trial indicate that the ladle shell temperatures exceed the offline modelled predications of 350°C. They also exceed the temperatures measured via a thermal imaging camera that is used as a safety system with measured values around 300°C. To validate these findings it was necessary to carry out a second thermocouple trial. The implications of the ladle shell being subjected to temperatures above 400°C present concerns to the deformation of the ladle shell and the thermal efficiency of the refractory lining. Thermocouples show the ladle shell should be measured between 30 and 60 minutes after the ladle is empty. However, further investigation into the thermal imaging camera suggested that the cleanliness of the

camera lens and the emissivity value had a greater impact than the time. A brief investigation into the emissivity value of the ladle shell suggested that a value of around 0.7 rather than 1 should be used to correlate with the thermocouple findings. However, further investigation into an accurate emissivity value of ladle shells is recommended for future work.

The measurements of the hot face of the insulation showed the material was subjected to temperatures that peak at 1036°C. To confirm this accuracy thermophysical lab testing was performed on the recovered thermally characterised post-mortem insulation. The findings from this can be found in Chapter 4 of this thesis.

There were differences in temperature recorded by the thermocouples in the bottom of the ladle and Ladle Watcher during preheating and in production. It was concluded that the overestimate of the temperatures recorded by Ladle Watcher were due to a tracking error of the state of the ladle. The temperatures recorded in the bottom exceeded the service temperature of the thermocouples. It was deemed necessary to use Pt-Rh thermocouples for the next trial as these can measure temperatures up to 1500°C. The overpredictions of the ladle after it had been in production for more than five cycles were attributed to the difference in thickness of the precast bottom insulating the thermocouples, compared to the average used in Ladle Watcher. This highlighted the challenges caused by modelling based on an average of a lining thickness and the importance of accuracy of the data being fed to a thermal model. It also highlighted the importance of recovering a sample of the insulation lining to show why the online Ladle Watcher was over predicting the temperatures of the ladle shell.

3.5 Thermocouple trial #2

3.5.1 Redesign of insulation box insert

To protect the thermocouples from the potential damage of another recycle event the insert that insulates the cavity opening needed to be redesigned. The original insert was made from refractory insulation wrapped in steel that reduced the cavity opening to a 5mm thin slot, just thick enough for the PTFE wires to exit. This was the weakest point of the insulation box for protecting the datalogger from the shell temperatures and thus the slot was kept to a minimum to reduce heat transfer. The original design of the insert can be seen in Figure 28.

Figure 28: Original insert designed with slot for PTFE cables to exit cavity.

The decision was made to have the sheathed thermocouple cables enter the cavity to ensure they were sufficiently protected by the box. Figure 29 shows the adapted insert design, which provided the space for twenty thermocouples with 3mm diameters to enter the box cavity.
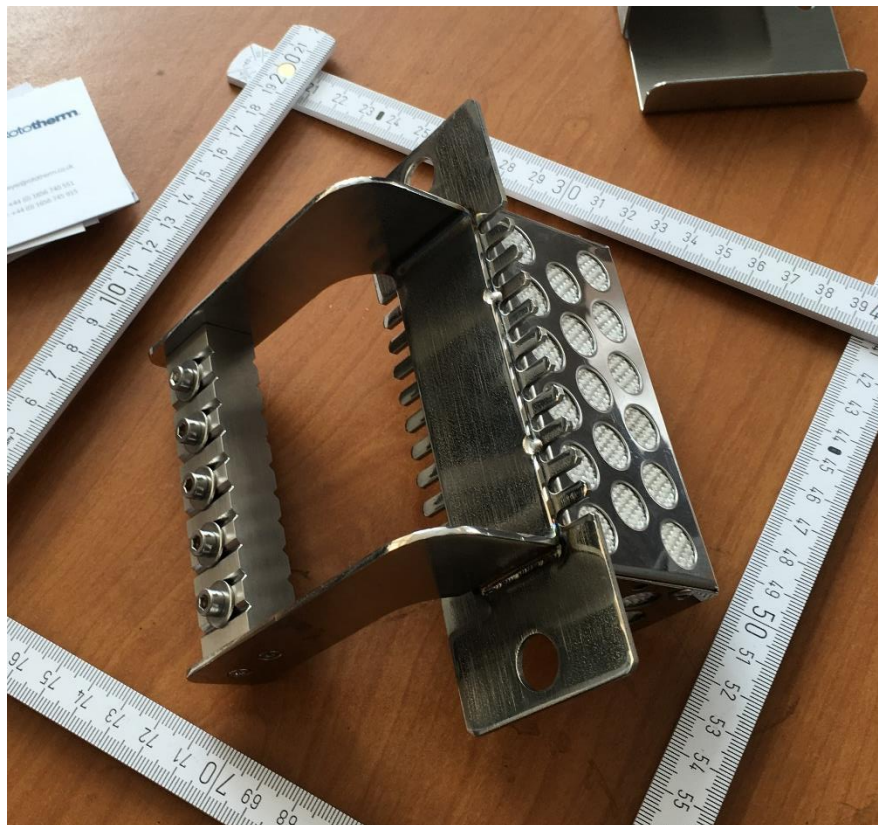
Figure 29: Adapted insert design with locking screws and increased gap for thermocouple cables.

3.5.2 Changes to ladle standard build for verification from thermocouples

The first thermocouple trial measured high temperatures for the ladle shell that were above the simulated values and values recorded in the plant safety systems. To validate these numbers a second trial was performed to determine if these values were repeated. From the first thermocouple trial it was also observed that the ladle bottom required more time in the preheaters to be thermally saturated for production than the barrel. By using simulations it was possible to show that by adding a layer of insulation to the bottom of the ladle it was possible to heat the refractories quicker. The location was decided to be between the safety lining and the precast bottom. This would provide the largest benefit from the insulation panels and the largest drop in temperature. The location of the insulation panel in relation to the other refractory layers can be seen in Figure 30. Also shown in Figure 30 is the location of the thermocouples, which were placed either side of the insulation layer.
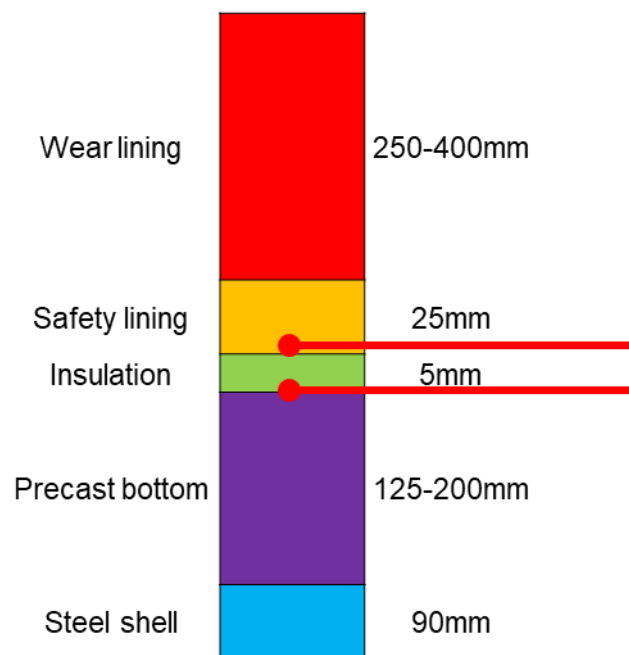
Figure 30: Refractory build of ladle bottom including insulation panel.

The verification of the benefits to the lining can be seen in Figure 31, which shows the thermal storage of the bottom of the ladle with and without the insulation layer, after 2.5 hours of cooling. The lining with the insulation layer had a higher thermal storage, shown by the temperatures across the lining. The theory was that the extra storage of heat reduced the amount of temperature pulled from the steel when the ladle was tapped into. This would then reduce the amount of reheating required to meet the casting temperatures. Because reheating has been shown to be around 50% of the cost

53

of refractory linings during steel production it had the potential for a large financial benefit to Tata Steel (31). It was later found that the ladle bottom had limited effect on the steel temperature losses. More detail on this can be found in Chapter 5. This justification was therefore no longer valid but the insulation would still reduce the thermal shocking by retaining the thermal storage. The theory was that with this added thermal storage there was a reduction in the wear rate of the bottom refractories.
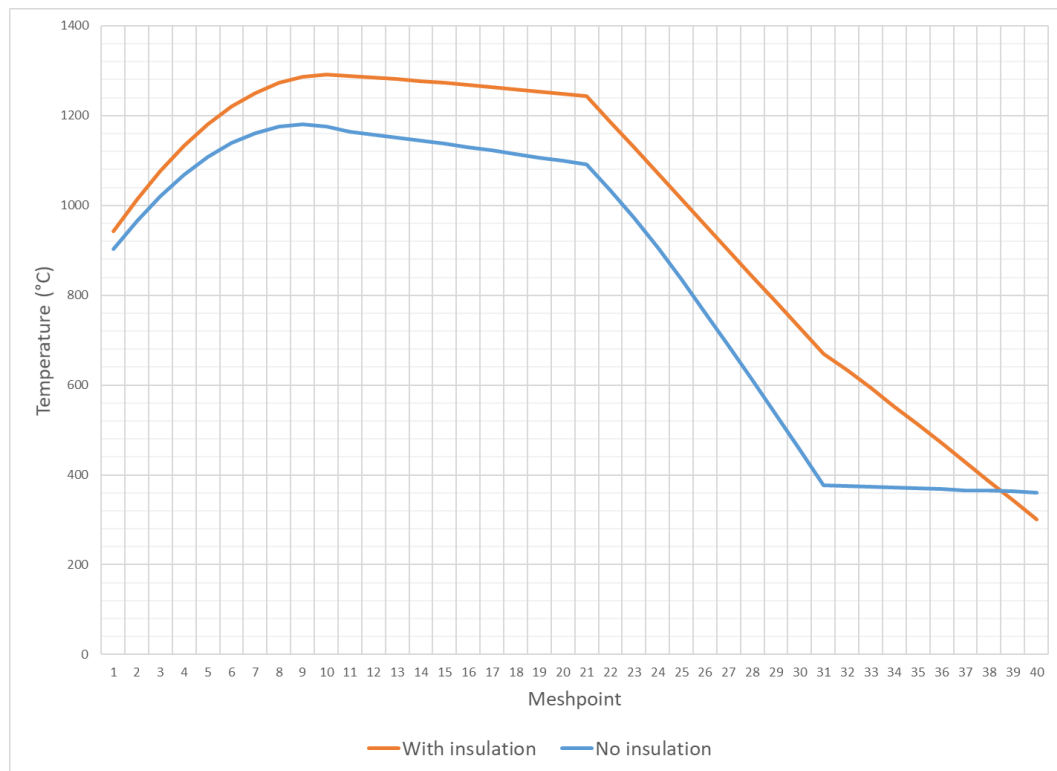
Figure 31: Ladle Watcher outputs of ladle bottom refractories with and without insulation layer, the Meshpoint refers to the thermal model outputs at the different layers of the refractory.

3.5.3 Data analysis and findings

3.5.3.1 Thermocouples installed in ladle barrel

The thermocouple measurements for trial #2 were kept in the ladle for a full wear lining campaign before the datalogger was subjected to excessive heat, which caused it to produce measurement errors. This was caused by a delay in the ability to access the equipment on the ladle due to production demands. At this point the trial was ended and future trials will need to ensure the water in the insulation box is filled more frequently. The thermocouples installed between the shell and insulation for this trial appeared to become damaged after ten days of data and nineteen cycles measured. This caused them to measure temperatures more than was logical and at this point the data was no longer accurate for analysis. During the initial nineteen cycles the shell

54

temperatures measured were consistently at or above 400°C with one thermocouple measuring temperatures up to 500°C. The hot face temperatures of the insulation did not exceed 950°C. This data, therefore, was able to confirm the measured temperatures of trial #1 and the insulation was deemed to be accurately thermally characterised to aid the post-mortem analysis of the insulation samples. The full data sets can be found in the appendices.

Due to the errors caused after the first ten days of data gathered the comparison of the thermocouple measurements to the outputs are of the first thirteen heats. The thermocouple data in Figure 32 was intended to be compared to the Ladle Watcher mesh point for the initial preheating of the lining. However, there was an error in the archiving of the Ladle Watcher data and this section of the data was missing. From the data that was available the thermocouples recorded temperatures lower than Ladle Watcher during the late stages of preheating and initial thirteen cycles of production. There were points during the preheating stage when two of the thermocouples and the Ladle Watcher correlated within a few degrees. It is interesting to note that the deviations in the thermocouple data and Ladle Watcher correlate uniformly. This indicated that a simple offset may need to be adjusted within the model to increase its accuracy. The deviations in area A coincide with the times when the ladle was removed from the preheater and then returned. This suggested the model was unable to correctly predict the temperature increase of a ladle that is partially heated when returned to the preheater. The flare programs cause a ramping of the temperature for the first period of the preheating programme. This caused the refractories to be cooled rather than heated for the initial state change in the model. From then on Ladle Watcher was tracking with the assumption that the temperature constantly increased since the ladle was on flare. However, the temperature had been reduced in the refractory from the preheater programme ramping. Therefore, it was not able to correlate with the predicted model temperatures before it was then taken into production. This highlighted the importance of fully understanding the process the ladle was subjected to when creating an online model. Adjustments are required to the preheater programmes to reduce this cooling effect and the model to better correlate its outputs with the temperatures of the refractories.
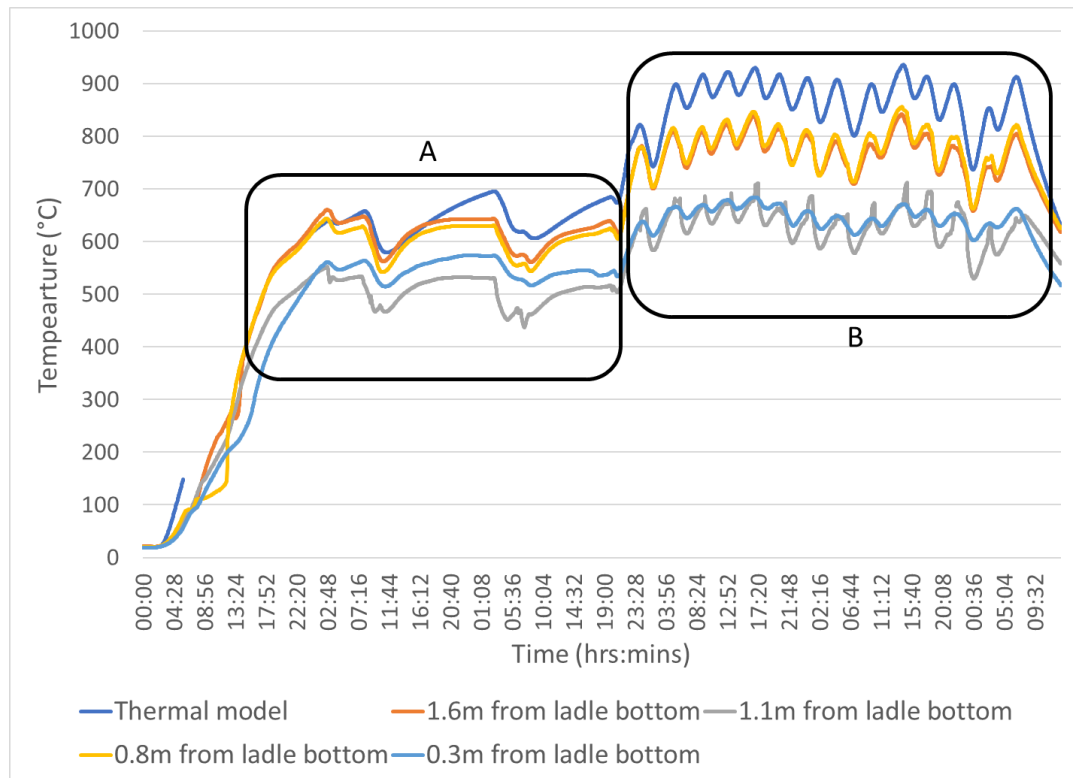
Figure 32: Comparison of Ladle Watcher data and thermocouple data, numbers in legend denote meters from the bottom of the ladle the thermocouples were positioned.

3.5.3.2 Thermocouples installed in ladle bottom

The installed insulation layer in the bottom of the ladle extended the drying time because it insulated the precast bottom, which has a water mixed castable refractory to secure in place. This meant the heat was unable to penetrate the insulation and heat the castable and this extended the drying process. A standard drying process takes around 24 hours before the ladle is ready for production. With the insulation layer the production team did not have the confidence to use the ladle until it had been on the preheaters for more than 60 hours. This extended period of preheating before the ladle had gone into production would have decarburised the ladle refractories and caused the premature failure of the ladle. Despite a management of change process, the effect of the insulation on drying time was not anticipated or identified until the preheating delays occurred. This then showed that it would not be beneficial to include an insulation layer in this location. However, after further analysis of the lining with the offline Ladle Watcher model. It was possible to change the location of the insulation layer below the precast bottom. It would still provide a benefit and would not insulate the heat from the castable and prevent drying from the preheater. It is likely that having the insulation below the preheaters would improve the drying process because the temperature in the castable would increase during drying as less heat was lost through

56

the shell. The output from the offline Ladle Watcher model can be seen in Figure 33. The Ladle Watcher parameters were set to be the same scenario with the insulation previously in Figure 31. The lining was fully saturated and met steady state scenarios and then simulated to cool the lining if the ladle was empty for 2.5 hours. However, the process benefits were found to be negligible in Chapter 5.
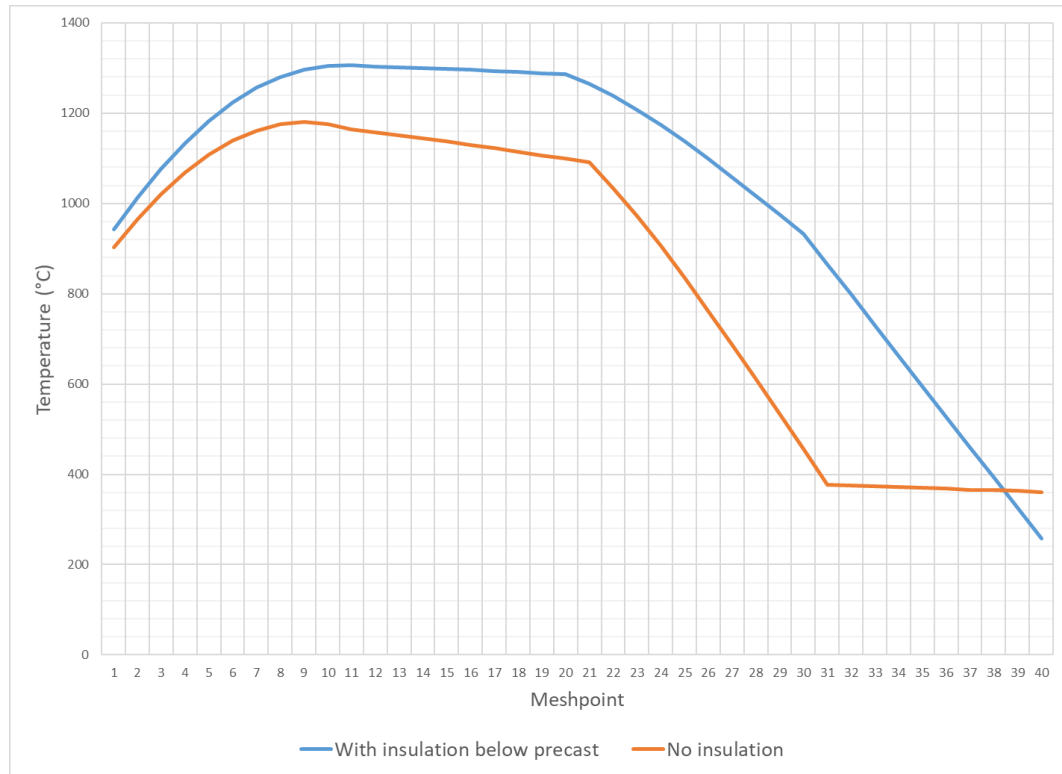
Figure 33: Output from offline Ladle Watcher model with insulation modelled below precast bottom.

The thermocouples in the bottom of the ladle failed during the preheating stage. Because of this it was not possible to conclude whether the thermal storage of the wear lining found was correct. It was concluded that the thermocouples failed due to mechanical issues. The lack of mechanical strength of the Pt-Rh thermocouples was determined to be the main cause and future trials would need to have a more robust sheath material to protect from the mechanical damage. It was not possible to determine from the temperatures measured the location of the thermocouple junction points and which layer of refractory is being measured. There were very small differences measured between the thermocouples installed on the hot and cold faces of the insulation. From the measurements recorded in the barrel for both thermocouple trials this also provided evidence of failure. The thermocouples continued to measure temperatures which suggested a new hot junction point had been formed. However, it was unclear where the thermocouples were measuring these temperatures in the

refractory build. Therefore, little conclusions can be made by the thermocouples installed in the bottom refractories and the data in Figure 34.
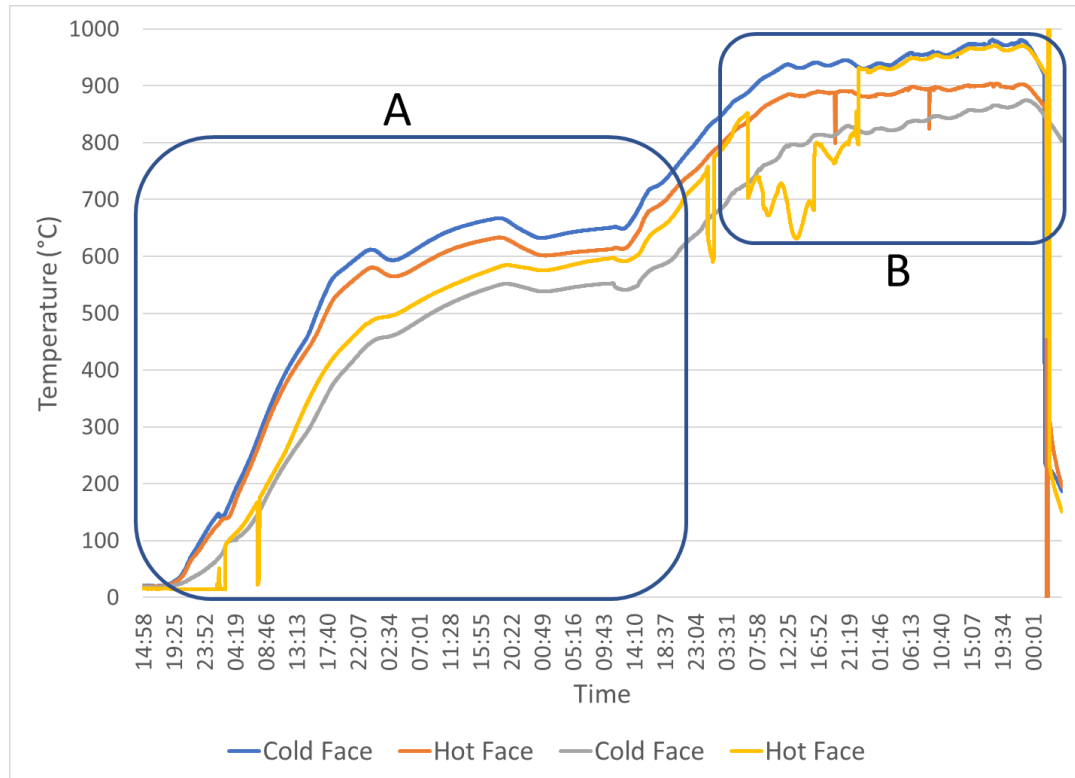
Figure 34: Thermocouples installed in bottom of ladle to determine if insulation layer provides benefit to thermal storage. Area A shows the duration of the ladle preheating process and area B shows the ladle during the first ten cycles of the steel plant.

3.5.4 Conclusions from second thermocouple trial

The second thermocouple trial was required to validate the findings of the trial #1. This was due to the large discrepancies found between the thermocouples and safety systems and offline model simulations of the ladle shell. This was achieved as the shell temperatures were consistently measured to be above 400°C, with one of the thermocouples measuring temperatures above 500°C. Due to the variations between the safety systems and measured temperatures a brief emissivity study was performed but it is recommended that this is confirmed with future work. The second trial measured the hot face temperatures of the insulation to be less than 1000°C. The differences in the post-mortem samples collected from these trials is compared in Chapter 4. The Pt-Rh thermocouples installed in the bottom of the ladle measured very similar temperatures even though they were installed in different layers of the refractory. No conclusions could be made from these measurements on the benefit of the insulation layer. It was found that the insulation needed to be installed below any layers that contained water. This would stop the heat being insulated from these areas

58

and allow for sufficient drying. It was concluded that the thermocouples were damaged, most likely due to mechanical forces. Therefore, future thermocouple trials are recommended to have robust sheath materials to protect the Pt-Rh sensors for higher temperature readings.

3.6 Conclusions

The two thermocouple trials performed in this chapter measured the temperature of the insulation material, ladle shell and refractory in the bottom of the ladle. From these trials the maximum temperatures recorded in each of the areas measured are presented in Table 4. These values were used to perform thermophysical tests on the Green and post-mortem insulation samples, which are detailed in Chapter 4.

Location of thermocouple	Maximum temperature recorded (°C)
Ladle bottom - Safety lining/Precast bottom interface	1233
Ladle barrel - Safety lining/Microtherm interface	1040
Ladle barrel - Microtherm/shell interface	519

Table 4: Maximum temperatures recorded in the different measured locations from thermocouple trials.

Peak temperatures recorded at the insulation hot face in thermocouple trial #1 were higher than in trial #2. Post-mortem material was recovered from both trials and analysed in Chapter 4. Samples recovered from the ladle have been closely thermally characterised and can now be tested with a good understanding of what they have been subjected to. The next chapter of this thesis will discuss the findings from the thermophysical characterisation of the post-mortem insulation.

It was noted if the accuracy of thermal imaging could be improved it would be less intrusive than thermocouple trials and could be used to monitor all ladles in a BOS plant. An improved approach to thermal imaging the teeming ladle refractory hot face is applied in Chapter 5. This could then be utilised as a calibration point for an online model tracking the in-situ ladle fleet.

From the findings in this chapter it was possible to disprove H1 because the ladle insulation was thermally characterised via thermocouples and post-mortem samples

were recovered from the teeming ladles. The next chapter will discuss the findings of the thermophysical testing of the thermally characterised post-mortem samples of microporous insulation.

Chapter 4 – Analysis of post-mortem insulation for quantification of the degradation in insulative properties

4.1 Introduction

Q1 of the literature review asked whether an insulation sample could be recovered from a teeming ladle after production. Q2 questioned whether the recovered sample would show a change in thermophysical properties. This chapter will look to disprove the hypothesis (H2a): the in-situ properties of microporous insulation do not change or degrade in performance.

The ladle insulation material was thermally characterised in the previous chapter and samples were recovered from the ladle that then went through thermophysical testing. The results of the thermophysical tests are presented in this chapter. Using the temperatures recorded in the ladle it was possible to determine if any phase changes occurred in the material whilst in production. The samples retrieved from the ladle also provided good evidence of the reduction in thickness that occurs in the material whilst in the ladle. Agreement can be found between multiple studies that the insulation layer has the largest effect on retaining the temperature of the steel in a teeming ladle (2,3,42). Gupta (2004) quantified that 55-60% of the heat lost from the ladle is lost through the side wall without the presence of an insulation layer (3). Rahm et al. (2014) were able to quantify through thermal models that the heat lost through the top of the ladle could be reduced by at least 50% by using an appropriate slag covering on the ladle when it was full (66). When the ladle is empty, however, the top of the ladle becomes the highest form of heat loss. Rahm et al.'s study was able to quantity that if a 67-tonne ladle is lidded when empty it would reduce the cooling effect on the steel by approximately 31°C. There is a good understanding of heat losses through the top of the ladle and the benefit of using insulation if the ladle is modelled with the supplier's information. The question was clear from the literature – what is the benefit of the insulation when it has been thermally cycled and compressed? The motivation to measure the properties of the post-mortem insulation should therefore be high and well researched. However, the author was able to find very little literature available and only one study on microporous insulation, the most common used insulation for teeming ladles (35,37). It was concluded that lack of literature on this

subject is due to the challenges of physically recovering insulation from a teeming ladle in a BOS plant; the collaboration and coordination of multiple departments to recover the insulation during a relining; and the lack of desire for manufacturers to prove (or otherwise) the degradation of their own materials. Therefore, the need to quantify any degradation in a microporous insulation layer and determine the effect this has on the temperature losses in the steel was still required.

Mazzetti-Succi's (2013) study looks at the compression of insulation boards, which are currently considered the most compression resistant form of insulation, and found a reduction of thickness from 10mm (original thickness) to 3-5mm (35). Unfortunately, Mazzetti-Succi's (2013) study does not include thermophysical testing of the recovered material. Because of this, the assumptions present in Glaser's (2011) study that degradation of insulation materials has a significant effect on the steel temperatures, was neither confirmed nor disproved (24). Buhr (1998) produced a study on microporous insulation and noted a reduction in thickness and a degradation in the thermophysical properties which was attributed to carbon impregnation of the insulation material (37). This is a very relevant and informative study but the refractories used in teeming ladles have changed considerably since 1998. The desire to protect the shell from temperature has meant a reduction in the carbon content of the linings and new chemistries of refractory are used with different levels of expansion (31). With these studies considered there was still the need to recover a full panel of the microporous insulation from a teeming ladle after production. The insulation panels are installed with a fibreglass bag to allow the compressed fused silica fragile board to be installed. Due to the fragility of the panels careful attention is required during installation. Because of this, when speaking to industry professionals there was the assumption that the fused silica material drops to the bottom of the fibreglass bag due to the movement of the ladle and the harsh production environment. When the insulation panels were recovered from the ladle it was observed that there was consistent coverage of insulation material across the panel and this common myth in the industry was disproved. This reduced some of the uncertainty surrounding microporous insulation in-situ.

Buhr et al. (1998) concluded that there was an increase in carbon of the post-mortem sample collected for their study (37). This theory was tested, and the opposite was found. The carbon content was found to be less in the post-mortem samples when

compared to the Green sample. The challenge was then to find the thermophysical changes of the insulation material. Thermal models require key parameters to determine the thermal performance of a material. These include the density, specific heat capacity and thermal conductivity. From this the thermal diffusivity, the rate at which heat transfers through a material, can be calculated using Equation 1. When the thermal diffusivity is then calculated the thermal model considers Fourier's law of thermal contact conductance using Equation 2. With these two parameters known thermal models have the two key metrics required to plot the thermal profile of the refractory linings (31). As previously mentioned in Chapter 2 both the thermal diffusivity and thermal contact conductance are dependent on knowing the thermal conductivity of the materials. There is a large amount of uncertainty regarding microporous thermal conductivity in-situ. This was the justification for creating an experimental procedure that would be used to determine the thermal conductivity of the post-mortem insulation material and provide this information.

By using the laser flash method, it was possible to find the thermal diffusivity. Using the thermal diffusivity relationship in Equation 1 it was then essential to calculate the thermal conductivity and density of the post-mortem insulation. To calculate the thermal conductivity, it was then essential to determine the specific heat capacity. This was measured via differential scanning calorimetry. The density was measured via several methods without success. The tap density method was then utilised to give the best estimate of the material density change.

From the data gathered it was possible to conduct a comparative study of the Green and post-mortem sample data. This was then cross referenced to the supplier's data and, using the factors of difference for the measured post-mortem values, the supplier's data was converted to post-mortem values.

4.2 Sample preparation and recovery

The insulation material is installed in a fibreglass bag which is not able to withstand the harsh process of removing and replacing the refractory lining in the ladle. Therefore, to recover a post-mortem sample of the insulation material it was necessary to protect the material from mechanical damage during this process. However, it was also essential that the material was not insulated from any heat it would otherwise be subjected to and not increase its compressive strength. The solution developed was to

protect the insulation with 1mm thick steel. This would provide the mechanical strength needed whilst limiting the compression resistance. As steel is highly conductive and the gauge used was very thin, it would transfer nearly all the heat to the sample contained in the steel protection. When modelling the ladle shell, which is 40mm thick, the temperature drop observed is consistently <10°C. This is with a gradient of 400°C on the hot face and environmental temperatures on the outside. This was justification enough to suggest the steel protection would absorb <1°C. The steel protection was designed to be folded around the insulation panel as this increased the likelihood of a representative sample due to a seamless protective envelope. This also removed any requirements to weld the steel, which would risk heat treating the insulation and cause errors when testing the materials. Figure 35 shows the fabricated steel envelopes, which were marked with an arrow prior to fabrication. This insured the installed orientation of the sample could be confirmed when it was recovered from the ladle. By knowing the orientation it was then possible to see if there was a difference in thickness between the top of the sample and the bottom. This also disproved the industry assumption that there is no material at the top of the panels.

Figure 35: Fabricated steel envelope around insulation panel.

Thermocouples were installed in the same ladle as the protected insulation panels. This made it possible to track the temperatures the insulation was subjected to and verify the changes caused by the temperature through lab testing. The protected panels were placed at three different heights in the ladle – one sample in the slag-line, one two

thirds up the barrel and one a third up the barrel. The samples were installed using the same method as the standard panels. The only differences were that the panels needed to have an overlap to ensure the integrity of the insulation was not compromised, as the steel envelopes were slightly larger than the insulation panels. To avoid confusion after installation, the ring number was recorded. By knowing the height of each brick it was possible to calculate the height of the sample in the ladle. Figure 36 shows a sample of the protected insulation installed in the ladle.

Figure 36: Sample installed in ladle with number of rings recorded to calculate height of sample in ladle.

The samples were recovered after the lining had been removed from the ladle with the samples from the slag-line being removed after 155 and 126 cycles of production. Unfortunately, the samples in the barrel of the ladle were not able to be recovered, even with the added protection. The material was too far into the ladle and it was not safe for a member of the team to recover the samples before the refractory was tipped out. With the large amount of refractory that was loose at this point the tipping process either damaged the sample to the point where analysis was not possible or it simply was not possible to find the sample. Therefore, future work is needed to develop a method that can recover a sample from the barrel of the ladle. Figure 37 shows the

ladle lining removed from the barrel and the harsh process the samples would need to withstand if a method cannot be developed to recover the sample prior to this process.

Figure 37: Insulation samples damaged or lost within the refractory bricks in the ladle.

Once the refractory bricks had been dislodged from the ladle it was safe to enter the ladle to recover the steel envelopes from the loose bricks.
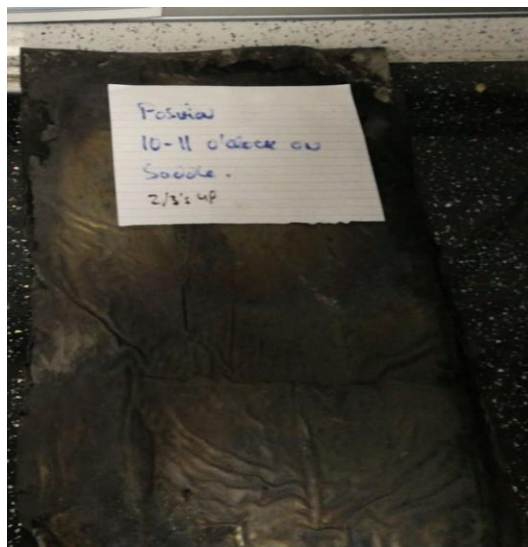
Figure 38: Recovered steel envelope from barrel which no longer had a sample of the insulation material contained.

When the sample was removed from the ladle it became apparent the insulation material had been lost during the recovery process. The steel envelope had been damaged at the edges and the insulation had then fallen out during the removal of the refractory from the ladle.

The successfully recovered samples still protected by the steel needed to be removed from the steel envelope. This required carefully opening the envelope with tin snips and using pliers to pry the steel apart. This was achieved and access to the insulation sample inside was possible with minor damage to the sample. The panel then needed to be broken into manageable sized pieces for testing, ensuring the least damaged areas of the panel were sampled. Figure 39 shows the steel envelope opened to gain access to the insulation sample under a vacuum hood to remove any particulate that became airborne.

Figure 39: Steel envelope opened to reveal ladle insulation sample inside.

Figure 40 illustrates the sampling approach, taking care to select the samples from different areas of the panel. The thickness of each sample was then measured five times across five different angles and averaged to give a general thickness of the sample. The samples were then individually stored ahead of further analysis in sealed containers with the average thickness and sample position noted.

Figure 40: Insulation sample broken into manageable pieces and the thickness measured.

Table 5 shows the samples produced from the first post-mortem insulation panel, recovered from the ladle after 155 cycles in the slag-line. The differences in thicknesses observed in this sample show the variance in forces applied by the edge of the brick compared to the centre of the brick during the expansion of the wear and safety linings. This was obvious from the imprint of the brick on the steel envelope. Samples were only taken from the area that did not have the folded steel or panel overlap. Again, this was easy to determine as a clear sign of clay and extra compression produced a line on the envelope. To ensure the samples were not affected by this samples were not taken within 30mm of this compression line. This is indicated by the box drawn on Figure 41.

Figure 41: Recovered protected insulation panel with sample area marked to ensure samples were not taken from overlapped area.

The first sample recovered did not have an arrow imprinted on the steel protection, so it was not possible to retrospectively deduce the orientation in the ladle. The addition of an arrow on the second sample recovery was a learning from this process.

Sample	Location of panel	Location in brick	Average thickness (mm)	Standard deviation (mm)	Reduction in thickness (%)
PM155A	Edge	Centre	2.9	0.10	41.8%
PM155B	Centre	Centre	4.6	0.03	8.0%
PM155C	Edge	Edge	3.8	0.06	23.3%
PM155D	Edge	Centre	4.0	0.23	19.5%
PM155E	Edge	Centre	2.5	0.23	49.9%
PM155F	Centre	Edge	2.3	0.08	54.4%

Table 5: Samples recovered from insulation panel installed in the slag-line for 155 cycles and recorded average thicknesses and the change in thickness as a percentage.

Table 6 shows the sample thicknesses of the insulation panel from different locations on the panel. Contrary to the generally held assumption that all the material sinks to the bottom of the casing the data clearly shows there is material across the whole of the panel. This sample was in production for 126 cycles.

69

Sample	Location from panel	Location in brick	Average thickness (mm)	Standard deviation (mm)	Reduction in thickness (%)
PM126A	Bottom left	Edge	3.0	0.14	40.7%
PM126B	Top right	Middle	2.8	0.21	44.3%
PM126C	Upper Middle Left	Middle	3.5	0.21	30.8%
PM126D	Upper Middle Right	Middle	3.4	0.14	32.0%
PM126E	Top Left	Edge	2.8	0.38	43.1%
PM126F	Lower Middle right	Middle	3.4	0.09	32.8%

Table 6: Samples produced by slag-line panel after 126 cycles and recorded average thicknesses and the change in thickness as a percentage.

A range of the panel samples were also pulverised and homogenised to create powdered samples. This was performed on both of the recovered panels that produced the samples in Table 5 and Table 6. This was performed because it was necessary to produce powdered samples for several of the thermophysical tests discussed in the following sections.

4.3 Post-mortem thermophysical testing

4.3.1 Carbon testing

It was first essential to confirm or disprove Buhr et al.'s (1998) theory that the degradation of the insulation properties in microporous insulation is due to the impregnation of carbon (37). This was achieved by using a carbon/sulphur analyser that combusts the materials in a purified oxygen stream. The carbon and sulphur are oxidised and two non-dispersive infrared (NDIR) cells then detect the SO_2 and CO_2 produced by the sample. The test method can detect the carbon to within ±0.04% and the sulphur to within 0.001% in the ranges measured.

Sample	Carbon (%)	Sulphur (%)
Green	0.19	0.006
Post-mortem (155 lives)	0.16	0.026
Post-mortem (126 lives)	0.08	0.005

Table 7: Carbon and sulphur percentages from Green and post-mortem insulation.

The Green sample was found to have the highest content of carbon when compared to the post-mortem samples. There is an increase in sulphur but the overall effect on the performance of the insulation is negligible. The temperatures the microporous material is subjected to range from 300°C – 1000°C when in production. Literature shows that

sulphur has a thermal conductivity of 0.01303W/m.K in solid form (67). The supplier states the microporous material tested has a thermal conductivity of 0.039W/m.K, therefore the presence of sulphur has a negligible effect on the insulation properties and can't definitively state that it causes a degradation (68). This contradicts Buhr et al.'s (1998) study and shows the change in refractories between 1998 and the time of writing has influenced carbon impregnation of the microporous insulation (37). Consequently, the requirement to determine the degradation effects from the post-mortem insulation is still required (37).

4.3.2 Phase change analysis

4.3.2.1 X-Ray Diffraction

With the carbon theory disproved it was noted from the thermocouple measurements that the rated service temperature of the microporous insulation is reached and exceeded. The material is pyrogenic fused silica based and it is understood in the literature that this material will undergo phase changes at 900°C (69). Therefore, to understand if the post-mortem insulation had evidence to suggest these phase changes had occurred in the material when in production X-Ray Diffraction (XRD) was conducted on the Green and post-mortem material to find the crystalline structures. Figure 42 shows the data produced by the XRD and the analysis performed to produce Table 8. XRD was performed on a control sample of the Green insulation to determine the crystalline structures of the Green material. This data acted as a base line for the post-mortem samples to determine how much the insulation material had crystallised. The insulation recovered from the slag-line after 155 cycles (PM155) was used to compare to the Green sample and the results can be seen in Table 8. The various parts of the PM155 sample were measured using the XRD to determine if there were increases in the crystalline structure. Due to the highly insulative properties of the material it can be assumed with confidence that there is a large temperature gradient between the hot and cold face. Therefore, both the hot and cold faces were measured to determine the extent of this effect and a homogenised powdered sample was measured to give an average.
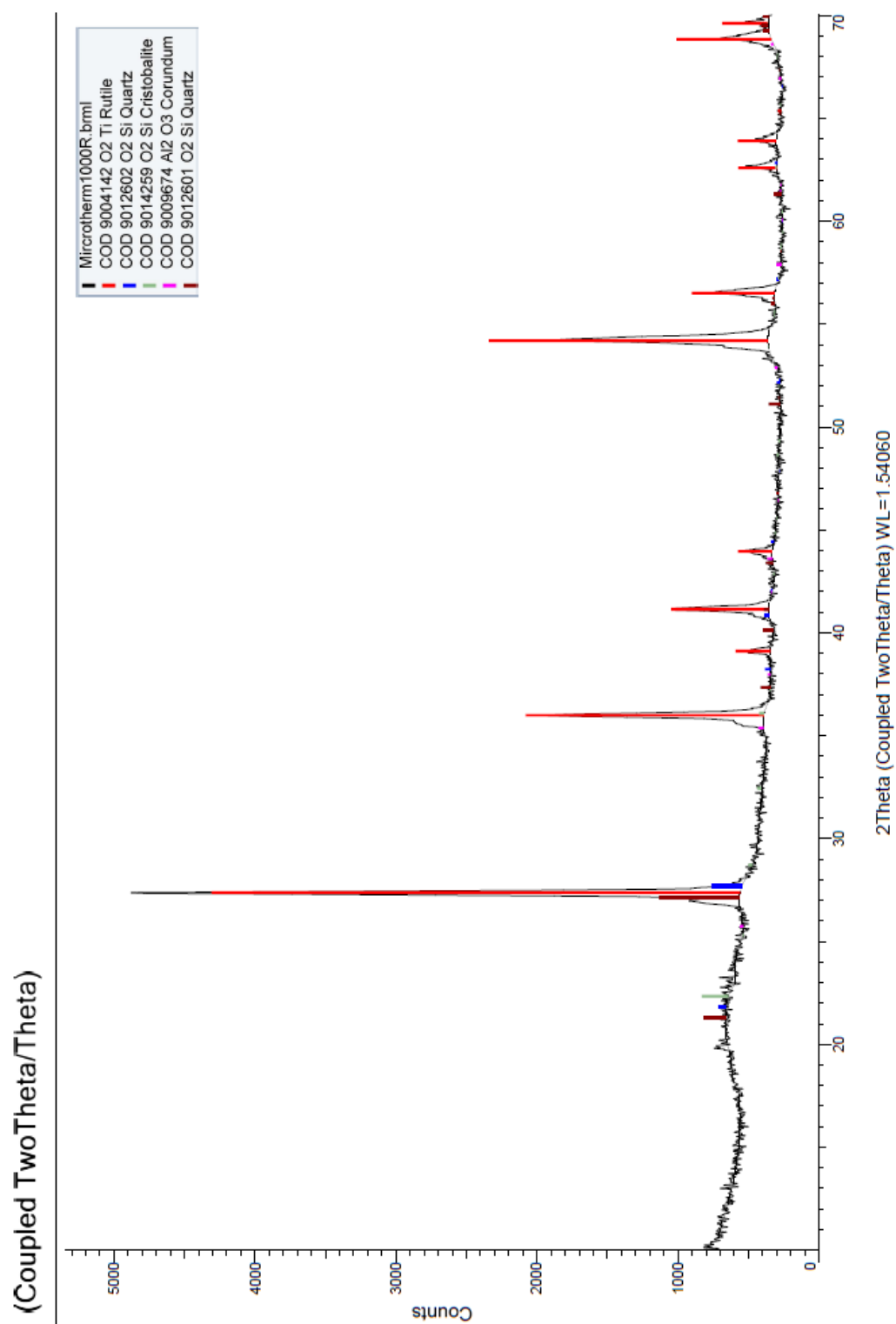
Figure 42: XRD data and analysis for crystalline material present in insulation samples

Microtherm 1000R HY	Corundum	**Quartz**	Rutile	**Cristobalite**
Green	3.1%	**4.9%**	86.8%	**1.9%**
PM155 homogenised powder	1.5%	**4.0%**	91.6%	**3.0%**
PM155 cold face	1.0%	**3.9%**	80.8%	**2.2%**
PM155 hot face	0.4%	**4.5%**	84.2%	**16.8%**

Table 8: XRD results of microporous insulation.

The results in Table 8 prove the hypothesis that the fused silica material is progressively crystallising during the production process. The crystalline forms of silica, highlighted in bold in Table 8, are the indicators of the phase changes from the fused silica. This is most apparent in the hot face sample, which is to be expected as this is subjected to the full heat and any sublayers are then insulated from this. The increase in the Cristobalite phase from 1.9% to 16.8% demonstrates this. The total crystalline silica increases from 6.8% to 21.3% of the total crystalline constitutes of the microporous insulation. The testing method now looked to determine the temperatures the phase changes occurred in the microporous insulation and cross reference this to the thermocouple measurements in Chapter 3.

4.3.2.2 Differential Scanning Calorimetry

4.3.2.2.1 Determining phase change temperatures

Differential Scanning Calorimetry (DSC) was utilised to determine the phase change points of the XRD results on the homogenised samples of Green and PM155. They showed little difference in the XRD analysis with only an extra 0.2% total crystalline silica between the PM155 and Green sample. The DSC will measure the heat flux of the two materials to determine when phase changes occur. The hypothesis being that the two materials have very similar crystalline phases. Therefore, they will undergo similar phase changes at similar temperatures. This is because, other than the hot face, the majority of the PM155 has been insulated and kept below its service temperature.

4.3.2.2.1.1 Initial tests

Homogenised powdered samples of the Green and PM155 insulation were heated in an argon rich atmosphere to 1000°C. They were held in an isothermal state for 2 hours before increasing the atmospheric temperature to 1200°C. Again, the samples were held in an isothermal state for 2 hours before returning to room temperature. These temperatures were selected because the peak temperature measured by thermocouples

in Chapter 3 was 1040°C on the hot face of the insulation. The service temperature of the microporous insulation is 1000°C. If it was seen that phase changes were occurring at 1000°C then it can be concluded that they will occur at an increased rate at 1040°C. Literature states that fused silica devitrifies at 1100°C into a transitional phase of cristobalite but the stable form of cristobalite is not possible until the fused silica reaches 1450°C (70). The 1200°C value was used as this is 200°C above the maximum service temperature of the material and the maximum temperature the equipment could achieve. The 1200°C heating was used for this test to accelerate the devitrification of the fused silica and determine the phase changes. From the XRD analysis the chemistry of the microporous insulation is mostly a combination of alumina, titania and silica. A ternary diagram of these three chemistries is shown in Figure 43, Figure 44 and Figure 45 show the phase diagram for pure silica and titania. There is no phase diagram for pure alumina as pure alumina has no phase transformations. It can be seen from the XRD analysis that most of the crystalline phase material in the microporous insulation is titania. This is because the fused silica, which makes up the majority of the material, does not show up on XRD analysis due to its amorphous nature but this information is provided by the manufacturer (68). Therefore, the areas of the phase diagrams of highest interest are the areas with high silica and high titania. The homogenised powders were created to provide a wide range of samples and there was a mixture of chemical concentrations still contained in these powders. The pure silica and pure titania show phase changes occurring around 600°C at atmospheric pressure. It is understood that fused silica devitrifies at 1100°C and no transformation is present below 867°C (70). For the concentrations of alumina and silica there may be some phase changes occurring between 1000°C and 1200°C as shown in Figure 43. Figure 43 shows that for the purity of silica no phase changes occur below 1540°C with its interactions with titania. Figure 43 shows there may be some initial phase changes starting to occur as the transition to α-Al_2O_3 and rutile occurs at around 1100°C. However, the XRD was able to show the titania is already in the form of rutile, therefore, these phase changes will not occur at this temperature. These transitions and phase changes are considered during the analysis of the DSC results.
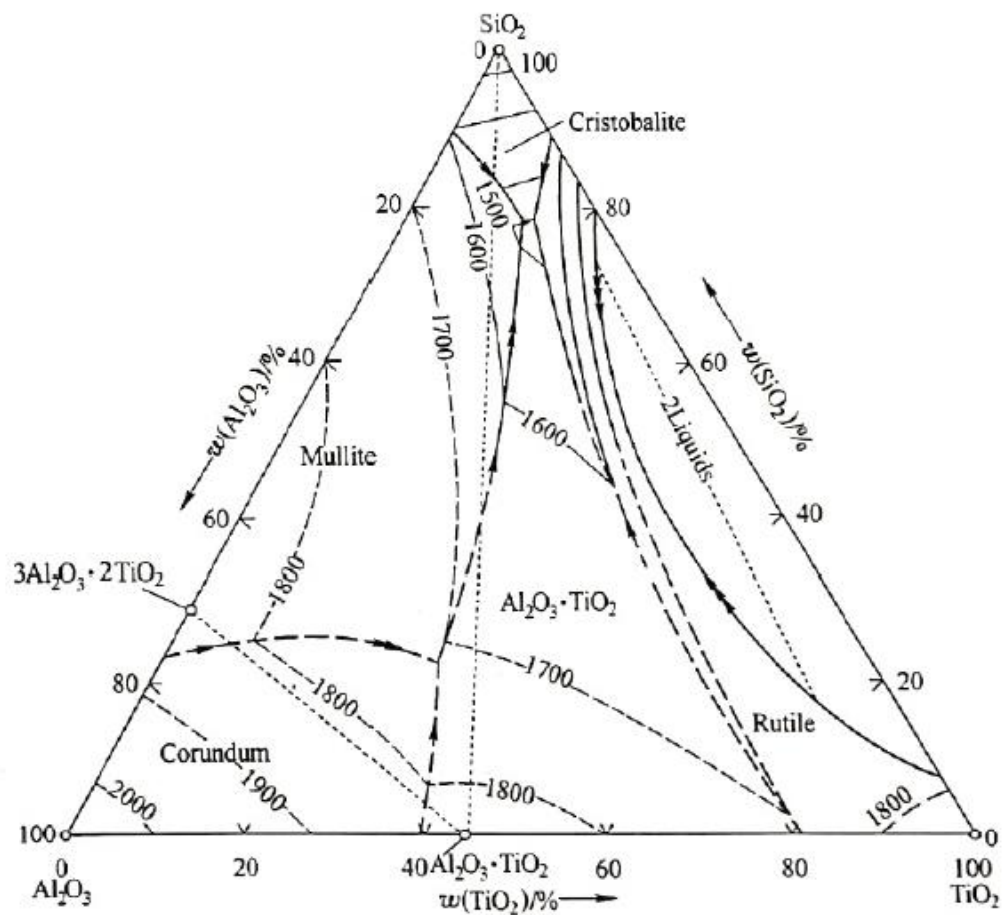
Figure 43: Ternary diagram of SiO2 - TiO2 - Al2O3 phases taken from (71).
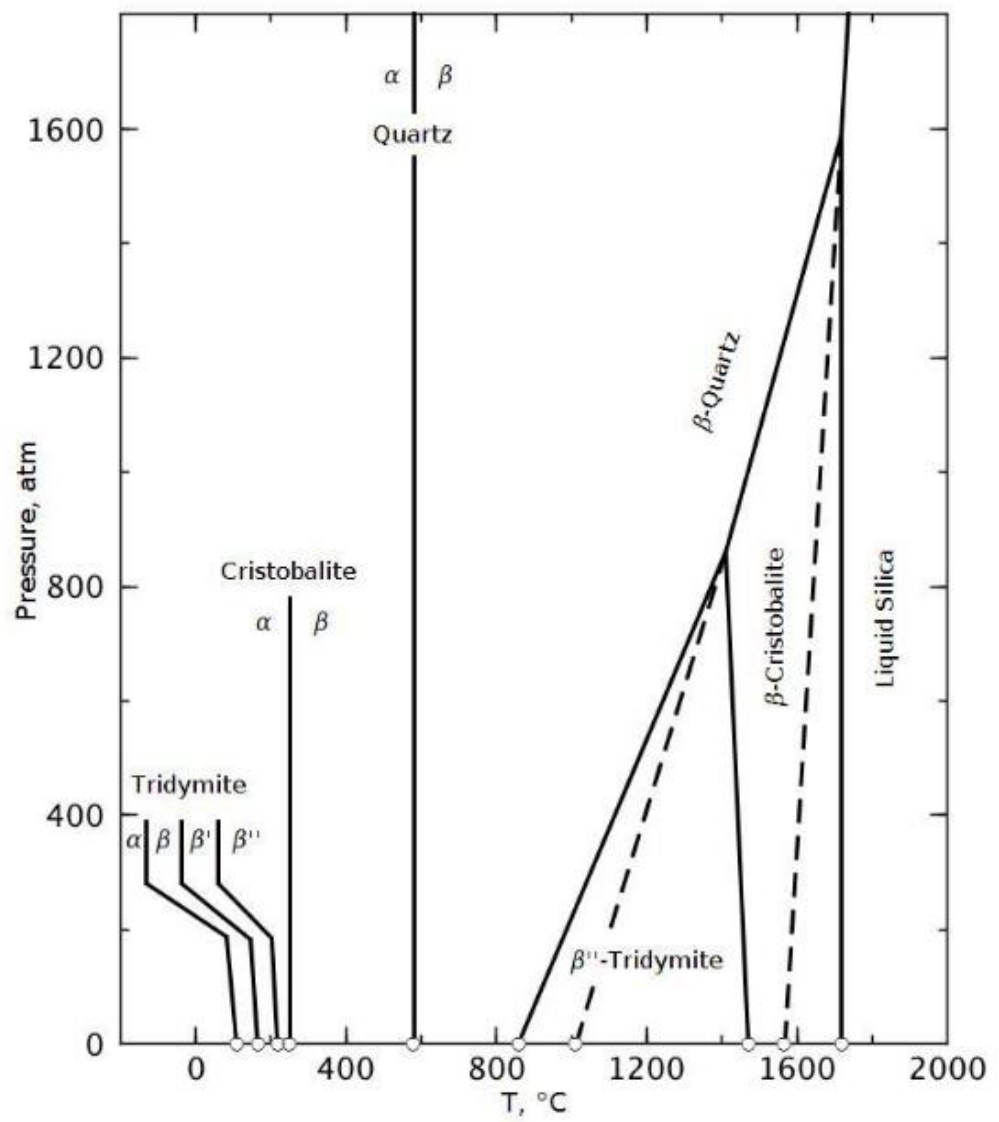
Figure 44: Silica phase diagram taken from (75).
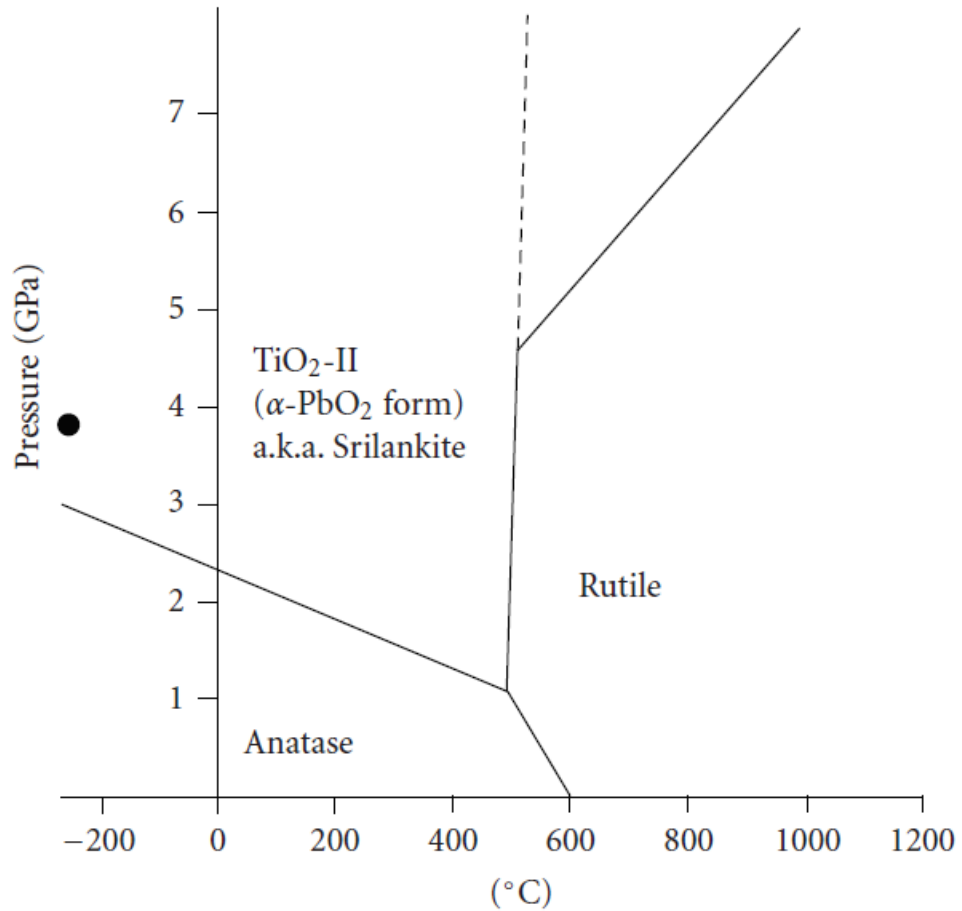
Figure 45: Titania phase diagram taken from (76).

Figure 46 is the output from the initial test which applied the heating method for one cycle. It can be observed that the Green material with the green line undergoes a much larger phase change compared to blue line of the PM155 material. This is indicated by the different gradients of the DSC plots seen in the transitional heating up to 1000°C. These changes are attributed to the titania phase change from anatase to rutile, as shown in Figure 45, and the α-quartz into β-quartz and then HP-tridymite, as seen in Figure 44. The isothermal stage at 1000°C shows a steady phase change occurred. this is attributed to the devitrification of the fused silica initiating. During the 1200°C isothermal stage a very large change in gradient is observed for the Green sample. Here it can clearly be seen the devitrification of the fused silica to cristobalite phases. This starts as the sample is heated from 1000°C to 1200°C and is expected due to the 1100°C devitrification temperature taken from the literature (70). It can be observed from Figure 46 that whilst the Green sample was going through these phase changes far less phase changes were occurring in the PM155 sample. This can be explained as the phase changes have already occurred in this sample. The data suggests the sample

had been heated to at least 1100°C and potentially 1450°C due to the lack of transitional phases of cristobalite behaviour. To determine if the cristobalite had reached its stable phase in the Green sample cyclic testing was required. Therefore, it was deemed necessary to run further tests using the same thermal pattern with a larger number of cycles.
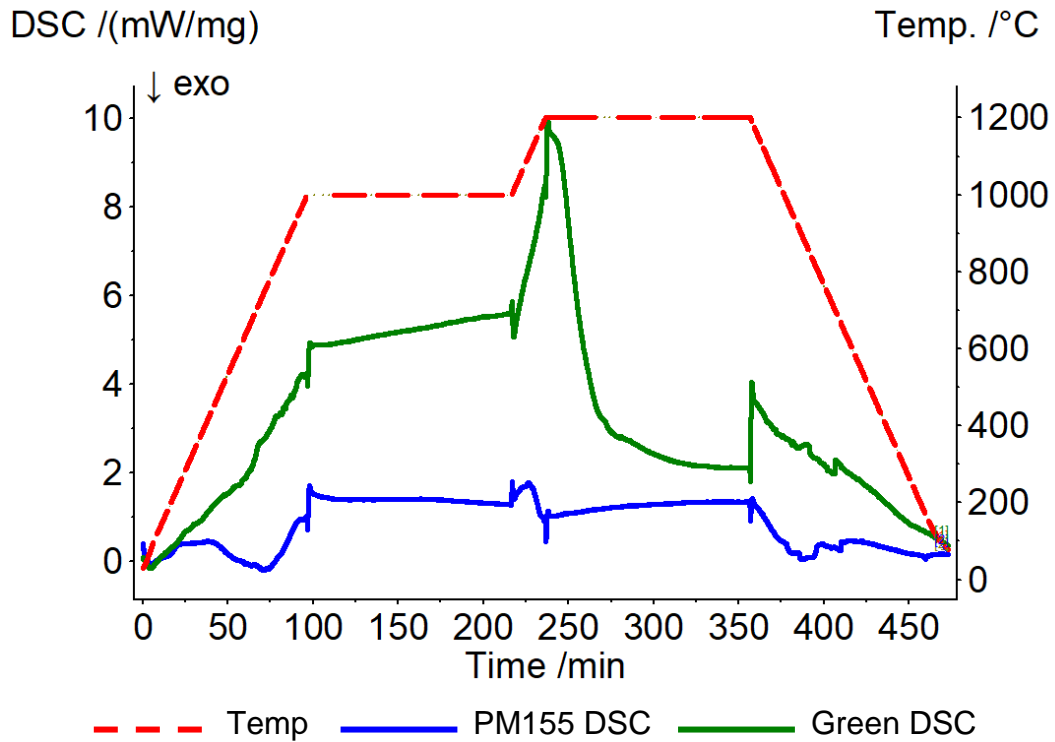
Figure 46: DSC results of Green insulation and post-mortem insulation PM155.

4.3.2.2.1.2 Cyclic testing

The powdered Green and PM155 materials were tested again using the DSC and the same thermal cycle but cycled ten times. The sample was returned to room temperature before beginning the next cycle. Figure 47 shows the cycled testing of Green and PM155. It can be observed that the DSC curves for the materials are very different for the first cycle and these have almost converged by the tenth cycle. This suggests the phase changes found in the PM155 could become stable after being heated for a relatively short period of time at 1200°C. Due to the time taken to perform these tests enough convergence had been found to make it impractical to perform a larger number of cycles for this thermal profile. The reduction in the peak of the Green sample at cycle three suggests at this point the phase changes are no longer reversible and that

these phase changes can occur at 1200°C. This is higher than the recorded thermocouple measurements and as a convergence was found and a stable phase change can be seen in the Green sample. Therefore, it was deemed necessary to reduce the peak temperature to 1000°C, the service temperature of the material, and the regular temperatures recorded on the insulation hot face. If a convergence can then be seen and a stabilisation of the phases in the Green sample at 1000°C it can verify the temperatures recorded by the thermocouples were accurate.

Both materials underwent phase changes during the 1200°C isothermal point. The DSC curves for the Green and PM155 start to converge after the fourth cycle and fully converged by cycle ten. This shows a higher amount of phase changes occurred in the Green material that was not present when the material is heated to 1000°C. The PM155 sample displays consistent DSC curves from the third cycle showing there has already been significant phase changing occurring in the material before it was subjected to this test.
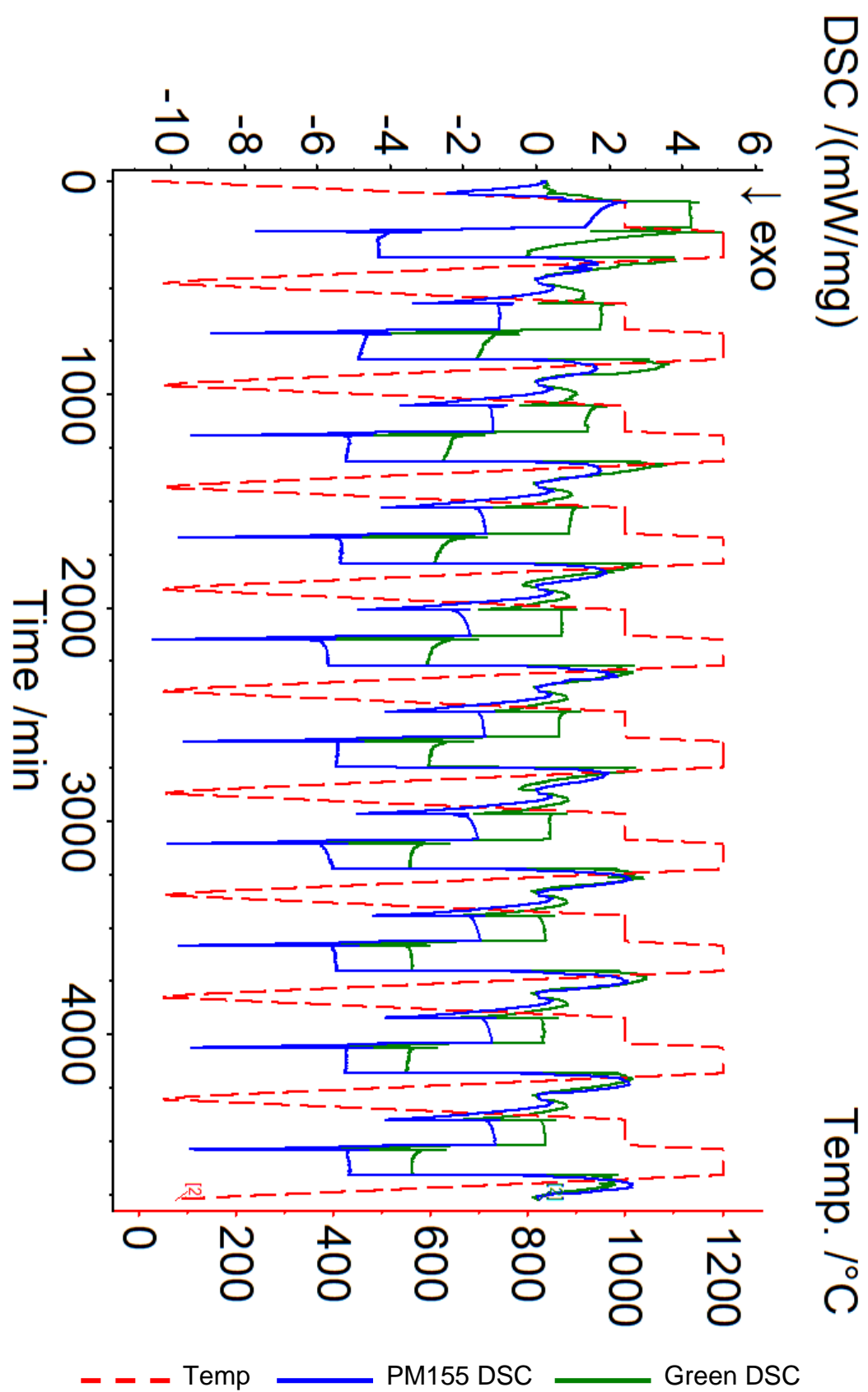
Figure 47: DSC results of ten cycles with peak temperature of 1200°C for the Green and PM155 samples.

Figure 48 shows the Green insulation and PM155 samples cycles ten times up to 1000°C. The Green material shows little phase changes occurring at the isothermal

points in the cycle. However, for each cycle the PM155 reaches 1000°C the material is undergoing phase changes for the first five cycles before these level out. This shows there has been some degradation in the post-mortem material and that it is now undergoing phase changes even at 1000°C which is only observed in the Green insulation at 1200°C. As phase changes absorb energy the reduction in PM155 phase changes occurred would mean the material is transferring more energy now it has degraded compared to the Green material. The reversible phase changes seen in the Green sample are not completely reversible in the PM155 and it must have been heated to between 1000°C and 1200°C based on the differences observed in Figure 47 and Figure 48. This makes the 1040°C temperature measured by the thermocouples very plausible.
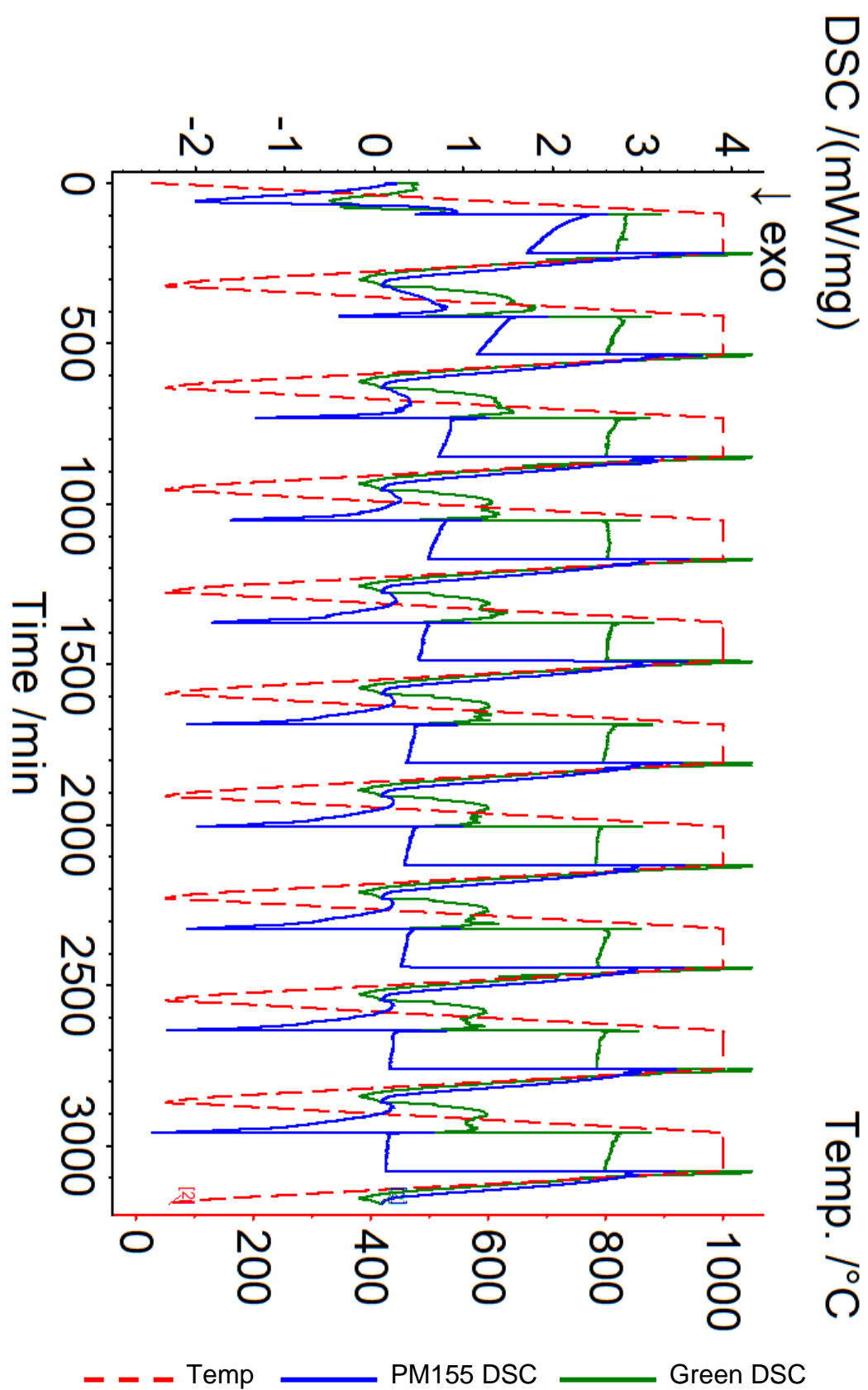
Figure 48: DSC curves for PM155 and Green materials ten cycles to 1000°C.

82

4.3.3 Density analysis

Pyrogenic silica has particle sizes <30nm so it would not be possible to determine the true density with XCT or SEM (77). However, these tests were performed to determine if the particles had bonded to form large particles to the size of the XCT voxels of 4µm or the SEM resolution of <1µ then a comparison could still be made. The material was not durable enough to utilise the Archimedes principle and fell apart when it was submerged, making this test not possible. Tap density testing was used to give a difference of the packing factor. This was then used to calculate the change in density based on the supplier's information and the change in volume size from the recovered compressed sample.

4.3.3.1 X-Ray Computed Tomography Scanning

X-Ray Computed Tomography Scanning (XCT) was performed to understand the internal structures that are present in the Green and post-mortem samples and provide a density value for use with Equation 1. XCT also has the advantage of revealing the 3D interconnectivity of particles on which the material properties depend. Post-mortem samples were mounted on a thin piece of wood to allow the material to rotate during the scanning. The Green material was too fragile to mount so was suspended in epoxy resin before mounting for the XCT measurements. Figure 49, Figure 50 and Figure 51 show single slices of the XCT data that can be considered representative of the volume for the Green material and two post-mortem samples from the PM155 panel noted PM155D and PM155F which have been compressed to 80% and 50% of the original thicknesses respectively, as previously mentioned in Table 5. PM155F has large cracks that run through the cross section whereas the scans of PM155D show a much more homogeneous structure.
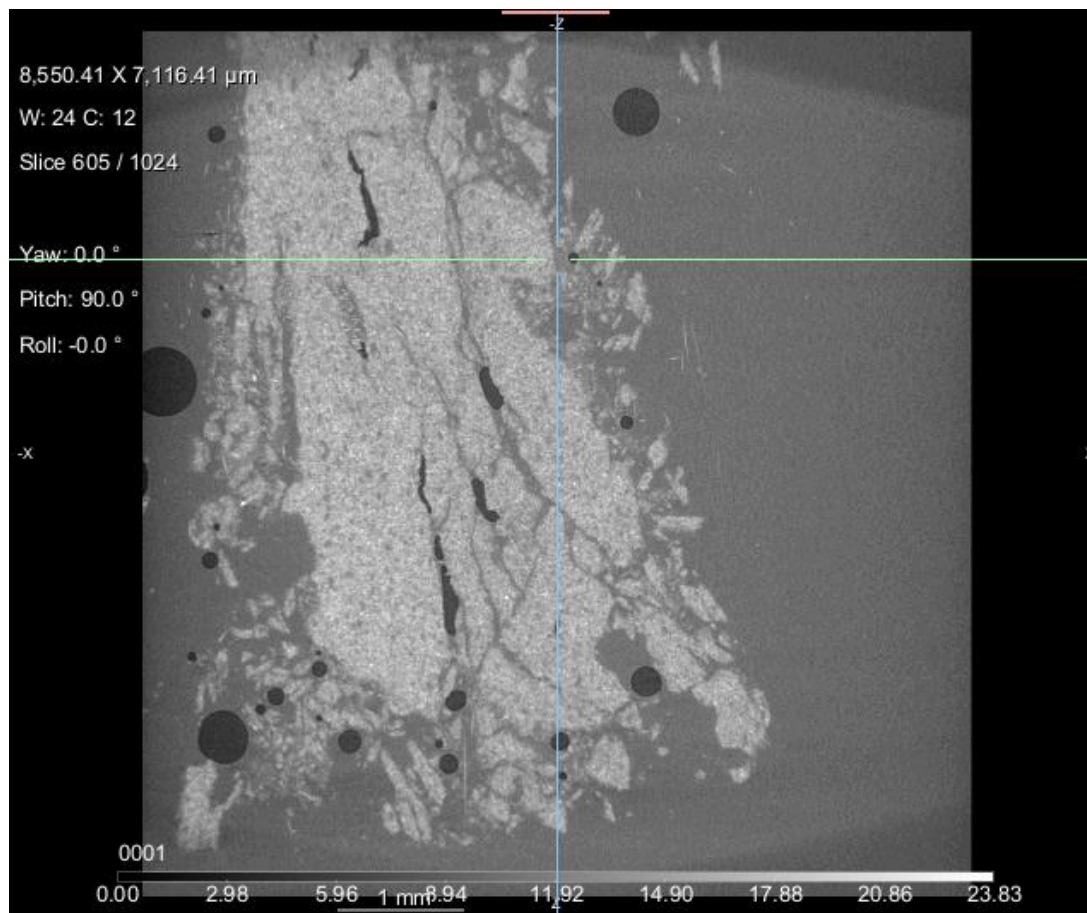
Figure 49: XCT image of Green sample with voxel size in top left corner (this was consistent for Figures 52-55).
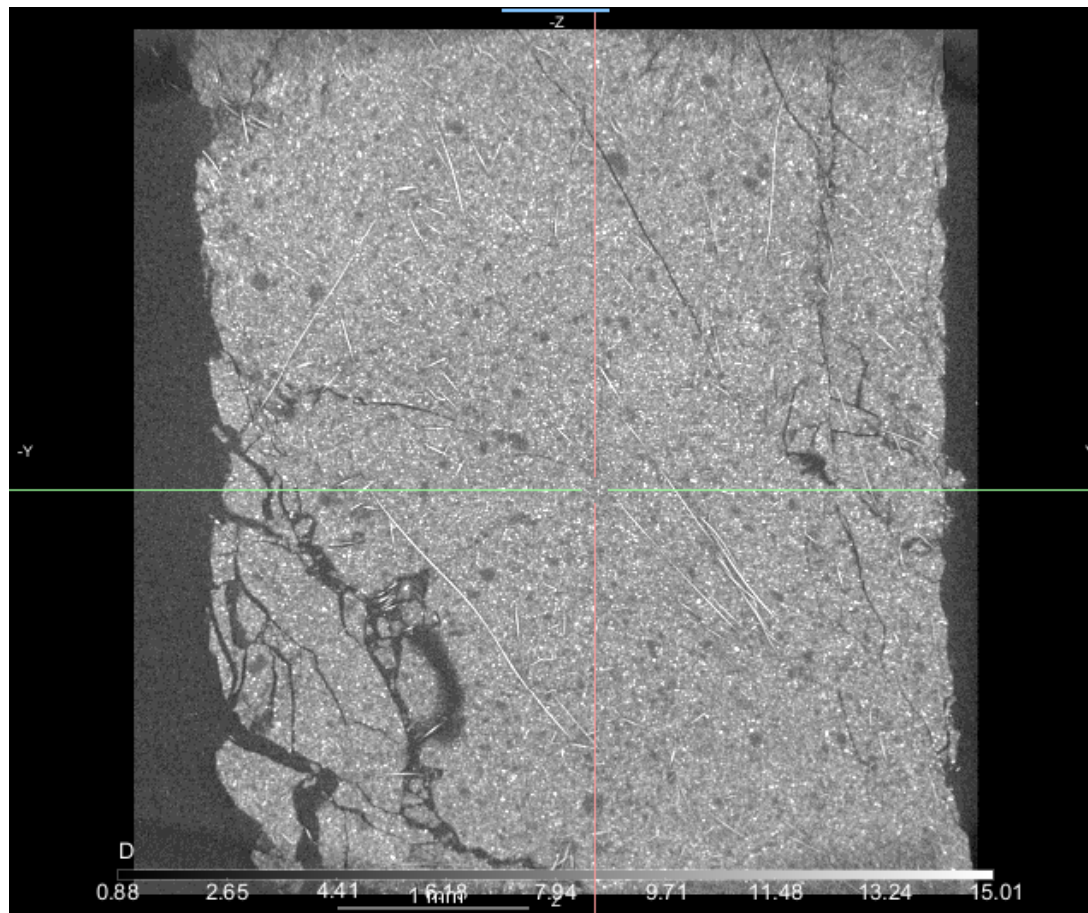
Figure 50: XCT image of PM155D sample.
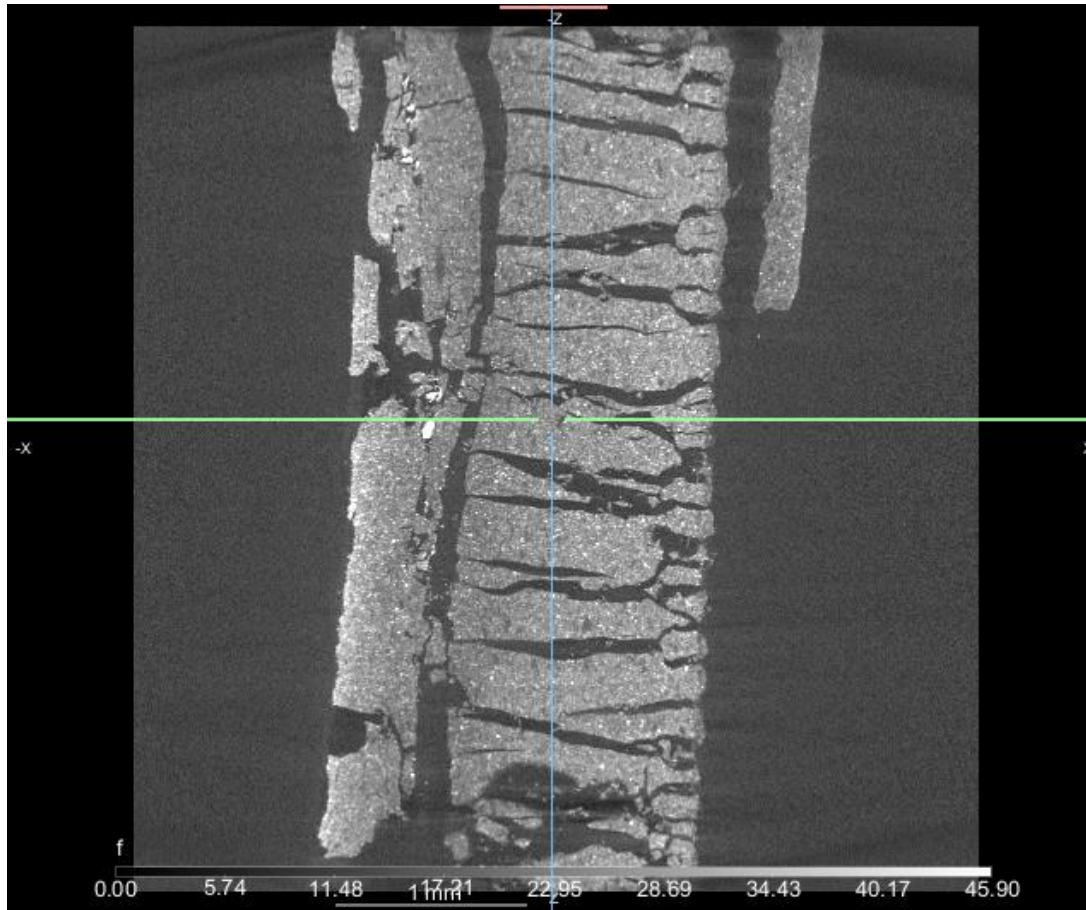
Figure 51: XCT image of PM1155F sample.

Figure 52 and Figure 53 show outputs of the insulation scanned with the XCT of the PM126 samples. The homogeneity of the samples is much more similar to the Green sample and the PM155D sample previously scanned and shown in Figure 49, Figure 50 and Figure 51.
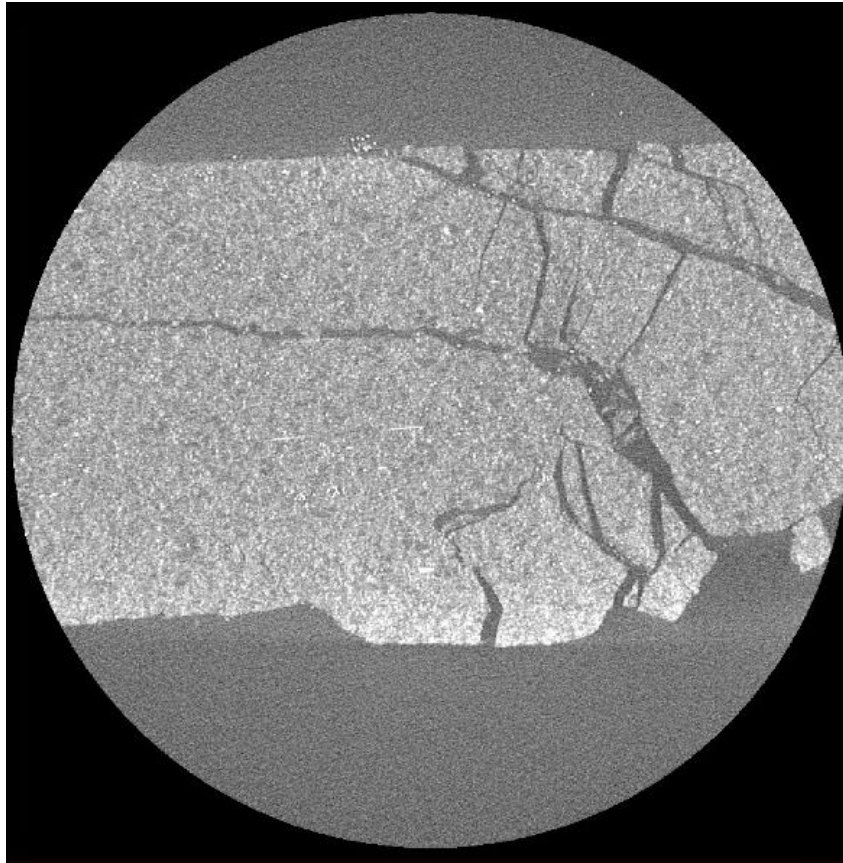
Figure 52: XCT image of PM126B sample.
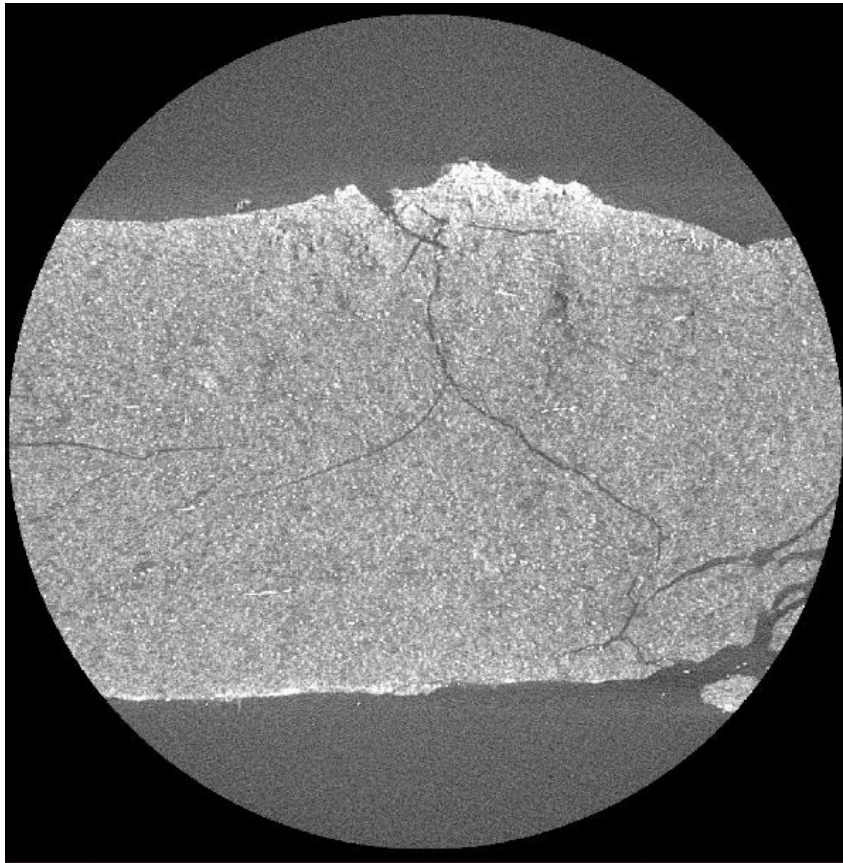
Figure 53: XCT image of PM126C sample.

87

Unfortunately, it was realised at this point that the resolution of the voxels from the XCT scans was too coarse and was not picking up the nanoporous voids in the materials. The voxel size was consistently 4.6μm for all the scans, however, the values produced showed no correlation to the visible images produced. The large cracks in sample PM155F showed a higher volume fraction and it could not be conclusively said this was accurate. On close inspection of the scans one voxel was imaging a void and thus it was concluded a higher resolution technique would be required to characterise the density.

4.3.3.2 Scanning Electron Microscopy

Due to the voxel size issues with the XCT scanning technique Scanning Electron Microscopy (SEM) was used to image the Green and PM155 samples. Samples were coated in carbon to aid electrical conductivity and imaged using the back-scattered electron method to elucidate compositional differences. The samples were mounted in resin and prepped for the SEM imaging with grinding discs going through the same method to keep the samples constant for scanning. Although there were some clear differences between the Green sample and the PM155 samples it was not possible to see the smaller voids at the field widths assessed. SEM images of the Green, PM155D and PM155F sample can be seen in Figure 54, Figure 57, and Figure 60 respectively. The Green materials get damaged during installation and sample prep, which is shown in the Green SEM image in Figure 54, with additional particle boundaries. It is not possible however to determine from the SEM images whether these boundaries add significantly more porosity than contained within the pyrogenic silica. Therefore, it is inconclusive as to whether this influences the microporous porosity significantly and future work should look at this with a technique that can measure to a scale that can quantify this. Unfortunately, these were inconclusive with regards to porosity and therefore density determination. The SEM images did highlight areas of the TiO_2 which is used in the microporous insulation as an opacifier to reduce the radiation transfer through the material. This is highlighted in the EDS images in figures XXX
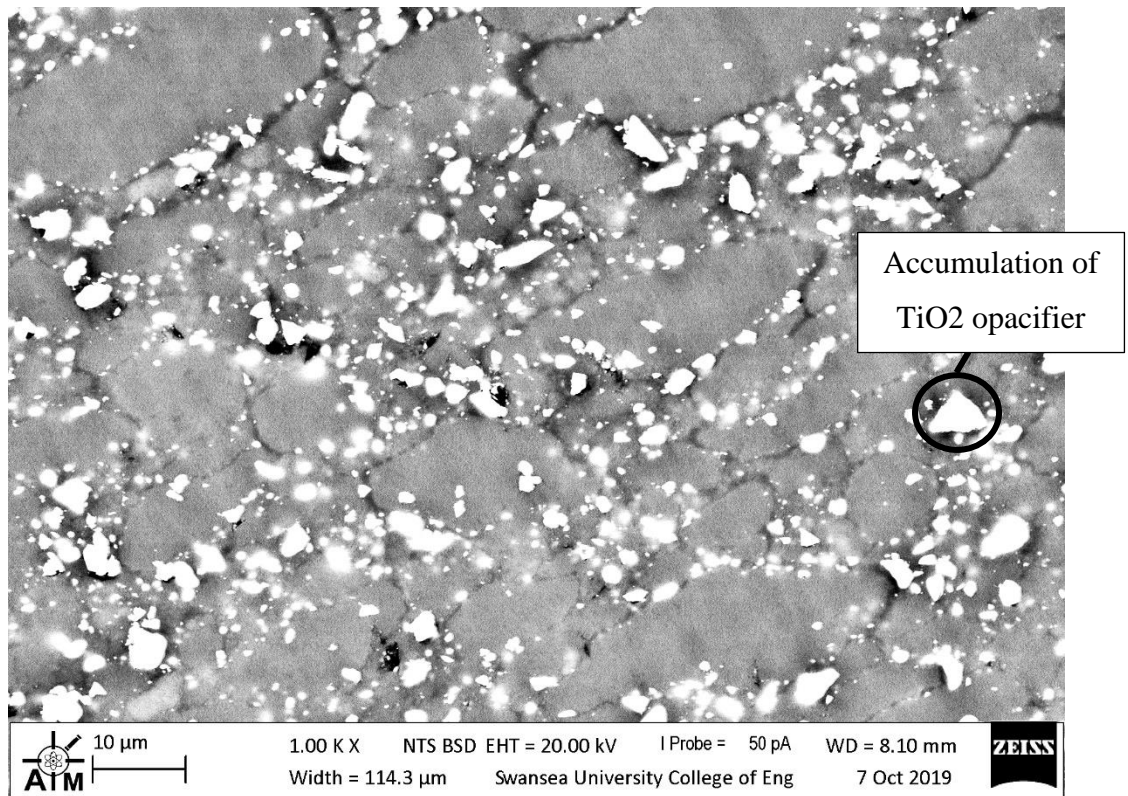
Figure 54: SEM image of Green sample.
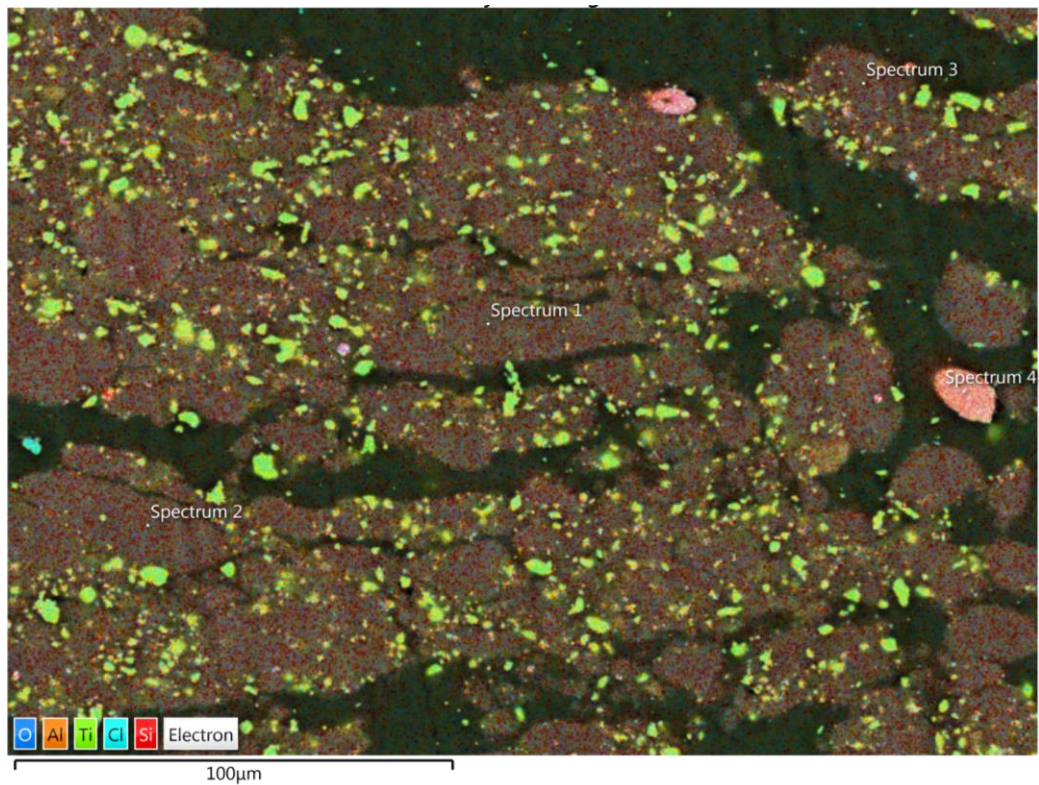
Figure 55: EDS image of Green sample with multiple spectrums

100μm
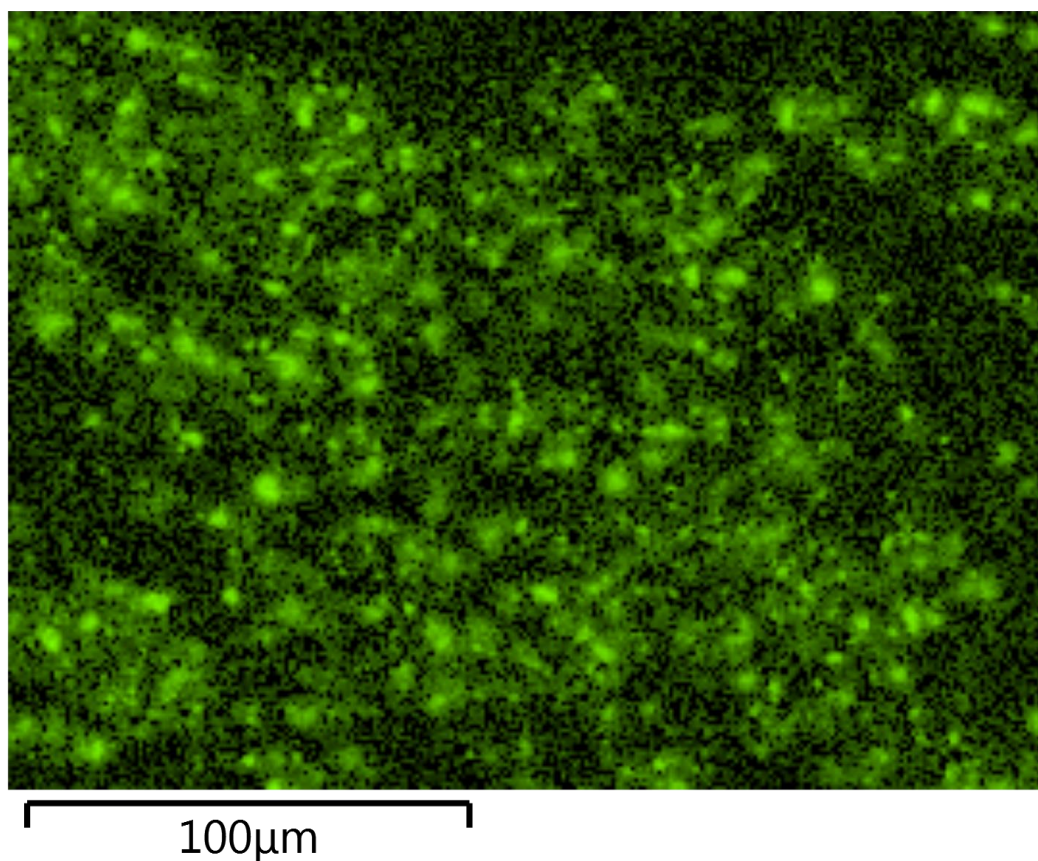
Figure 56: Ti spectrum from EDS image showing TiO2 opacifier across Green sample and accumulations highlighted in SEM image

Accumulation of TiO2 opacifier

10 μm   1.00 K X   NTS BSD EHT = 20.00 kV   I Probe =   50 pA   WD = 8.24 mm
Width = 114.3 μm   Swansea University College of Eng   7 Oct 2019
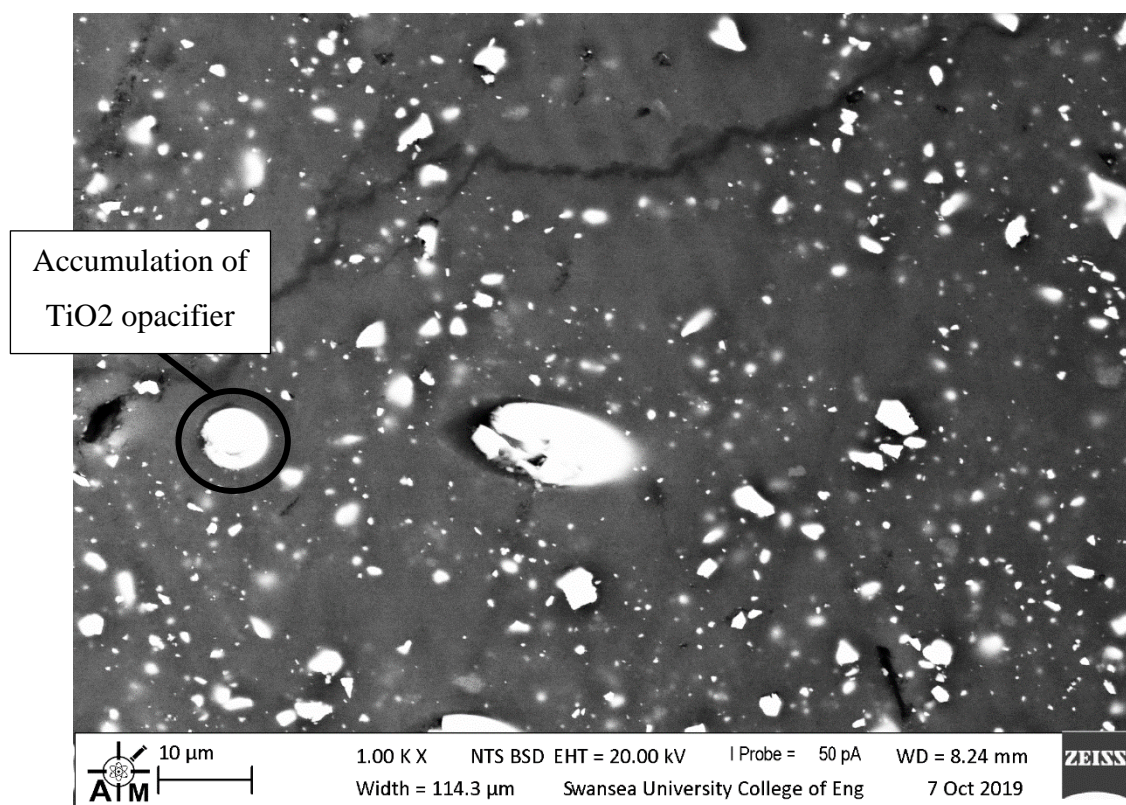
Figure 57: SEM image of PM155D.
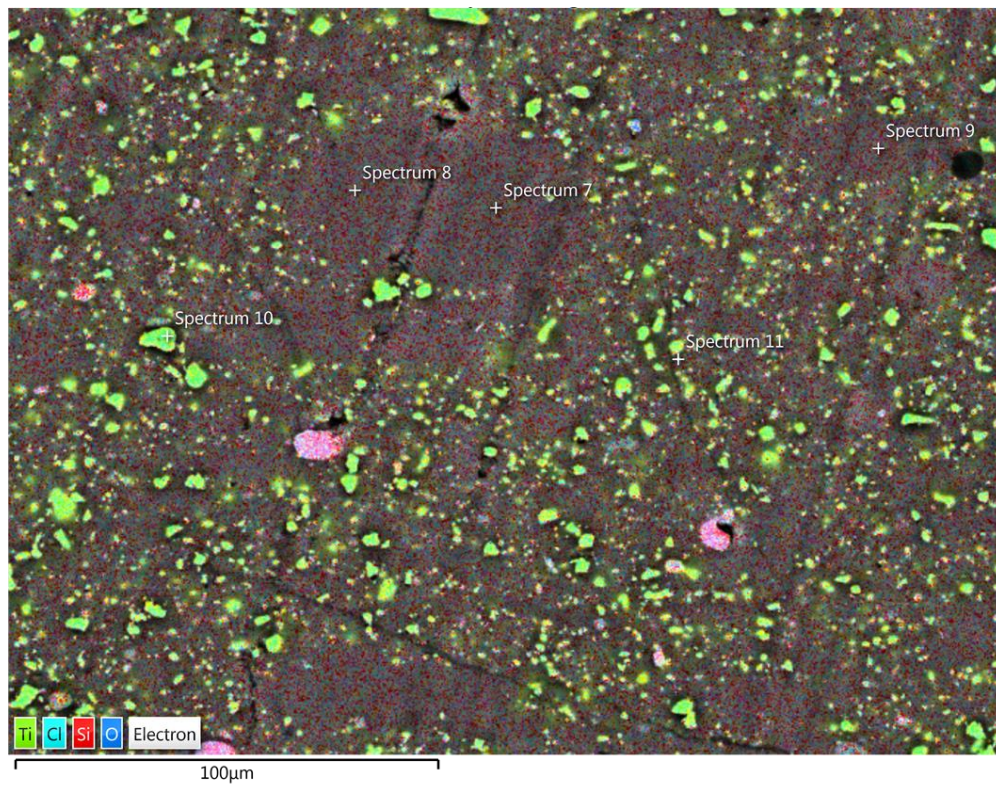
Figure 58: EDS image of PM155D with multiple spectrums
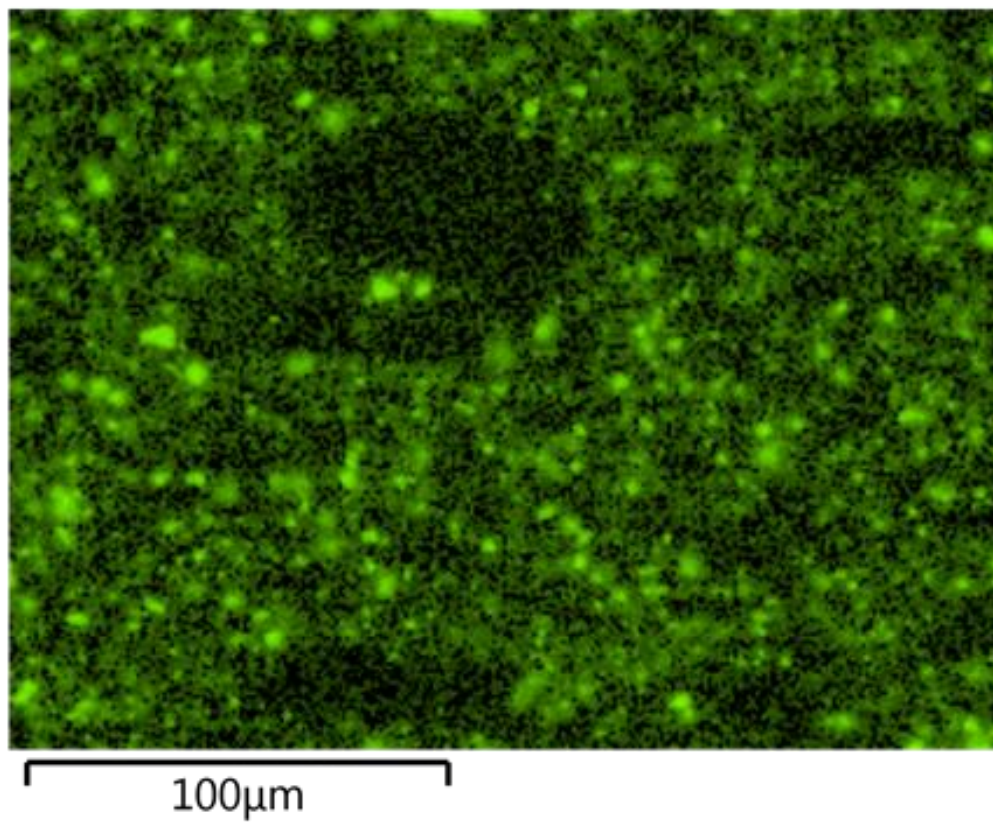
Figure 59: Ti spectrum from EDS image showing TiO2 opacifier across PM155D sample and accumulations highlighted in SEM image
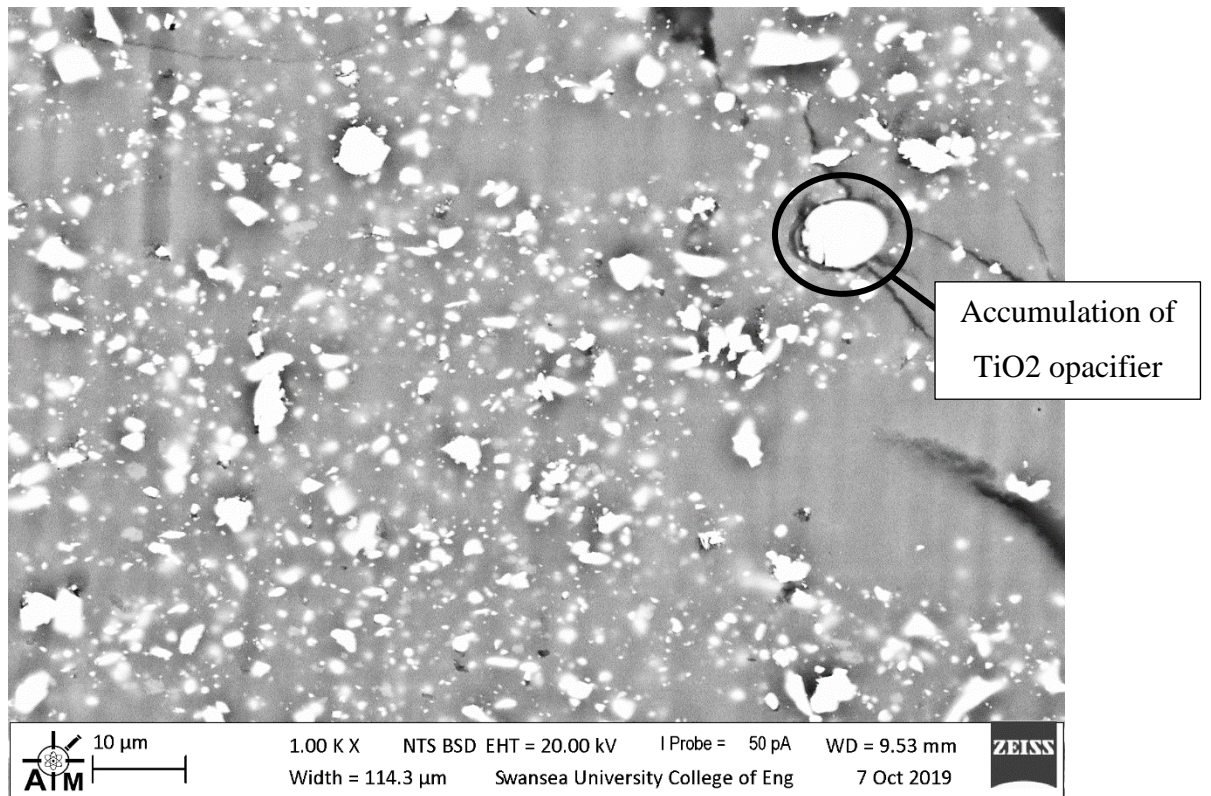
Figure 60: SEM image of PM155F.
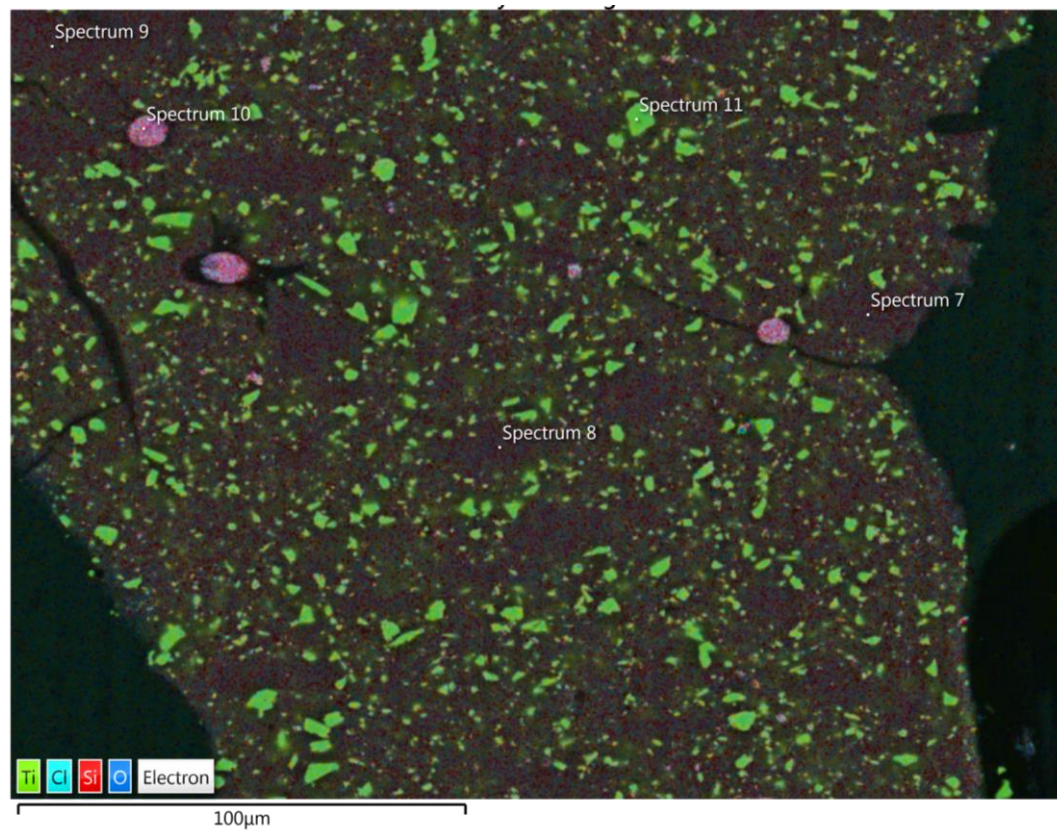
Figure 61: EDS image of PM155F with multiple spectrums
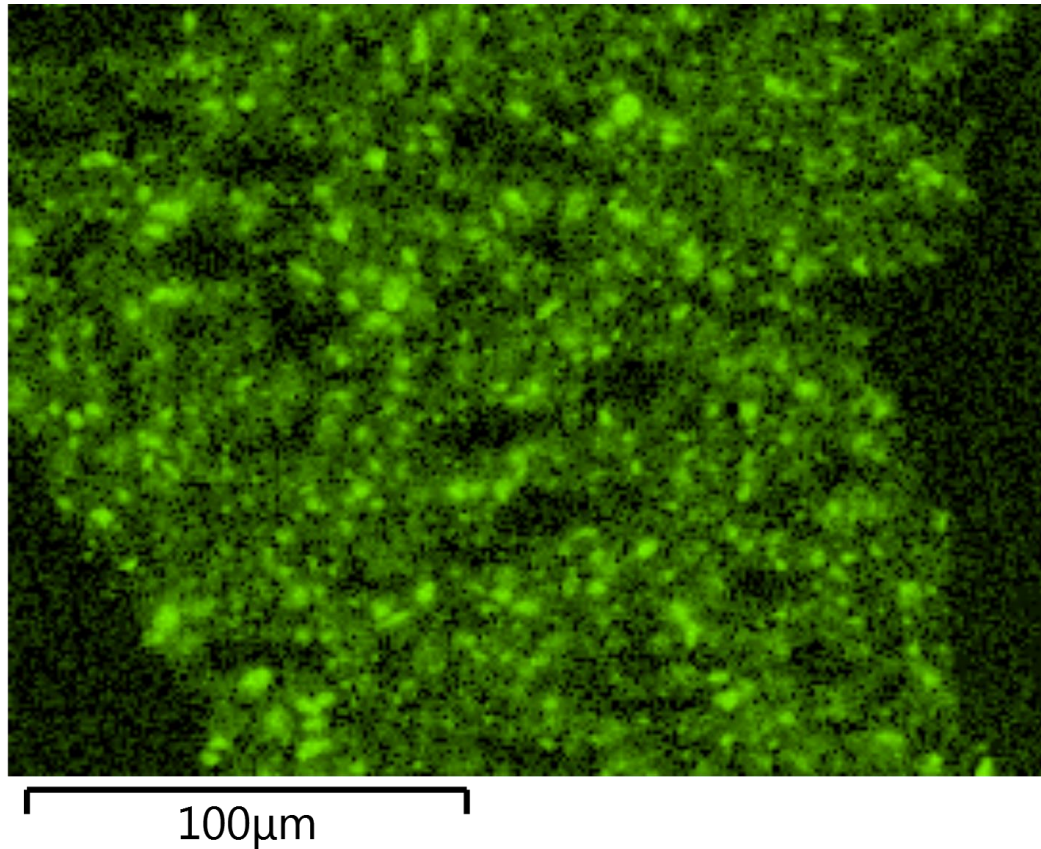
Figure 62: Ti spectrum from EDS image showing TiO2 opacifier across PM155F sample and accumulations highlighted in SEM image

As the SEM had not been able to identify the voids that could differentiate the density between the Green and the PM155 samples it was not possible to determine differences from this test. Therefore, tap density of the powdered material was conducted to provide density differences.

4.3.3.3 Tap density testing

Because the imaging techniques were unable to determine the density of the samples the tap density method was utilised. The method applies only to powdered samples so this study would be conducted on powdered homogenised samples. The tap densities were then converted to panel densities by taking the average thickness of the PM155 and PM126 panels, from Table 5 and Table 6 and difference in tap densities to give the in-situ density. This information can be found in Table 9. The methodology for the tap density measurements is to fill a tube with the powder, tap the tube fifty times, scrape the excess powder off and then weigh the sample. Because the volume is known, and the starting weight of the tube is also known, the density can then be

calculated by the change in mass. The values recorded for the tap densities can be seen in Table 9.

Sample		Mass (g)	Tap density (kg/m3)	Average panel thickness before converted to homogenised powder (mm)	Panel density from powdered density change and panel thickness (kg/m3)
Green	1	3.66	146.4	6.0	260 (control)
	2	3.74	149.6		
	3	3.95	158.0		
	Average	3.78	151.3		
	St. Dev	0.12	4.9		
PM 155	1	6.62	264.8	3.4	759.6
	2	6.24	249.6		
	3	5.93	237.2		
	Average	6.26	250.5		
	St. Dev	0.28	11.3		
PM 126	1	4.47	178.8	3.1	368.8
	2	4.67	186.8		
	3	4.63	185.2		
	Average	4.59	183.6		
	St. Dev	0.09	3.5		

Table 9: Tap density results for Green and post-mortem samples.

The tap density outputs were able to give the difference in packing factor between the Green and post-mortem samples. As the volume changes and the panels' starting density was known it was possible to calculate the in-situ density of the microporous insulation by combining these two sets of data.

Now, with a value for the density of the Green insulation and the two post-mortem samples, the specific heat capacity was needed to then calculate the thermal conductivity with Equation 1 from the thermal diffusivity output of the LFA.

4.3.4 Thermal properties of post-mortem insulation

4.3.4.1 Specific heat capacity values of powdered samples from DSC measurements

The specific heat capacities (Cp) of the Green and post-mortem materials were calculated using the DSC in relation to a known standard and the DIN 51007 method for finding this value. The Cp of the insulation samples was an essential property as it was required to calculate the thermal conductivity of the post-mortem samples. The ratio of the Cp values measured between 80°C and 900°C for the Green and post-mortem samples can be found in Figure 63. This temperature range covered the working temperatures of the insulation. The values produced from this technique far exceeded the published Cp values for fused silica and the other chemistries found in

the material. Horbach et al. (1999) found the specific heat of fused silica to be 1.236kJ/kg.K (78). This is almost a factor of three smaller than the peak measured values of the microporous insulation. However, because of the precision and consistency of the results, it is still possible to do a comparative study even though the values recorded do not reflect the literature.
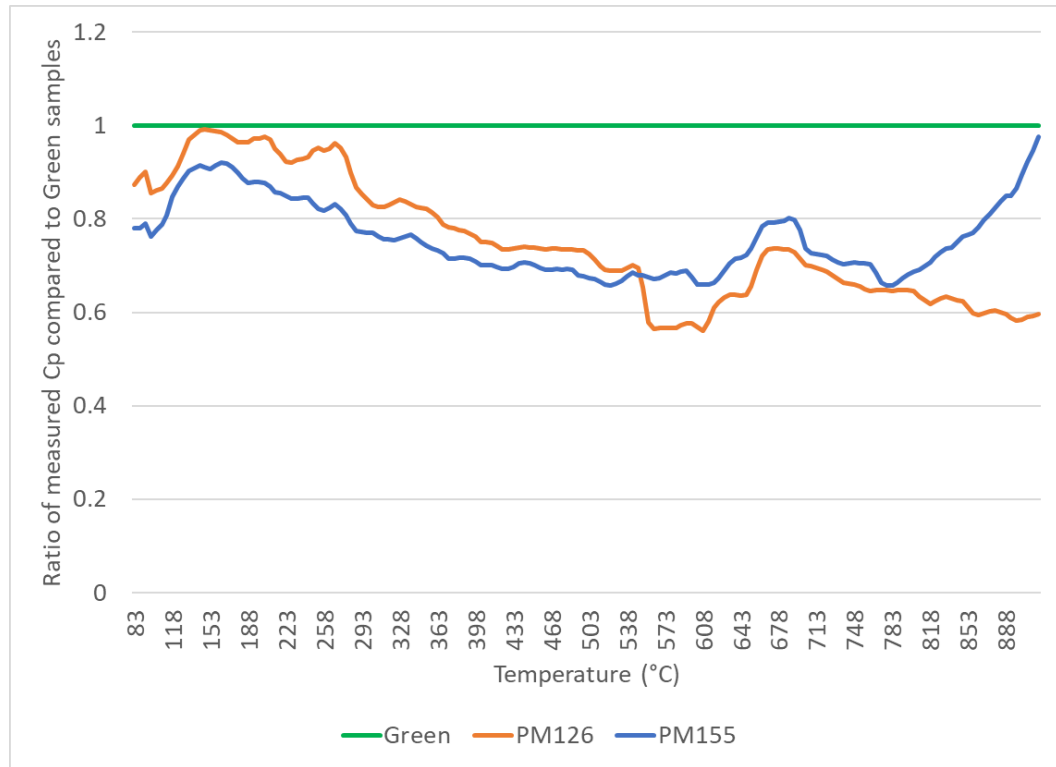
Figure 63: Specific heat (Cp) of the Green and post-mortem insulation materials measured via DSC displayed as a ratio of the properties compared to the Green sample measurements.

The calculated Cp values can be seen in Figure 64, which utilised the ratios shown in Figure 63 with the supplier's data to give an indication of the Cp of the in-situ insulation. The samples measured by the DSC were powdered homogenised samples of the Green, PM126 and PM155 samples. To get the in-situ Cp values of the post-mortem insulation the ratio of the measured post-mortem samples with the Green sample was calculated. This was then used to calculate Cp values by relating it back to the supplier's data for a panel. The Cp values can now be used to calculate the thermal conductivity of the post-mortem insulation from the diffusivity output of the LFA.
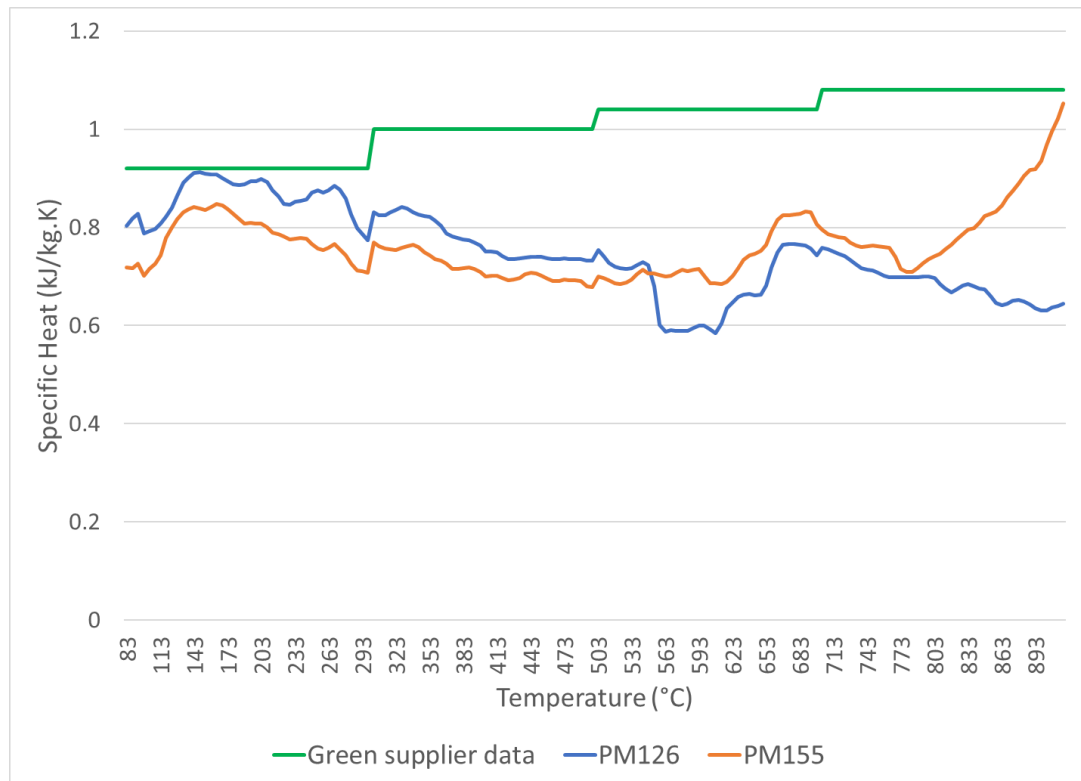
Figure 64: Specific heat of Green and post-mortem insulation materials calculated by ratio of measured samples and supplier data.

4.3.4.2 Laser Flash Analysis

4.3.4.2.1 Background

Laser Flash Analysis (LFA) uses a high-powered laser to heat a sample from the bottom. A thermocouple measures the top surface to determine the time delay for the heat transferred through a sample. The output of the test gives the thermal diffusivity of the material. As the Cp and density have been calculated from the DSC and tap density measurements, once the thermal diffusivity was measured it was possible to use Equation 1 to calculate the thermal conductivity thereby determining the degradation of the insulation in-situ.

4.3.4.2.2 Method

Powdered homogenised samples were tested of the Green and post-mortem samples. The relationship between the Green properties and post-mortem properties were calculated. The ratio of the measured Green properties and the supplier's data for the panel was then calculated. By using the calculated relationship of the Green and post-mortem samples, and the ratio of the recorded and published data, it was then possible to calculate the thermal diffusivity of the in-situ post-mortem panels. There is not a standard in place for the measurement of powders using the LFA method. Because of

this the testing method followed the guidance of the BS EN ISO 22007-4:2017 for LFA measurements of plastics (79). LFA is a relatively new measurement method and there are limited standards available to reference from. Even though there is not currently a standard Lian et al.'s (2016) study demonstrated it was possible to use LFA to find the thermal conductivity of porous thermal insulation (39). Therefore, the method followed utilised Lian et al.'s findings and used these stages:

1. Due to the low mechanical strength of the materials it was essential they were tested in pots designed to hold powders. This was to protect the equipment from any falling debris and reduce the chance of the equipment getting damaged.
2. Each of the samples is prepared in the powder pot with an extra volume of material so that air gaps are kept to a minimum as the lid is added to the sample holder.
3. The testing area was first purged of air, in an argon rich environment, because the changes in thermal properties of the argon are better known and were accounted for in the output data.
4. The thermocouple that records the heat change on the top of the sample is cooled via liquid nitrogen to remove any ambient heat. At each temperature interval of 50°C, from 50-1050°C, the diffusivity of the sample is measured.
5. The recorded data from the NETZCH LFA 457 was an average of the three measurements and the standard deviation of these measurements is also provided to give an indication of the repeatability of these tests (80).
6. Of the Green, PM126 and PM155 samples each measured for both the homogenised powder and panel states of the insulation two samples were created of each variation, which then meant that six tests were ran at each temperature.

The two average outputs from the LFA 457 for each sample type were then compared to determine if further testing was required to ensure repeatability of the results. The following section will discuss the results produced by the LFA 457 and analyse the relationship of the different forms of the microporous insulation.

4.3.4.2.3 Results and analysis

The data from the tests can be seen in Figure 65. From the data it was possible to see there was little difference between the Green material and the post-mortem material until the samples reached 950°C. At this temperature the results diverge, and the post-mortem samples diffusivity increases at a much higher rate than the Green sample. It was observed that devitrification occurs when the material is held at 1000°C. The energy absorbed by this phase change suggested this was the reason for the differences in diffusivity for these results.
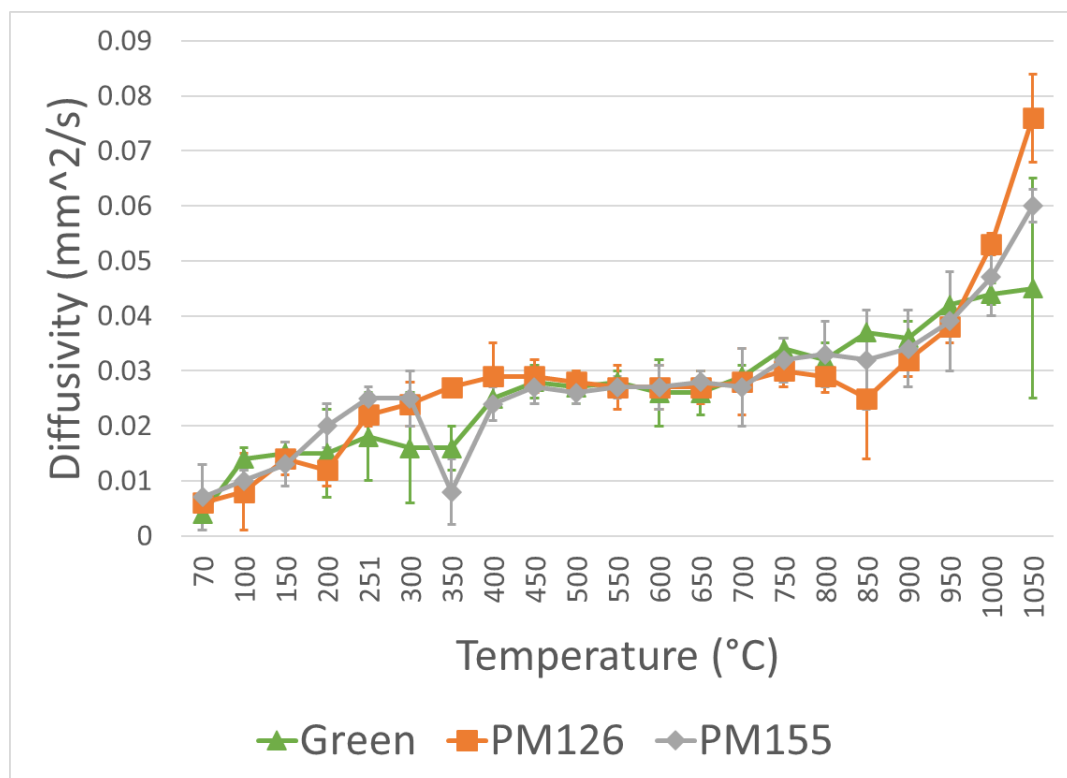
Figure 65: LFA results of powdered homogenised Green and post-mortem samples.

The reliability of the results from the LFA is strong as the NETZSCH LFA 457 is capable of accurately measuring the thermal diffusivity of materials in the range of 0.01 mm^2/s to 1000 mm^2/s (81). Most of the samples of the microporous insulation were comfortably in this range and the standard deviations from the tested samples were low in relation to the recorded values. When attempting to measure the PM126 panel material errors occurred and improbable values far exceeding previously recorded data were produced. Therefore, it is only possible to compare the Green and the PM155 panel material properties as seen in Figure 66. It is recommended that future work be conducted on a larger range of panel materials to expand on the knowledge gained from the powder samples.
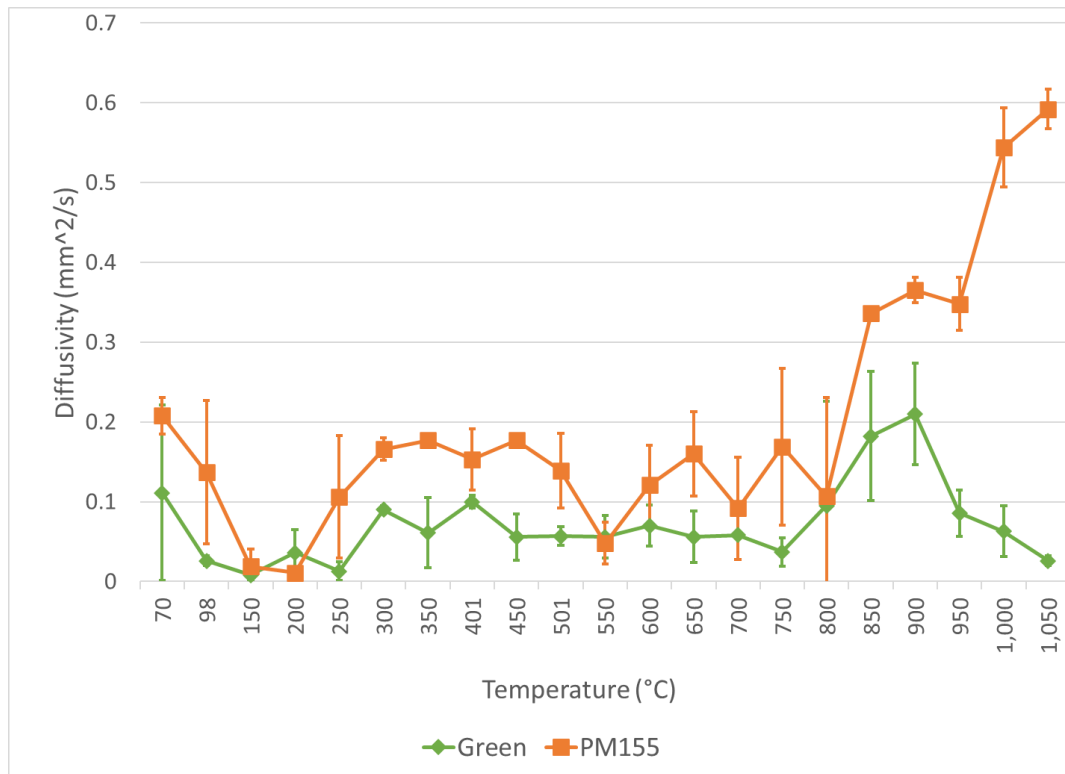
Figure 66: LFA data of Green and PM155 panel material.

4.3.5 In-situ thermal conductivity

The data gathered from the LFA, DSC and tap densities was used to calculate the thermal conductivity of the in-situ microporous material using Equation 1. The measured thermal diffusivity of the Green material was used to back calculate the thermal conductivity of the Green material. This was then used to determine by how many factors the LFA was measuring higher than the supplier data. This is because the LFA results showed consistency in the measurements of both the Green and PM155 data this factor could then be used to calculate the in-situ thermal conductivity of the PM155. The comparison of the Green and PM155 material can be found in Figure 67. The variability of the calculated data suggests that future work is still needed to verify these calculated figures. Smith et al. (2013) suggest that for this material the hotplate method can be used to give more accurate results and future work could be done to verify these findings by using one of these techniques (82). However, there is currently no published data of in-situ microporous insulation and Green data produced by the supplier or educated estimates must currently be used to model this material. With the testing that has been conducted on the microporous material this study has been able to demonstrate differences in the density, Cp and diffusivity. Therefore, it is very clear that modelling refractory linings using Green data is

99

inaccurate. From discussions with leading experts in the field, estimations based on best educated guesses were used for these materials using an increased value from the quoted thermal conductivity provided by the supplier. Therefore, the measured data is a step change in the understanding of the properties in-situ and modelling accuracy can be increased from this data. The trend line of this data showed that the in-situ thermal conductivity of the microporous material is between 0.1W/m.K and 0.15W/m.K in the temperature range of 100°C-900°C. This is a factor of four or five times larger than the Green material properties. Therefore, it has been possible to disprove the hypothesis that the material retains the same properties throughout the in-situ production. This was able to demonstrate that there is a real degradation of the insulation material from the forces and temperatures that are applied to it in-situ.
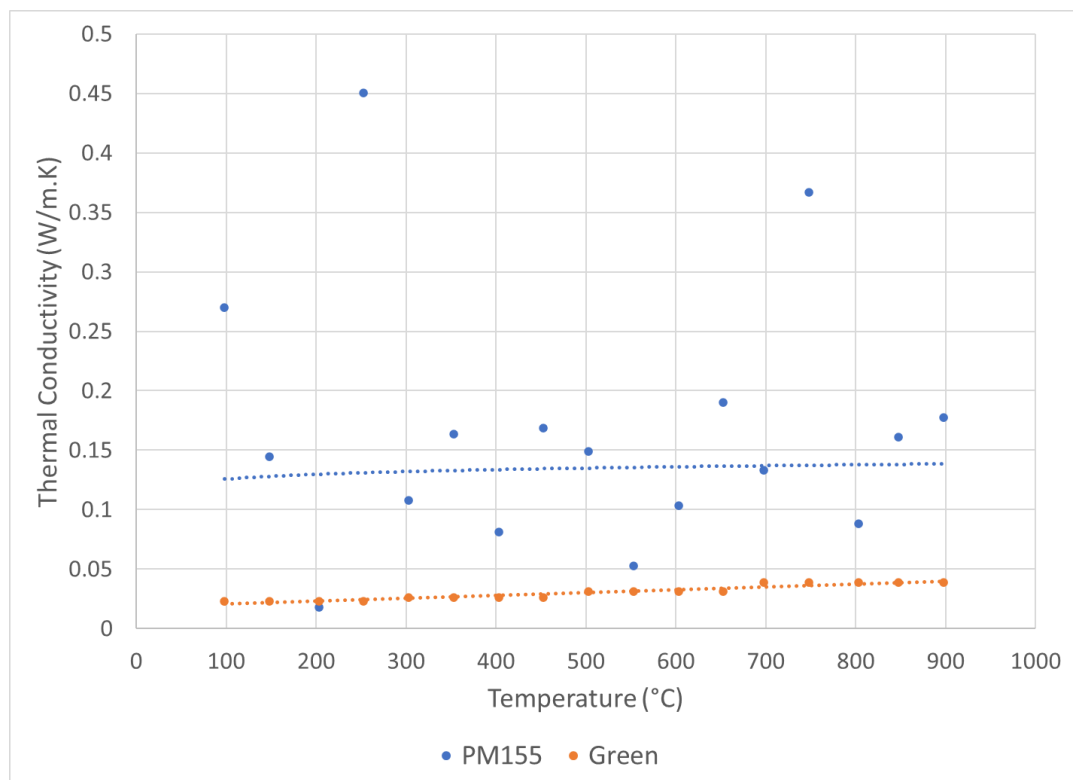
Figure 67: Thermal conductivity of the Green material from supplier data and the in-situ thermal conductivity of the insulation (PM155).

4.4 Conclusions

Two post-mortem insulation panels were recovered from a teeming ladle after the material had been in production for 126 and 155 cycles. Thermophysical testing was performed on the material via multiple methods. From this analysis it was determined, using XRD, that there was an increase in crystalline silica present in the post-mortem samples, compared to the Green sample. DSC measurements were able to verify the

temperatures that these phase changes occurred at, which validated the thermocouple measurements in Chapter 2. Analysis was then conducted via XCT, SEM and tap density to provide a density figure that was used to calculate the in-situ thermal conductivity of the insulation. The Cp of the materials was measured using the DSC and compared to a known standard. The density and Cp were then used with the thermal diffusivity values found via the LFA method to find the thermal conductivity of the samples. Using the difference between the calculated thermal conductivity of the Green material, then referencing this back to the supplier's information, it was possible to conclude that the thermal conductivity of the in-situ material had increased by a factor of five in the most extreme case. The Green thermal conductivity of the microporous material ranges from 0.023W/m.K to 0.039W/m.K dependent on temperature. This study was able to calculate that the thermal conductivity of the in-situ insulation ranges from 0.10W/m.K to 0.15W/m.K. This increase in thermal conductivity will cause higher in-situ ladle shell temperatures. This in turn was theorised to increase temperature lost from the steel compared to models that use the Green properties, which was disproved in Chapter 5. These findings disproved H2a and demonstrated that there is a large difference between the Green thermomechanical properties of the microporous insulation and the in-situ properties. The calculated density increases from the tap density measurements and supplier information showed the in-situ insulation panel increased from 260kg/m^3 to 759.6kg/m^3, which is almost three times the density of the installed insulation. The Cp was far more variable with temperature and ranged from being almost the same to being 50% of the installed value. It can be concluded that the density had the largest change that then caused the increase in thermal conductivity. Therefore, if insulation materials can be designed to retain their installed densities, this study suggests this would provide an increase in performance. It is recommended that this study be repeated to verify the findings and to use the hotplate method to measure the thermal properties of the insulation as recommended in Smith et al.'s (2013) study (82). The information gathered in this study provides an insight into the in-situ properties of the insulation material that, before the time of writing, had to be decided based on assumptions and educated guesses. With the data from this study it is now possible to model the heat transferred to the ladle shell with a higher level of accuracy. This will then increase the accuracy of simulated predictions of steel temperature losses due to refractory temperature,

thereby improving the accuracy of through process temperature predictions and improving steel quality.

Chapter 5 – Use of in-situ insulation properties to accurately model steel temperature losses due to degradation

5.1 Introduction

This chapter addresses Q2 and will state that the change in insulation properties caused an increase to the cooling effects of the teeming ladle refractories (H2b). From Q3 it can be stated that the cooling curves would not allow for an accurate prediction of the cooling effects from a hot face temperature measurement (H3).

In previous chapters it has been possible to prove that the assumption used in thermal models of teeming ladle refractories causes errors. It has also been possible to quantify the in-situ thermophysical properties of the insulation layer from post-mortem sample analysis. As previously stated by Glaser (2011) and Gupta (2004) the insulation layer integrity is theorised to have the largest effect on the thermal efficiency of the refractory lining (2,3). It can be concluded from their findings that degradation in this layer will cause an increase in temperature losses to the steel. Seibring et al. (2012) were able to quantify that a steel temperature losses range from 10-20°C per cycle can be attributed to a ladle without an insulation layer in the barrel (14). However, it was not possible to quantify the in-situ degradation in the insulation layer until the analysis for this thesis was performed, as covered in Chapter 4. Therefore, it was not clear how much temperature was lost from the insulation degradation and how close to the values in the Seibring et al. (2012) study it degrades to before the lining is changed. This chapter will discuss the results of the simulations conducted on the teeming ladle under the same scenarios with changes to the insulation properties. These changes are; the estimated properties used in the Ladle Watcher configuration, the Green properties, and the measured post-mortem properties. A comparison was then made of the effects on the refractory cooling rates and a quantification of the cooling effect on the steel. This looked to disprove the hypothesis that the insulation has a large effect on the molten steel cooling due to the refractories, as theorised in the literature (2,3,25–27).

This chapter will also quantify the steel temperature losses caused by the ladle bottom and the changes in thickness of the precast bottom. These were theorised as the reasons

for differences between measured and modelled temperatures. It was very apparent from the findings in this chapter that the differences in refractory temperatures need to be very different for it to influence the steel temperatures.

5.2 Simulation method

Plant data was analysed to produce a scenario based on production rates to simulate the cooling effect of the refractories on the steel. This then was then used to determine that the average ladle empty time was 1.5 hours during production. Therefore, ladles were simulated to determine their full saturation point, which typically took 15 hours of steel contact time. Although this was only observed on rare occasions in the plant data, a control point was required for the thermal storage in the refractory layers and the heat flux needed to return to this point. This then provided a worst-case scenario in terms of the cooling effects of the teeming ladle refractories on the steel in the ladle. It was then possible to compare the temperatures of the refractory lining and determine the heat flux required to bring it back to thermal equilibrium. This could then be converted into a temperature loss from the steel to validate H3 that insulation reduces the cooling effect of refractories (2,3,25–27). The method described was applied to the scenarios discussed in the following sections.

5.3 Ladle insulation effects

Steel temperature losses due to insulation degradation have little effect and were calculated to be within less than 1°C once the ladle had reached production temperatures. It was calculated that an additional 2°C from the steel was required to account for the difference in ladle shell temperatures. However, this loss would be spread across several heats because it takes 15 hours of steel contact time for the refractories to become thermally saturated. Therefore, the heat lost per cycle was calculated to be <1°C. This finding was consistent with the findings in the Siebring et al. (2012) study (14). This, however, disproves the theory that Glaser et al. (2011) stated that "a doubled conductivity of this layer would result in considerable increase in the ladle heat loss" (2). It was found that the temperature loss due to an unlidded ladle accounted for a temperature loss from the steel of 17°C for a ladle with Green insulation properties. This figure increased to 18°C when using the measured insulation properties from Chapter 4. This information is shown in Table 10.

Insulation properties	Temperature loss (°C) empty 1.5 hours no lid	Temperature loss (°C) empty 1.5 hours lid after 30 mins
Green	17	6
Measured	18	7
Model Estimate	17	6

Table 10: Temperature losses from steel due to ladle insulation property differences.

With such large differences in the insulation properties (calculated and shown in Chapter 4) it can be concluded that the difference in ladle reheating, shown in Table 10, caused by insulation degradation is negligible. However, it is important to note the steel shell temperatures increased from 282°C to 428°C with the changes in insulation properties. This validated the insulation properties measured in Chapter 4 because the simulated shell temperatures correlated with the consistent thermocouple measurements of around 430°C in Chapter 3. Such large differences in shell temperatures can cause safety concerns and reduce the service life of a teeming ladle shell. This confirmation of shell temperatures is of importance to the ladle shell modelled in this thesis as it is operating above its designed limit. The differences in the thermal profiles for the three different insulation properties and production scenarios can be seen in Figure 68, Figure 69 and Figure 70.

Lidding showed little difference compared to the differences in insulation properties, but it did show a significant benefit compared to the unlidded scenario. This highlighted a high level of impact and potential to benefit the steel quality and reduce reheating through lidding practises. Therefore, it was concluded that more scenarios surrounding lidding practises were needed and can be seen in the following section.
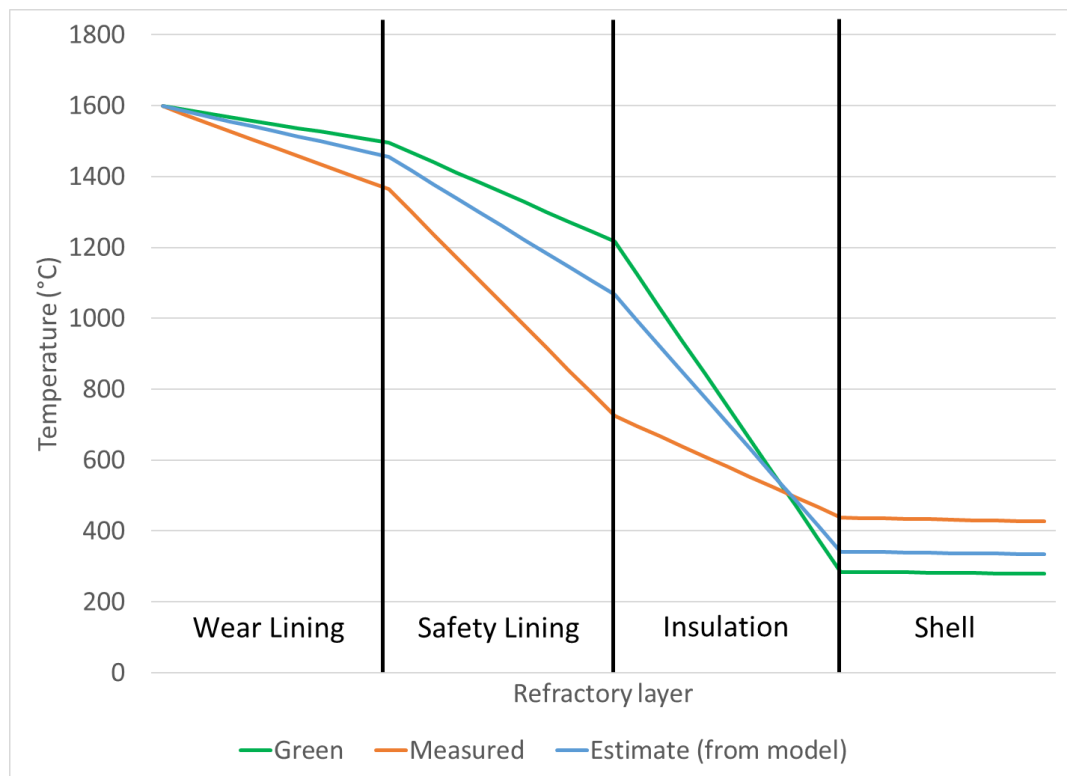
Figure 68: Ladle wall thermal profile fully saturated with Green, measured and estimated properties.
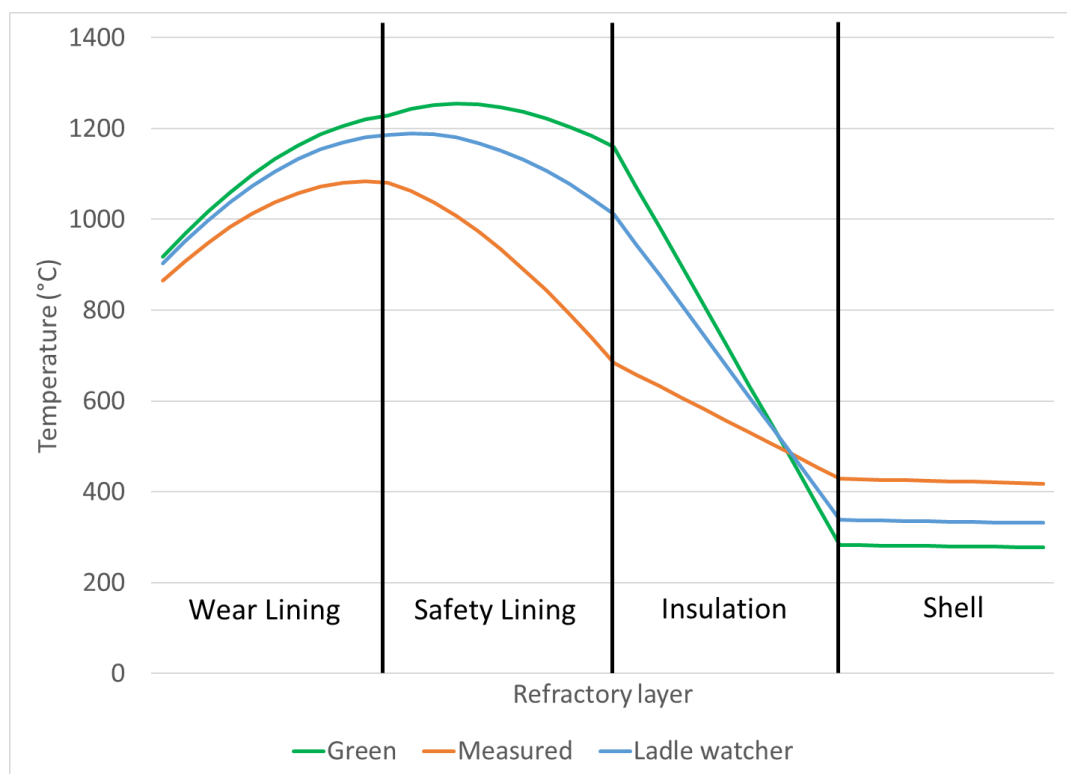
Figure 69: Ladle wall thermal profile empty 1.5 hours without a lid with Green, measured and estimated properties.

105
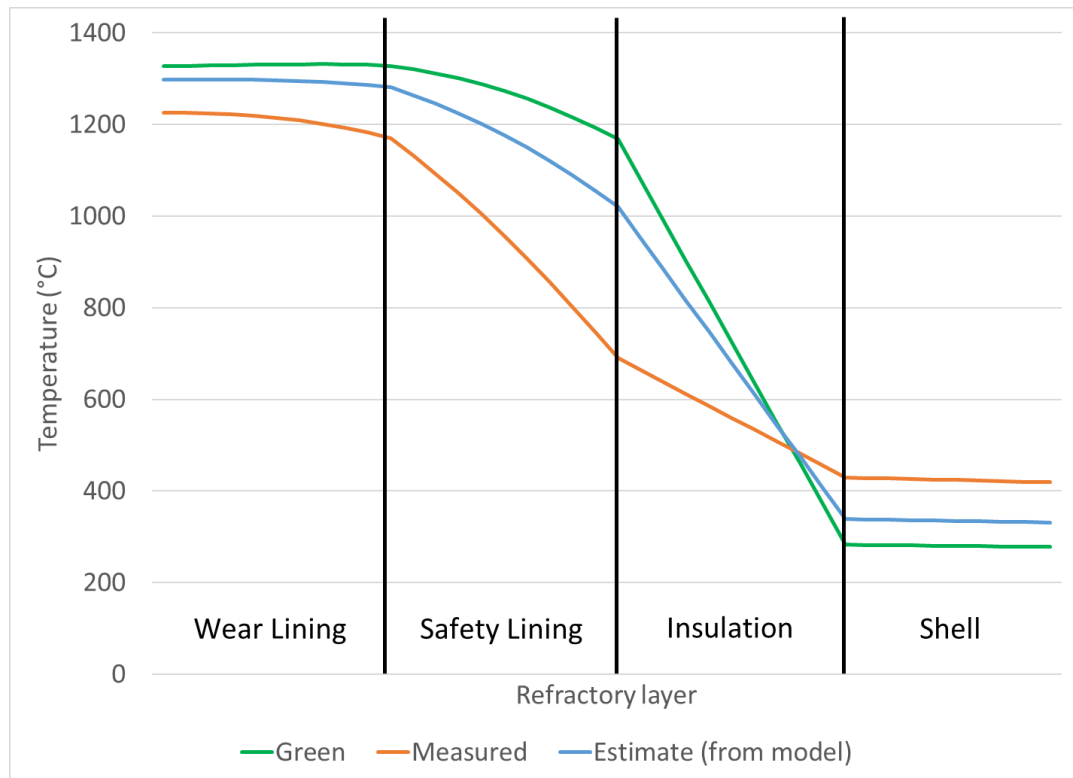
Figure 70: Difference of thermal storage for Green, measured and estimated properties of insulation.

5.4 Lidding benefits

The modelled results from the previous section were able to demonstrate the benefits of using lids to decrease the temperature losses from the ladle. The scenario modelled an empty ladle that was lidded after 30 minutes, a relatively short period of time for production to complete this task. Therefore, it was decided to model scenarios where the ladle was empty for 40 and 60 minutes before a lid was applied. This then provided the benefits if there were delays in production. It was also apparent from the plant data that the common empty time of 1.5 hours is often exceeded. Therefore, extended empty times, known as "turnaround times", were modelled to verify the benefits of lidding for these scenarios. Figure 71 shows the results from the additional scenarios modelled and associated temperature losses from these scenarios as temperature benefits from ladle libs. The temperature benefits value was calculated from the different scenarios modelled and the temperature losses caused by the difference in temperature of the refractory profile and a fully saturated ladle. The temperature losses of the lidded scenarios were then compared to the unlidded scenarios and the reduction in temperature loss of the lidded scenarios was shown as a temperature benefit. It was found that by lidding a ladle within 30 minutes would save 6°C of temperature lost, compared to 60 minutes for a 1.5 hour turnaround time. This would equate to

significant quality improvements and savings due to improved through process temperature management from ladle lids.
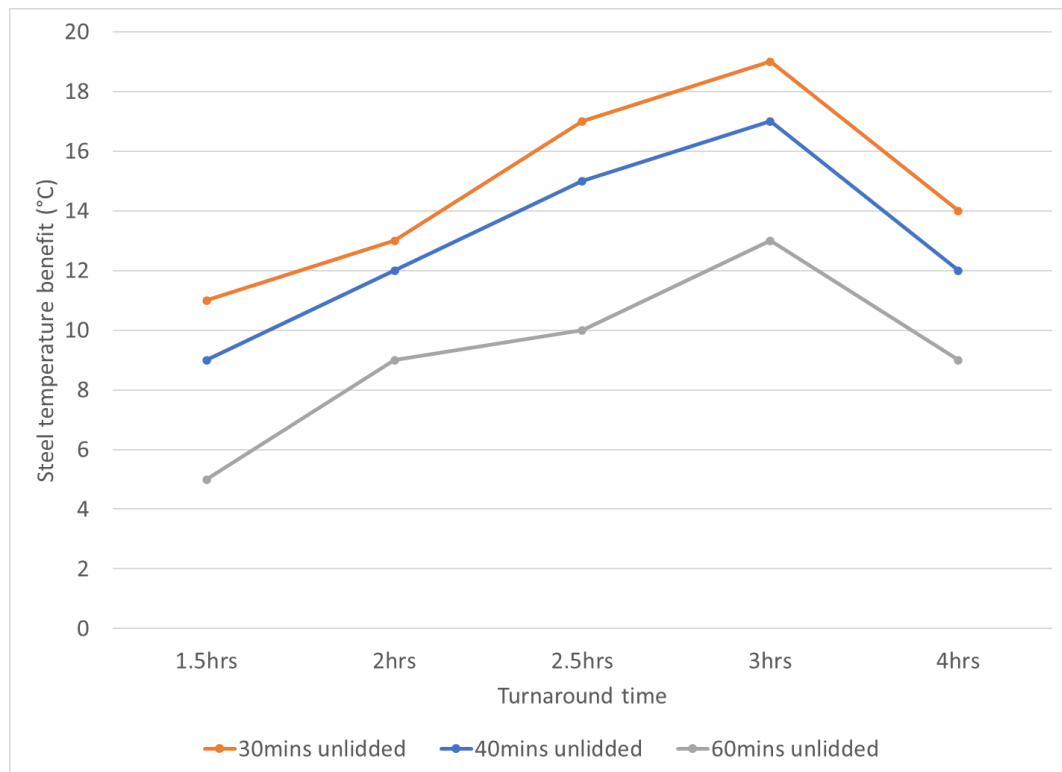
Figure 71: Graphed benefits of ladle lids with 30, 40 and 60 minutes ladle empty without lid before lidded.

5.5 Precast bottom effects

It was found that the ladle bottom accounted for a temperature loss of 2°C during a 1.5 hour cooling period. This figure was constant regardless of the precast bottom thickness. It was therefore concluded that the bottom refractories had little effect on steel temperatures when compared to the more significant temperature losses from the barrel refractories. With regards to thermal efficiency of the ladle bottom it can be concluded that the longevity of the bottom be the prime focus to reduce ladle repairs and relines. Little is required in terms of temperature management or thermal improvement. However, it was noted that there is a difference in the temperatures at the safety lining and precast bottom interface, which can be seen in Figure 72 and Figure 73. This difference peaks in the 1.5 hours of cooling with a difference of 150°C between the minimum and maximum thickness. This then also accounts for the temperature differences measured between the thermocouples and the model output as previously discussed in Chapter 3.
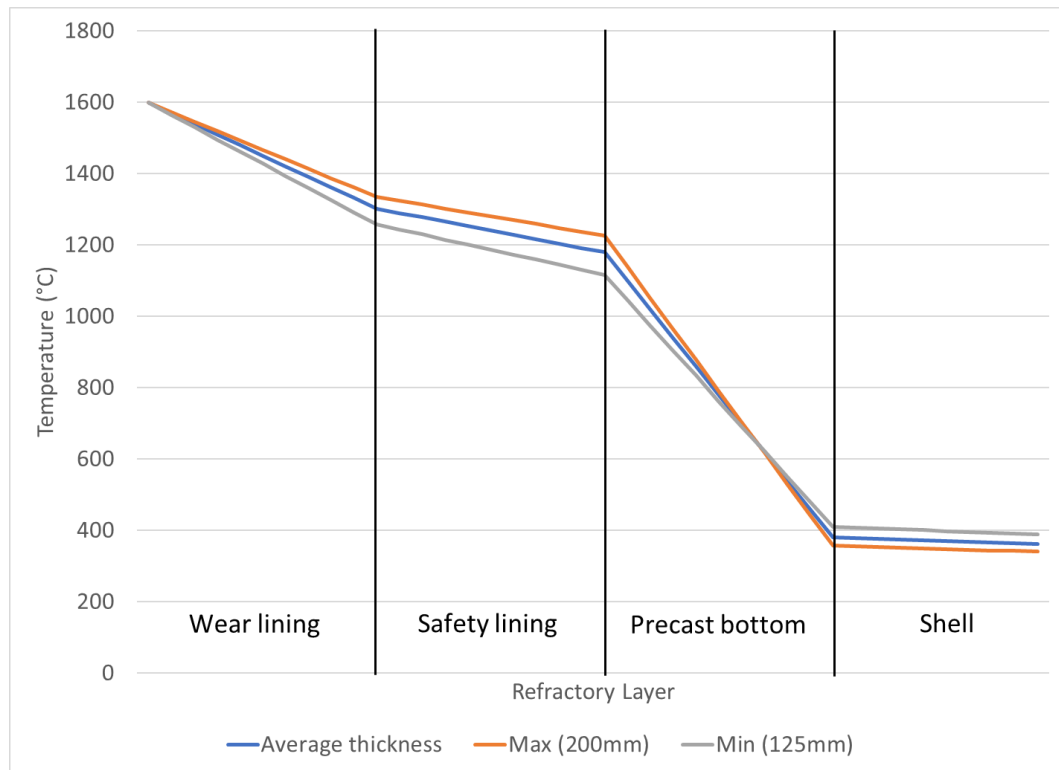
Figure 72: Ladle bottom with thermal equilibrium and variations in precast bottom thickness.
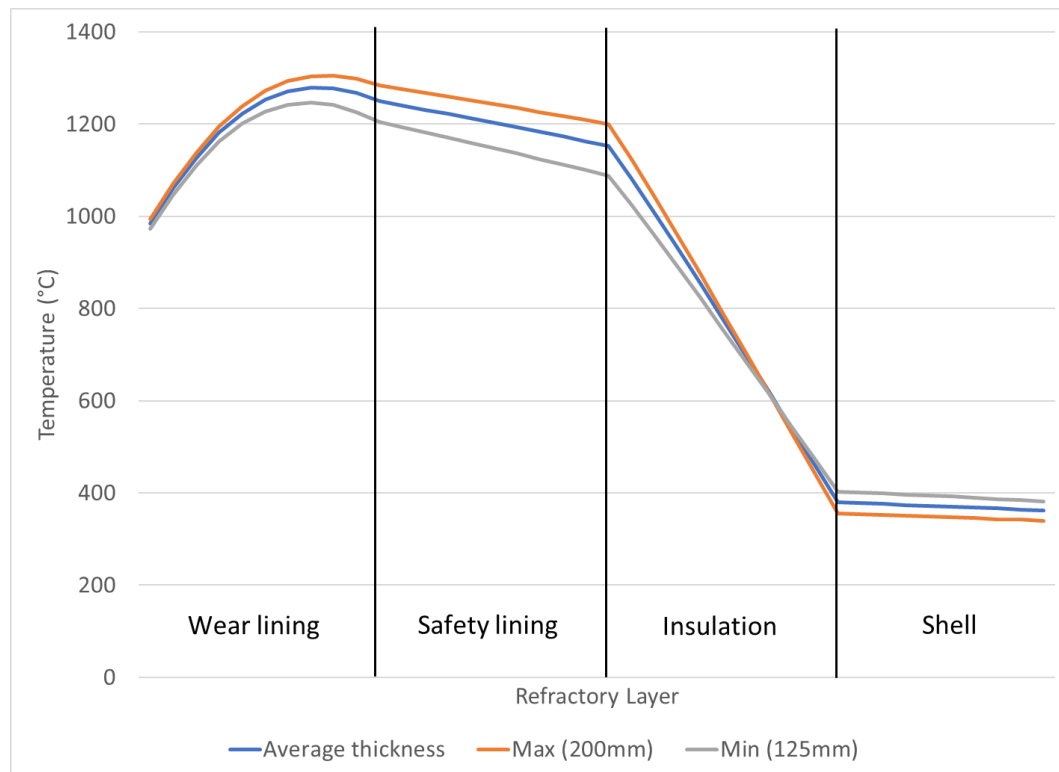
Figure 73: Ladle bottom thermal profile after ladle empty for 1.5 hours without a lid.

5.6 Conclusions

From the findings in this chapter it is possible to conclude that the degradation in ladle insulation has minor effects on product quality and thermal efficiency of steel

production, which disproves H2b. However, it does have a large effect on safety, and it was possible to show the degradation in insulation increased the ladle shell temperatures by 146°C. This has a significant effect on the ladle shell service life and in-turn the financial impact on the asset owner. The importance of accurately measuring the ladle insulation properties is a safety concern rather than a financial impact. The degradation in insulation only increased the cooling effect by 1°C. However, it was possible to demonstrate the benefits of using ladle lids. For the simulated ladle it was possible to show that a lid would reduce the cooling effect of the ladle by 8°C. The time the ladle is empty before a lid is applied was also investigated and it was found that a 30 minute delay caused an additional 6°C of cooling. This has a large financial impact (estimated to be £0.8-1.1mil/annum using Buhr et al.'s (2016) calculation (31)) and the author suggests future work should focus on reducing the time a ladle is empty before a lid is applied. The thermal profiles for the different scenarios modelled also showed that, if the history of the ladle state could be accurately recorded, the hot face temperature could be used to predict the cooling effect from the refractories, thereby disproving H3.

The approach used to quantify the cooling effects of the refractories relied heavily on the temperatures of the refractory material. Therefore, it is of high importance that the model tracks the ladle with a high level of accuracy. The suggestion from the literature was that a calibration point would increase the accuracy of thermal models. However, getting an accurate thermal measurement to calibrate the models was demonstrated to be a challenge. Thermocouples displayed a large amount of variability, can only track one ladle at a time and require a high investment of time to conduct a single trial. Therefore, it is not possible to rely on thermocouples for model calibration for a long-term strategy. If thermal imaging could accurately measure the ladle hot face this would provide the calibration point needed to improve the accuracy. Thermal imaging cameras can also be strategically placed to capture data on an entire ladle fleet with one camera. Therefore, the next chapter focuses on increasing the accuracy of thermal imaging.

Chapter 6 – Emissivity measurement and utilisation of ladle geometry enhancement for accurate thermal measurement of ladle hot face

6.1 Introduction

This chapter will address the final two questions from the literature review. From Q4 it was stated that the variability in the emissivity did not make it possible to get accurate measurements with a radiometer even with the enhancement from the ladle geometry (H4). It was possible to deduct from Q5 that accurate measurements of the hot face could not be used in combination with a thermal model to act as a calibration point for a thermal model (H5).

Thermal imaging is the ideal technology to act as a calibration point for online thermal models designed to track refractory temperatures in teeming ladles. The ability to measure surface temperatures from a distance and have a fixed point in the process where data on all the ladles can be gathered is what makes this technology so appliable. If the variability of the emissivity could be nominalised, and in turn the accuracy increased to a reliable level, it would be possible to utilise a thermal imaging camera for this purpose. To accurately determine the thermal efficiency of a refractory lining it is essential that the hot and cold faces are accurately measured. This data can then be used to increase thermal modelling accuracy so it can then be utilised to understand the steel cooling effects from the ladle. This would then provide production with the necessary information to heavily reduce unnecessary reheating and improve product quality. This chapter will outline the experiments performed to determine the spectral emissivity values of the teeming ladle refractory bricks and slag, and how the geometry of the ladle can be utilised to enhance the emissivity and subsequently reduce the emissivity variability. With this improved accuracy thermal imaging can now be used to accurately measure the refractory hot face and act as the calibration point needed to improve the accuracy and reliability of refractory thermal models.

Thermal imaging is a non-invasive form of temperature measurement that can be strategically placed to monitor an entire ladle fleet during production. Because of this it has the advantage over thermocouple technology and other contact thermometry which can only monitor one ladle at a time. Therefore, the desire to get accurate thermal imaging data has been the attention of several research studies, which were

discussed in detail in Chapter 2. The previously published academic research on the emissivity of refractories and slags has limitations in the experimental approach and the system errors are not quantified in these studies. The two most comprehensive and relied on studies found in the literature were produced by Glaser et al. (2011) and Jain et al. (2004) (24,42,51). However, these are not without fault as neither study accounts for the ladle geometry or background radiation effects. Glaser et al.'s study used incompatible wavelengths for the temperatures measured and Jain et al.'s study did not consider the effect of decarburisation of the refractory during measurement. This is somewhat surprising as geometry enhancement of radiometry is well understood and utilised in the production of blackbody cavities for radiometer calibration (6). Therefore, the geometry enhancement needs to be considered in the measurement of teeming ladle refractories when measuring the hot face.

To further knowledge in this field this chapter details the design and implementation of accurate methods for the measurement of the spectral emissivity through collaboration with Zhu (61) and The University of Sheffield. This experimental setup was able to measure the emissivity of materials to an accuracy of 0.0820 (k=2) in an inert atmosphere. The inert atmosphere is relevant as it heavily reduces the decarburisation errors identified in Jain's study (51). The experimental setup also accounts for the background radiation errors that are present in both Glaser's and Jain's studies and removes these through the use of a radiation shield (24,51,61). By utilising the equation of a cylindrical cavity in the MSL Technical Guide 35 – Emissivity of Blackbody Cavities it was possible to account for the geometrical enhancement of the ladle (6). This then made it possible to apply a single emissivity value to the ladle, which reduced and provided good understanding, of the error in °C from using that single value. The equation for a cylindrical cavity can be seen in Equation 6.

Emissivity is not the only factor that needs to be considered to ensure an accurate temperature measurement is recorded. The spectral radiance at different wavelengths and temperatures can be seen in Figure 6. The spectral radiance is the intensity at which a body radiates at a given wavelength. An example of this is when a body is heated to 625°C it appears to glow to the human eye. This is because the spectral radiance has increased to a level that can be registered by the sensitivity of the human eye in the visible wavelengths (0.4 – 0.7µm). This same principle can be applied across

the whole electromagnetic spectrum. The sensors used in pyrometers and thermal imaging cameras are selected to detect the wavelengths that correspond to the peak in spectral radiance at the object's temperature. As the peak radiance moves across the wavelengths the change in radiance received at those wavelengths also changes. This change in radiance changes the incoming signal for a pyrometer or thermal imaging camera and is what enables the temperature measurement of an object. If this signal change is large, for each °C change in the object temperature, the pyrometer or thermal imaging camera is better able to interpret the signal change and the potential for measurement errors is reduced (5).

Boone et al. (2018) were able to use this concept of spectral radiance changes with wavelength and determine how a deviation in emissivity is linked to a change in temperature for a radiometer (5). The equation Boone used for this is shown in Equation 5 (5). This information is contained in Table 2, which shows an emissivity deviation of 0.01 of a body at 800°C changes the recorded temperature by a LWIR radiometer by 7.7°C and a NIR radiometer by 0.7°C. It is worth noting that the current accuracy of emissivity predictions used is rarely within ±0.2 of the actual emissivity and, therefore, the measured temperature errors exceed ±140°C for a LWIR as used in Glaser et al.'s (2011) study (24). However, through the spectral measurement of the refractories and slag and application of the geometry enhancement this study has shown that the temperature measurement error can be heavily reduced.

6.2 Emissivity measurement

6.2.1 Equipment

Zhu et al. (2019) proposed a systematic isolated test procedure in which a material has a controlled environment and the furnace temperature deviations during emissivity measurements are accounted for (61). The method used in Zhu's study is able to measure the emissivity of a sample with a system error of 0.0820 (61). This uncertainty accounts for many variables including the changes in temperature of the sample during measurement and the accuracy of the temperatures measured. The system error is not presented in Glaser's or Jain's studies but. due to the cooling and background radiation of the furnaces, it is certain that the system error would be larger than Zhu's study (24,51). The measurement equipment also utilises a twin radiometer system where a blackbody is measured in-situ with the sample. A ratio is then used to calculate the emissivity of the sample. The temperatures of the blackbody were recorded with both

the furnace temperature monitor and a thermocouple was used to verify this figure. The radiometers used to measure the emissivity of the sample were in the spectral range of 0.85–1.1µm, which gives the largest level of accuracy in the measured temperatures of 800 – 1000°C. Therefore, this measurement procedure considered the variations in temperature of the sample, measured at the correct wavelength for the tested temperatures and accounts for the internal errors caused by the sensors in the radiometers. The equipment used in Glaser's study measured outside the recommended spectral range for the emissivity measurements. Both Glaser's and Jain's studies do not account for the temperature reductions of the sample surface, whilst the experiments allowed time for the background radiation to dissipate. Because of these reasons it was deemed necessary to measure the emissivity of the refractories and slag and adopt the measurement technique used in Zhu's study to acquire accurate spectral emissivity values of the materials recovered from the ladle. A schematic of the measurement equipment can be seen below in Figure 74.
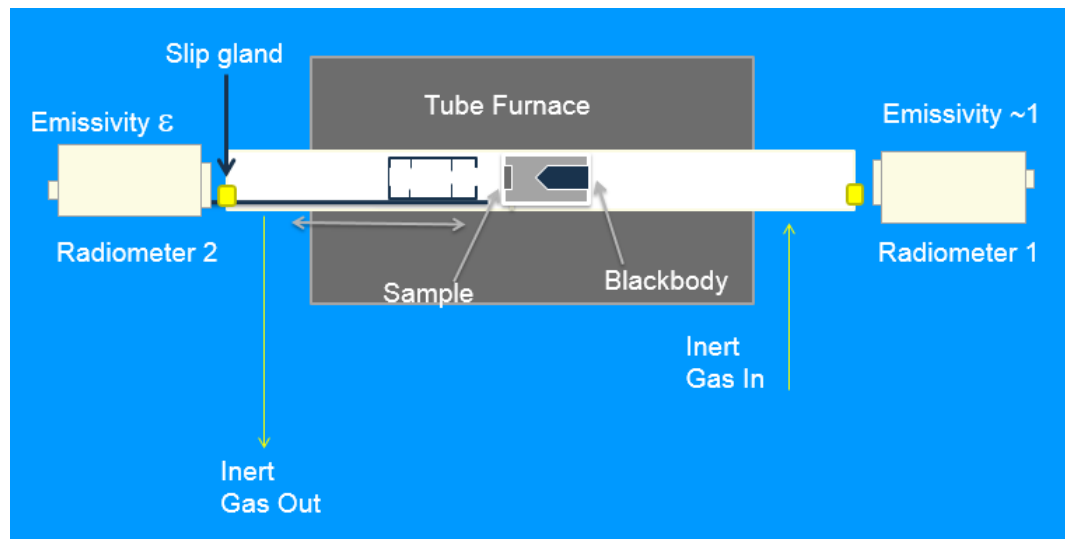
Figure 74: Equipment setup from Zhu et al. (2016) (61) *Copyright of The University of Sheffield.*

6.2.2 Measurement procedure

To measure the emissivity of the refractory and slag in a teeming ladle a sample of the material was heated in a tube furnace. The procedure used to measure the emissivity of the samples followed the same steps as detailed below and in Zhu's study (61):

1. Samples were cut to size and shape to fit into the housing.
2. Samples were mounted in the housing and then pushed into the centre of the furnace.

3. The radiometers were then calibrated and aligned to focus on the centre of the blackbody and the centre of the sample. The blackbody cavity was verified to be within the specified tolerances and the maximum uncertainty caused by the blackbody was estimated to be 0.0071.

4. The furnace was then heated to 200°C and held for 2 hours to remove any moisture.

5. The furnace is then heated to 1000°C (the highest temperature for measurement) and then stabilised for 30 minutes before the first measurement was taken. Even after stabilisation the variation in equilibrium of the equipment account for an uncertainty of 0.0040.

6. The radiation shield was then pushed into place to block the effect of background radiation during the emissivity measurement. The variability of positioning added an uncertainty of 0.0040.

7. The temperatures of the sample and blackbody are then recorded and used to calculate the emissivity of the sample as the blackbody emissivity is known. Once data is collected the shield is then retracted from the furnace. The minor temperature variation between the sample and blackbody accounted for a maximum uncertainty of 0.0176.

8. The furnace is then left to re-stabilise for 15 minutes to ensure the correct temperature of sample before recording the second measurement at test temperature and repeating steps 5 and 6.

9. Furnace temperature is then set to next measurement temperature, reducing the temperature by 100°C each time, and held for 30 minutes so the sample and furnace can re-stabilise.

10. Steps 5 to 9 are then repeated until all data is collected from the sample.

Where applicable the uncertainty errors have been matched to the points in the method to which they are related. Errors that were not included are electronic noise, thermocouple error, responsivity correction of the two pyrometers and fluctuation in temperature of the radiation shield and sample. Zhu (2019) quantified the total uncertainty in the form of the maximum relative combined uncertainty of 0.0820 for the equipment (61).

6.3 Results and discussion

The results gathered using this method will be discussed in this section. The geometry of the ladle is also utilised to reduce the emissivity errors further and increase the accuracy of ladle hot face thermal image data.

6.3.1 Spectral emissivity results

The raw data from the measurements are displayed below in Table 11. During testing some of the samples were visibly decarburised after taking the measurements at the higher temperatures. This provides the largest difference in terms of spectral emissivity, so these values are still valid. The slag showed very little decarburisation and was often the highest tested emissivity value throughout the temperatures. The largest difference is displayed for each sample as well as the average across the individual sample and temperatures. The maximum difference between the samples is then also shown in Table 11. This difference is used to determine the error in temperature (°C) if the measurement was taken with a LWIR or NIR radiometer, calculated from Equation 6.

Sample	Emissivity	Temperature (°C)		
		800	900	1000
New bottom brick	Test 1a	0.4820	0.5187	0.6483
	Test 1b	0.4824	0.5115	0.5892
	Test 2a	0.6033	0.6661	0.6806
	Test 2b	0.6506	0.7256	0.6666
	Mean emissivity	0.5546	0.6055	0.6462
	Difference + system error	0.2496	0.2952	0.1724
New barrel brick	Test 1a	0.4266	0.4958	0.6916
	Test 1b	0.4299	0.4704	0.6860
	Test 2a	0.6069	0.5582	0.5188
	Test 2b	0.4937	0.5017	0.5533
	Mean emissivity	0.4893	0.5065	0.6124
	Difference + system error	0.2613	0.1689	0.2538
Slag	Test 1a	0.6865	0.6604	0.6588
	Test 1b	0.6845	0.6697	0.6387
	Test 2a	0.7641	0.7291	0.7294
	Test 2b	0.7978	0.7075	0.7183
	Mean emissivity	0.7332	0.6917	0.6863
	Difference + system error	0.1943	0.1498	0.1717
Max - min emissivity + system error	NIR	**0.4532**	**0.3408**	**0.2926**
Max - min emissivity converted to °C error	LWIR	349	262	225
	NIR	32	24	20

Table 11: Results from spectral emissivity measurements of slag and refractories.

Figure 75 shows the mean emissivity values of the different samples in Table 11. The error bars in Figure 75 are calculated by the maximum difference in the sample plus the system error of the measurement method.
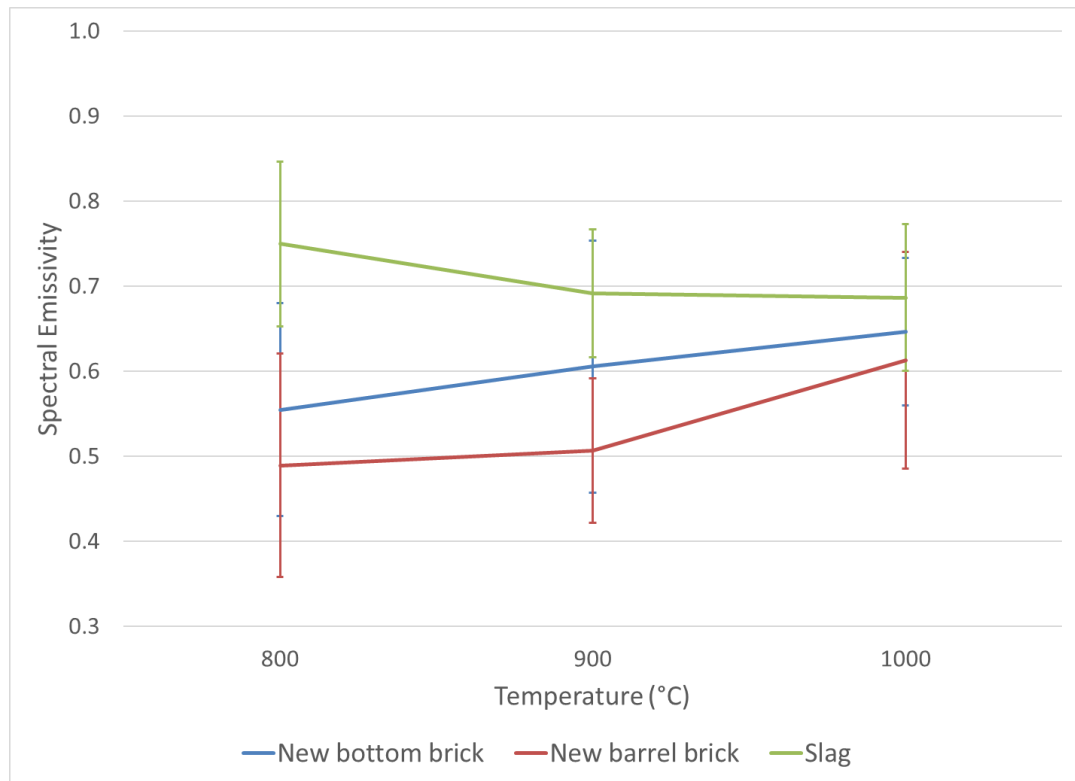
Figure 75: Spectral emissivities measured with error bars.

Figure 76 is a graphical representation of the measurement errors caused by using a LWIR and NIR radiometer for these temperatures. This is a comparative error from the results in Table 11 if a similar study was conducted for the LWIR and factored in system error. This comparison would also apply if a prediction for emissivity were used and accurate to the errors found. This has previously been stated as being unlikely and the error would be significantly larger for common use of thermal imaging cameras. As previously mentioned, Glaser (2011) does not calculate the system error of his method measured at LWIR. The resultant system error will be larger than this study because of the cooling and background radiation (24). Therefore, the quantification of the LWIR temperature error below is a good estimate for the Glaser (2011) study.

117

Figure 76: Max temperature error of refractory hot face due to differences in spectral emissivity measured for LWIR and NIR wavelengths.
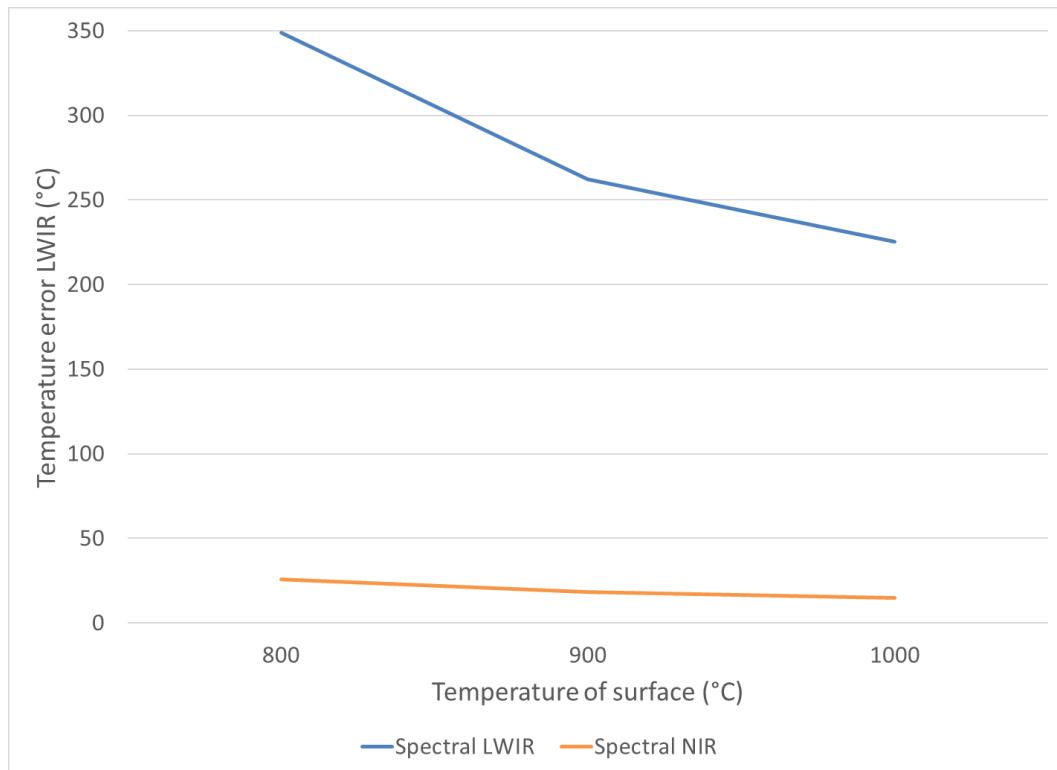
6.3.2 Emissivity enhancement results

Emissivity enhancement essentially removes the error caused by different spectral emissivity values. From this it was then possible to compare the errors of the different wavelengths. Whereas previously it must be assumed similar errors were caused by wavelengths, here the reduction in error makes that assumption more valid. Due to the geometry of the teeming ladle it is possible to benefit from the enhancement of the emissivity when measuring the hot face of the refractories. This concept of geometry enhancement is well understood and utilised in the production of blackbody cavities (6). Blackbodies are the standard used to calibrate radiometers, using the principle that the more an object absorbs radiation the higher the apparent emissivity. This then can be used to create geometries that reflect the radiation internally and increase the absorption of the cavity. Therefore, the emissivity of the system is increased.

This method is very successful with blackbodies having a calculated emissivity as high as 0.99995, i.e almost the theoretical maximum. Measuring the teeming ladle hot face perpendicular to the ladle bottom creates less enhancement due to the geometry being an approximate, but not a perfect approximation, to a blackbody cavity. Consequently, it is possible to utilise the blackbody equations with the understanding that the ladle

geometry enhances the emissivity at all wavelengths. The ladle is most similar to the blackbody cavity for a flat-bottom tube as detailed in Equation 6. The geometry of a flat-bottom tube was utilised to calculate the enhanced emissivity of the ladle and reduced measurement error (6).

Utilising the similarity of geometry of a teeming ladle and a cylindrical cavity, Table 12 shows the resultant geometry enhancement of the emissivity values. This then produces subsequent reduction in variability of the emissivity between the refractory materials and slag. The system error was applied to the maximum and minimum recorded spectral emissivities at each temperature. This then gave the largest possible difference between these values but still accounted for the enhancement.

Temperature (°C)		800	900	1000
Max enhanced emissivity		0.96	0.95	0.95
Min enhanced emissivity		0.86	0.87	0.88
Max enhanced - min enhanced		0.10	0.08	0.07
Max - min enhanced temperature error (°C)	LWIR	80.4	60.4	51.9
	NIR	7.3	5.5	4.7

Table 12: Enhanced emissivities of all samples showing the extreme maximum and minimum values and the subsequent error produced.

From the findings in Table 12 it is now possible to set a thermal imaging camera's emissivity to 0.91 and record data with certainty that the temperatures recorded between 800 and 1000°C were accurate to within ± 5°C. Figure 77 is a graphical representation of the data in Table 12, where the error bars take into account the difference in measured emissivity and the system error of the measurement method.
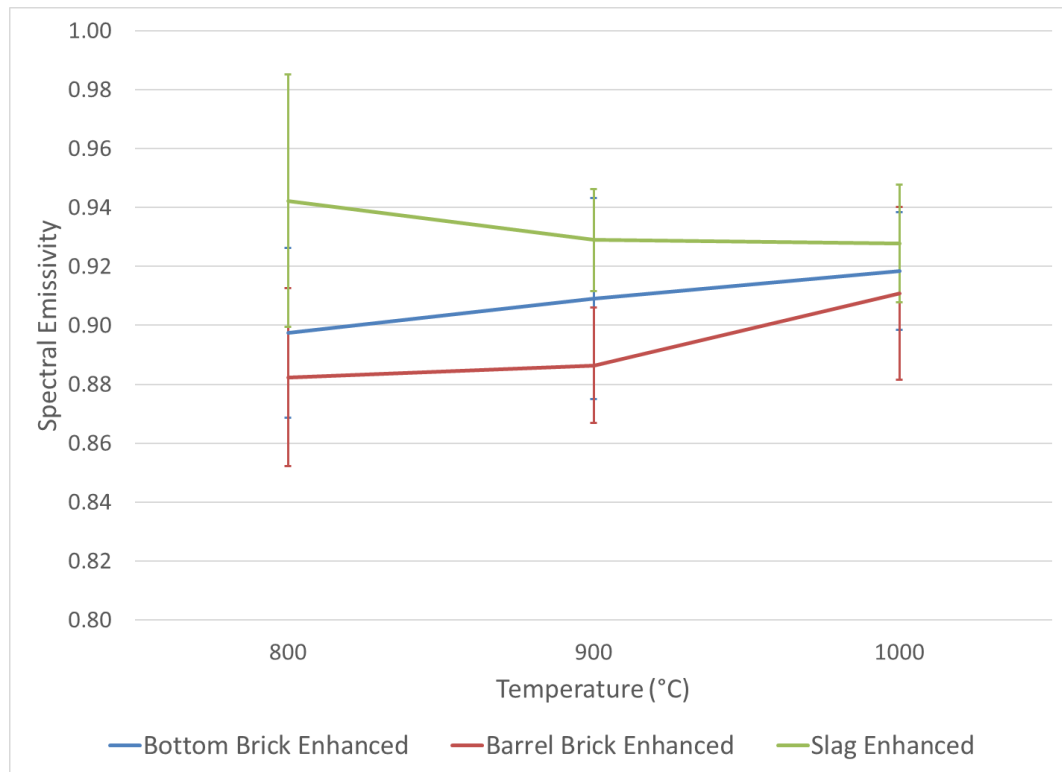
Figure 77: Enhanced emissivity values of refractories and slag from Table 12.

Figure 78 shows the maximum error due to the variation in the enhanced emissivities of the refractory and slag of a teeming ladle. Due to the enhancement of the emissivity the errors produced by both cameras is greatly reduced when compared to the spectral emissivity errors. It does also show that even with the emissivity enhancement the correct wavelength needs to be selected based on Plank's radiation law in Figure 6.

Figure 78: Errors at different wavelengths with spectral and enhanced emissivity differences.

6.3.3 High definition thermal imaging

Using the enhanced emissivity measurements calculated it was then possible to take measurements of a teeming ladle with a high definition thermal imaging camera developed at The Uni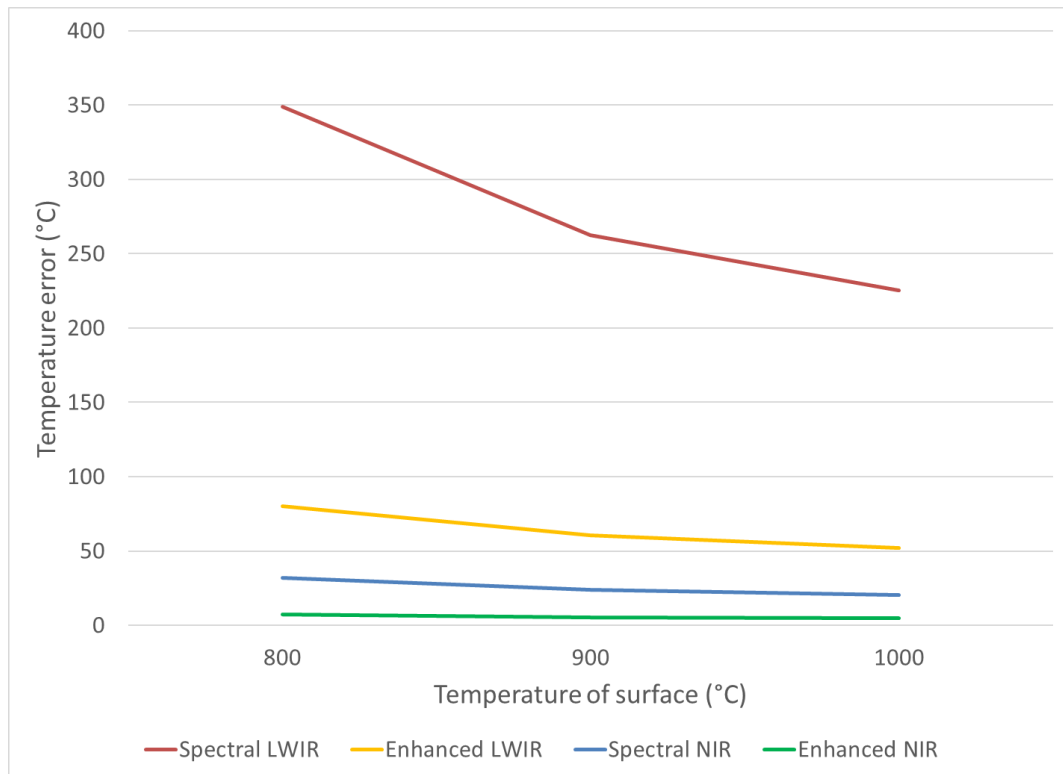versity of Sheffield. This camera utilises a DSLR camera and removes the RGB filters to get a light intensity that can then be interpreted with the emissivity value to give an accurate temperature (83). The high definition of the DSLR sensor provides a much higher density of information. The differences in textures were apparent in the bottom of the ladle. It is now possible to highlight areas where refractory bricks can be seen and it is also possible to tell the differences between the slag and frozen steel. The areas highlighted in Figure 79 show the different surfaces. The red circle shows an area of refractory that was exposed. It is clear this is an area refractory because the outlines of the bricks are visible due to the definition in the image. The white circle highlights cast steel in the bottom of the ladle that is due to the more uniform appearance than the refractories but smoother topography than the slag. The yellow circle highlights an area of slag that has adhered to the bottom of the ladle and was not removed during the tipping of the ladle after casting. The rough topography and lack of brick outlines are the characteristics of this being slag. The steel is shown to have an intensity in the image between the refractory and the slag. It

121

can therefore be concluded that the emissivity of the steel was within the range of these materials measured and does not warrant further testing. It was possible to determine this because when ladles are wrecked and tipped the steel and slag is still present and have very different physical appearances, as shown in Figure 80 and Figure 81.
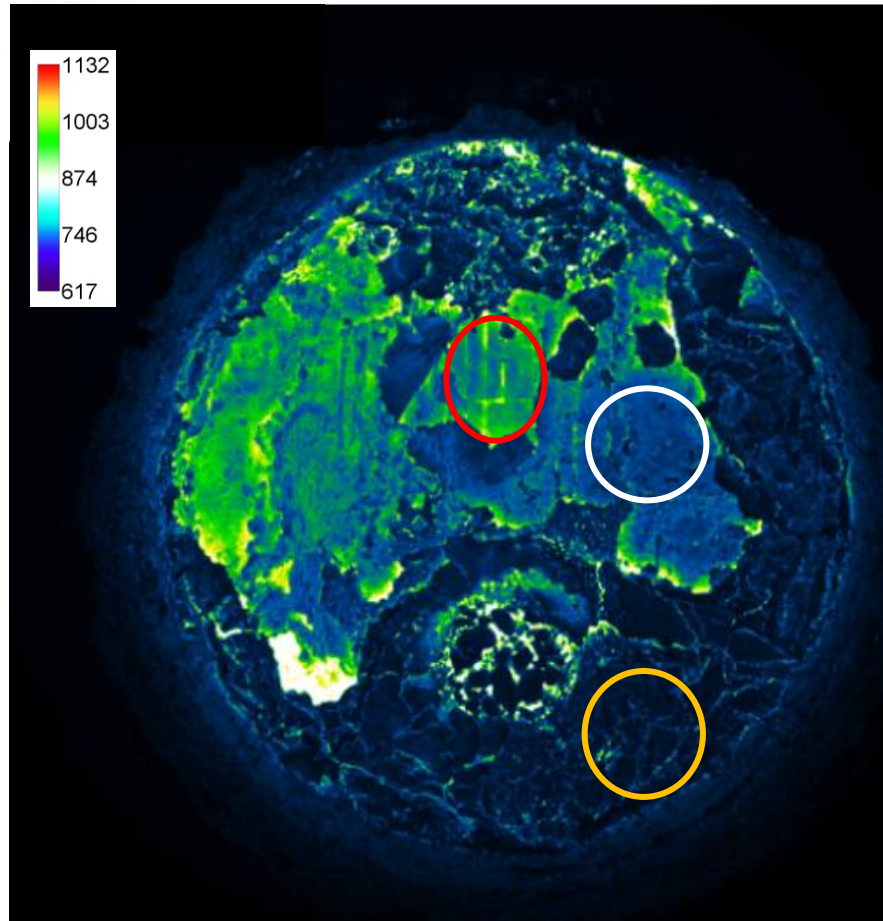
Figure 79: High definition thermal imaging camera utilising equipment detailed in Boone et al.'s (2018) study (5) scale shows temperature of object in °C.

Figure 80 shows a sample of slag that was taken from a ladle and Figure 81 shows a steel sample that was taken from the same ladle. The difference in topography of the frozen steel and slag is notable and makes it possible to characterise the areas in Figure 79. Through a basic brittleness test it was possible to determine the sample in Figure 80 was slag and the sample in Figure 81 was steel. This was verified through XRD analysis, which confirmed there was minimal iron present in the slag sample in Figure 80 but the steel sample was mostly iron in Figure 81.

Figure 80: Slag sample collected from ladle.



Figure 81: Steel sample collected from ladle.

Figure 82 shows the teeming ladle in the lade pits during the process of melting the steel and slag in the well block ready to re-sand the ladle to heavily reduce losses of containment and allow free flow of the steel at the CCs. This image highlighted the

importance of selecting the correct scale for the object as there is a lot less detail visible in Figure 82 than in Figure 79. It is important to note the temperature scale is correct for both images, however, the refractory surface in Figure 82 is hotter and falls into an area of the scale that makes it difficult to interpret the surface textures and negates the high definition of the image produced. This increases the difficulty in the analysis of surface textures to interpret the quantity of steel and slag in the bottom of the ladle. Therefore, this needs to be taken into account when selecting the correct scale and was a learning from the data set collected.
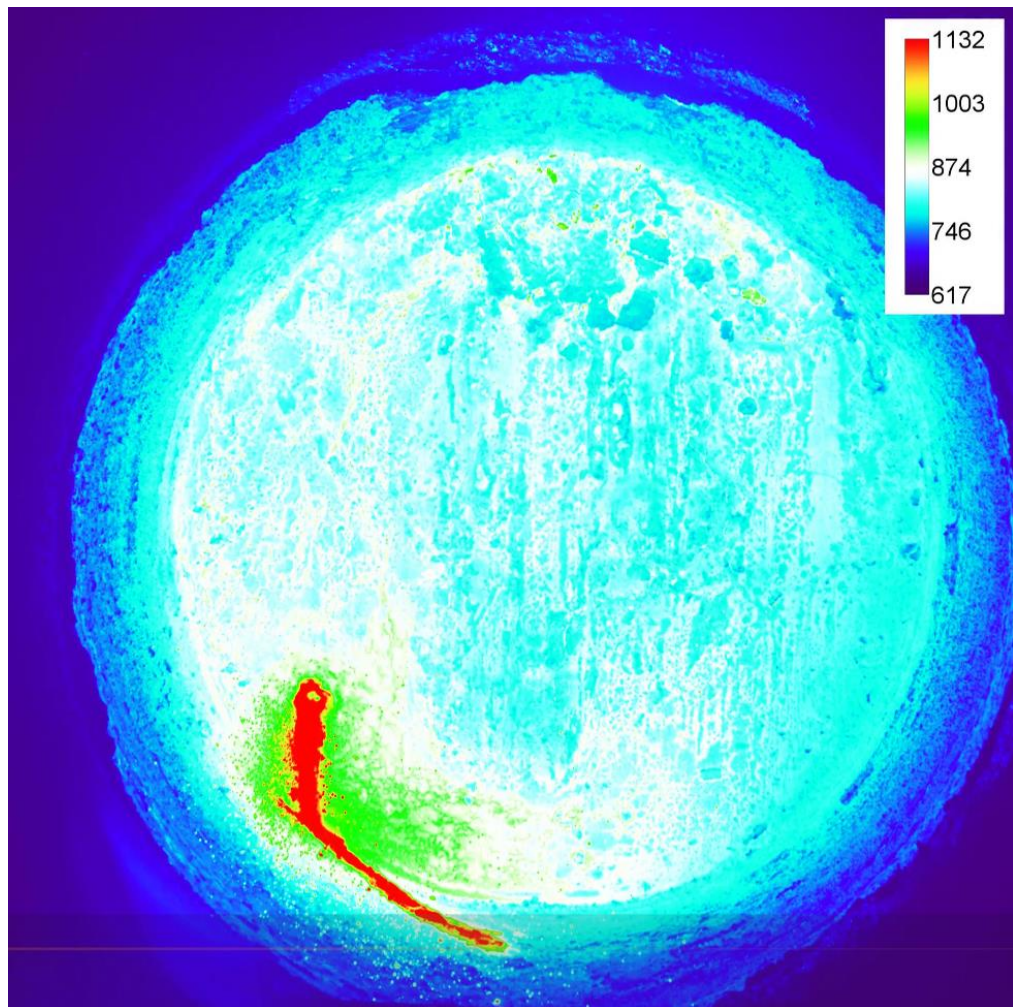
Figure 82: Image of teeming ladle during melting of steel and slag in well block ready for re-sanding the ladle to greatly reduce the likelihood of losses of containment, scale shows temperature of object in °C.

6.4 Conclusions

Previous literature on refractory and slag emissivity measurements had limited information and understanding regarding the system errors introduced from the methods adopted. The work presented utilised a method with a quantified uncertainty of 0.0820 of the measured spectral emissivity values. Both refractories and slag were

measured at the correct spectral response for production temperatures. Utilising the research into geometry enhancement of emissivity, and applying the theory to teeming ladles, it was possible to create emissivity independent data with an accuracy of ±5°C in the temperature range of 800-1000°C, thereby disproving H4. This is much lower than the predicted accuracy of ±175°C when using LWIR and the spectral emissivity methods adopted in the Glaser (2011) study. Now this level of accuracy for emissivity has been achieved, with a reliable method of measuring the emissivity, it can be used to accurately measure the ladle hot face regardless of whether the ladle is coated in slag or steel. The differences found between the slag and refractory emissivity are included in the temperature error stated. Now the refractory temperatures can be accurately measured they can be used to quantify the cooling effect on the steel during transport combined with the use of a thermal model and disproves H5. This can then give greater accuracy to through process temperature control and reduce unnecessary reheating and cooling, thereby giving an increase to product quality.

The geometry enhancement can apply to other steelmaking vessels, including hot metal ladles and converters. With this enhancement and the benefits of the higher resolution images it is possible to improve analysis of temperature fluctuations from the cooling effect of refractories. This improves the through process temperature controls throughout the process and further benefits the product quality.

Conclusions

The review of the literature informed five research questions (Q1-Q5) and generated five associated hypotheses (H1-H5) that this thesis has attempted to answer.

It was theorised that the ladle insulation degradation caused significant losses to steel temperatures during production. After thermally charactering the insulation via in-situ thermocouple trials, it was possible to determine the peak temperatures it was subjected to were 1040°C. This value was then used to perform thermophysical testing on the insulation samples to quantify the degradation of the material. The degradation in the insulation was primarily from an increase in density and this study was able to demonstrate that the density increased from $260kg/m^3$ to 759.6 kg/m^3. This thesis was able to quantify the in-situ thermal properties of the microporous insulation and determine that, even with a significant increase from 0.039W/m.K to 0.15W/m.K, had a negligible effect on the cooling of the transported steel when compared to lidding of ladles. It was verified that this created a loss in thermal storage in the safety lining and wear lining. However, no significant cooling was created when comparing the Green properties and in-situ properties. The effect of lidding was found to be consistent for the Green and in-situ scenarios and, even with the reduced thermal storage, the benefit of the lid remained constant. It was found that lidding a ladle when it is empty saved 11°C in temperature losses, whereas the degradation in insulation increased the temperature losses by <1°C. Emphasis for increasing the thermal efficiency of teeming ladles should be placed on using lids rather than insulation alone. The insulation degradation did increase the thermal loading on the ladle shell. The simulated shell temperatures validated the temperatures recorded by the thermocouples. This in turn highlighted issues of the thermal imaging cameras used to monitor ladle shell temperatures. The author suggests that the thermal imaging cameras used to monitor ladle shells should be validated through emissivity studies to ensure they are not producing false data.

The author was unable to find evidence in the literature of a thermal model with a temperature calibration point from production data. It was concluded this was due to the personnel hours required for thermocouple data and the errors produced in thermal imaging measurements. An emissivity study was performed on ladle refractories and slag combined with the geometry enhancement of the teeming ladle. It was possible

to produce emissivity independent thermal images with an error of ±5°C. With this accuracy it is now possible to create a calibration point and a step change in predictive thermal modelling of refractories in a ladle.

Future work

Previously it was stated that the unknown changes in the microporous insulation created a large amount of uncertainty to the thermal losses in steelmaking. The only quantifications that could be found compared the refractory profile with and without the insulation layer. The insulation properties were quantified using LFA, which has conflicting suitability in the literature and could suggest it is not accurate for a low thermal conductivity material. However, with the large increase in the thermal conductivity of the insulation material, and the limited effect it has on liquid steel temperature retention, it suggested the quantification was sufficient. This work has been able to quantify the degradation in the insulation layer and conclude that it has little effect. From this the doubt over the effect of the insulation layer has been removed. The author suggests modelling should focus on quantifying the temperature losses due to the ladle and process. Future work should look to include slag and residual steel to the quantification of the temperature losses to increase the accuracy of the prediction. The microscopy used was not able to quantify the porosity present in the silica particles and could not conclude whether the cracks present in the Green material increased the porosity significantly. It is recommended that future studies use microscopy techniques that have the necessary magnification to quantify this porosity.

When the degradation in insulation properties were modelled it showed an increase in the thermal stresses across the safety lining. This could increase the degradation rate of the safety lining. When the safety lining is replaced, the insulation also must be replaced, therefore, both these layers need to be extended together to increase the service life. Future work should look to quantify the degradation rate of the safety lining to provide benefits to the steel manufacturer by extending the service life of the refractory safety lining layers.

It was stated that if a model could have a temperature calibration point this would help reduce errors and drift from the actual temperatures in the ladle. The challenge previously was that the accuracy of the temperature measurement was insufficient. Thermal imaging cameras relied on spectral emissivity values and utilised cameras with unsuitable spectral responses to measure the hot face of a ladle. This then created large errors and prevented a reliable calibration point. With blackbody equations and accurate spectral emissivity measurements it was possible to reduce the emissivity

errors. The ladle hot face can now be accurately measured and a model with a calibration point is recommended as a step change in model accuracy that can then predict the cooling effects of the ladle in real time.

Thermal imaging cameras have been relied on to monitor ladle shell temperatures for several years. The understanding surrounding these cameras is of concern. The thermocouple study in this thesis was able to demonstrate the shell is subjected to much higher temperatures than the thermal imaging camera was producing. It is suggested that shell emissivity studies be performed. As thermal imaging cameras are often setup with an emissivity of 1, they give an underestimate to the shell temperatures. This means ladle shells are commonly subjected to higher temperatures than steel manufacturers are predicting. The high definition images gathered by Sheffield University and the author, utilising the collaboration developed by Tata Steel and Sheffield university, enable the possibility to distinguish between refractory, slag, and steel. Therefore, future work is recommended to validate these findings to quantify the residual slag and steel in the ladle to then determine the cooling effect this will have on the next production cycle. The high definition images can also detect joint formations in the bottom bricks and could act as a warning if bricks are at risk of coming loose. With development this could act as a warning system for production to repair this and extend the life of the refractory.

Industrial impact of research project

This study measured values for the microporous insulation at production temperatures and confirmed it was an important factor of safety for ladle shells. However, the study also showed it has limited effect on the cooling effect of refractories on the transported steel. This conflicts with several studies in the literature that state a degradation in the insulation would have a large effect on steel temperature but up until this research the in-situ properties were subjected to an educated guess.

It is now possible to take emissivity independent measurements of the teeming ladle refractory hot face with an accuracy of ±5°C regardless of whether it is coated in slag or not. This step was required before a model could economically be designed to have a hot face temperature input. Future work can now be conducted from these findings to create a model that has a calibration point with far more ease.

The cooling effects of refractories were found to correlate with previously published literature. However, with the in-situ insulation properties now known further emphasis can now be put on lidding. It was possible to demonstrate that the effect of ladle lids is far higher than the effect of insulation degradation, although in the literature it was concluded a doubled thermal conductivity would have a significant effect. The measured value was almost quadruple the value and had little effect compared to the speed of applying a ladle lid. If ladle lids can be used with a teeming ladle fleet within 30 minutes of the end of teeming it would save Tata Steel £0.8-1.1mil/annum. If ladle lids were used for every cycle, it would have a positive effect on the process that saves £1.5-2.1mil/annum in product quality.

The thermocouple data gathered in this thesis was able to highlight the teeming ladle shells were being subjected to temperatures above their service temperature. This is now being used to help justify a new teeming ladle fleet and has been used by a consultant to determine the risk of continuing to operate the ladle fleet with these elevated temperatures. The data will also be used to justify a change in the refractory build to reduce the thermal loading on the teeming ladle shells and has been used to justify a £6mil spend on new teeming ladle shells.

During the research project it was possible to analyse the ladle management system that tracks wear in the ladle for Tata Steel. With this analysis the author was able to highlight improvements that were implemented and saved Tata Steel £100k/annum in

refractory costs. This has amounted to more than £300k in savings on refractories at the time of writing and improved ladle availability, which in turn prevents plant stops and further reduces costs.

References

1. Institution BS. BS 1501 Steels for pressure purposes. Vol. 94. 1980. 1–35 p.

2. Glaser B, Görnerup M, Sichen D. Fluid flow and heat transfer in the ladle during teeming. Steel Res Int. 2011;82(7):827–35.

3. Gupta N, Chandra S. Temperature Prediction Model for Controlling Casting Superheat Temperature. ISIJ Int. 2004;44(9):1517–26.

4. Sichen D. Modeling related to secondary steel making. Steel Res Int. 2012;83(9):825–41.

5. Boone N, Zhu C, Smith C, Todd I, Willmott JR. Thermal near infrared monitoring system for electron beam melting with emissivity tracking. 2018;2–10.

6. Radiation B, Signal RT. MSL Technical Guide 35 Emissivity of Blackbody Cavities. 1992;(3):1–17.

7. Bi Y. Basics in refractories and their applications in steelmaking and casting. Vol. 1709825140. 2013.

8. Kleemans C, Bi Y, Siebring R. Ladle 11 breakout 13 May 2011 Report on CRC inspection 24 May 2011. 2011;(May).

9. Thomasberger J. Developments in Ladle Management System - better Energy, Materials and Asset Utilization in Steelmaking Process. 2014.

10. Ahualli FJ, Sagasti JG, Meyer S, Memoli F. Physical Ladle Tracking. AISTech - Iron Steel Technol Conf Proc. 2014;1567–76.

11. Jun C, Hong-Bing W. Ladle Monitor System Based on Vehicle Distance Measurement and Auxiliary Judgment Rules. In: 2014 International Conference on Identification, Information and Knowledge in the Internet of Things [Internet]. 2014. p. 262–5. Available from: http://ieeexplore.ieee.org/lpdocs/epic03/wrapper.htm?arnumber=7064043

12. USIT. USIT - Ladle Management System Brochure. 2017. p. 1–11.

13. Sintercast. Ladle Tracker (TM) - "Every Ladle, Every Minute." 2017. p. 1–2.

14. Siebring R, van Beurden P. Steel temperature loss of the Port Talbot steel ladle (2012). 2012.

15. Paul van B. Improving energy efficiency along the steel production route. In R&D Colloquium; 2014.

16. Specifications For Design And Use Of Ladles. Assoc Iron Steel Eng. 1991;August.

17. Specifications For Design And Use Of Ladles Part 2. Assoc Iron Steel Eng. 1991;(August).

18. Samuelsson P, Sohlberg B. ODE based modelling and calibration of temperatures in steelmaking ladles. IEEE Trans Control Syst Technol. 2010;18(2).

19. Samuelsson P, Sohlberg B. Modelling Heat Transfer in Multilayered Ladles - a Survey. In: SteelSim 2007. 2007. p. 164–9.

20. Zabolotskii A V. Model of heating of the lining of a steel-teeming ladle. Refract Ind Ceram. 2010;51(4):263–6.

21. Barber, B.; Zoryk, A. ; Walker KD. Process Model for the Determination of Liquid Steel Temperatures in the Ladle and Tundish. Process Technology Conference Proceedings- Iron And Steel Society; 1996. p. 131–6.

22. Zoryk A. On-line liquid steel temperature control. In: Steelmaking conference. 1993. p. 31–40.

23. Rong L, Nielsen P V., Bjerg B, Zhang G. Summary of best guidelines and validation of CFD modeling in livestock buildings to ensure prediction quality. Comput Electron Agric [Internet]. 2016;121:180–90. Available from: http://dx.doi.org/10.1016/j.compag.2015.12.005

24. Glaser B. Thermal Modelling of the Ladle Preheating Process. Steel Res Int. 2011;82(December):1425–34.

25. Santos MF, Moreira MH, Campos MGG, Pelissari PIBGB, Sako EY, Pandolfelli VC. Steel ladle energy saving by refractory lining design. 2017;1–24.

26. Campos MGG, Dos Santos MF, Moreira MH, Angélico RA, Sako EY, Pandolfelli VC. Holistic view of the insulating layer on the thermal efficiency of a steel ladle lining. Int J Ceram Eng Sci. 2020;2(3):113–29.

27. Santos MF, Moreira MH, Campos MGG, Pelissari PIBGB, Angélico RA, Sako EY, et al. Enhanced numerical tool to evaluate steel ladle thermal losses. Ceram Int [Internet]. 2018;44(11):12831–40. Available from: https://doi.org/10.1016/j.ceramint.2018.04.092

28. Samuelsson P, Sohlberg B. ODE-Based Modelling and Calibration of Temperatures in Steelmaking Ladles. IEEE Trans Control Syst Technol. 2010;18(2):474–9.

29. Vlček J, Jančar D, Burda J, Klárová M, Velička M, Machovčák P. Measurement the thermal profile of steelmaking ladle with subsequent evaluation the reasons of lining damage. Arch Metall Mater. 2016;61(1):279–82.

30. Beurden P Van. FEM based thermal process model of the Port Talbot steel ladle. 2016.

31. Buhr A, Bruckhaus R, Fandrich R, Dannert C. Trends in clean steel technology and refractory engineering. Stahl und eisen. 2016;136(9):25–34.

32. Wu P fei, Xu A jun, Tian N yuan, He D feng. Steel Temperature Compensating Model With Multi-Factor Coupling Based on Ladle Thermal State. J Iron Steel Res Int [Internet]. 2012;19(5):9–16. Available from: http://dx.doi.org/10.1016/S1006-706X(12)60093-4

33. Ogata M, Namba M, Uchida S, Maeda E. Saving Energy by using Working-lining Refractories with Low Thermal Conductivity. J Tech Assoc Refract. 2015;35:181–4.

34. Volkova O, Janke D. Influence of the Lining on the Thermal Behaviour of a Teeming Ladle. Steel Res Int. 2005;76(4):313–9.

35. Mazzetti-succi V. INSULATION BOARD INVESTIGATION AND TRIALS IN 300 TONNE STEEL LADLES AT ARCELORMITTAL DOFASCO. In: Unified Interantional Technical Conference on Refractories. 2013. p. 703–8.

36. Bakker J, Sinnema S. Thermal analysis on steel ladle linings. In: Stahl und

eisen. 2001. p. 165–6.

37.   Buhr A, Bauer W, Felsch T, Feja D, Hoever P. Auswirkungen der alterung von mikroporosen warmedammstoffen aur die temperaturfuhrung von stahlgiebpfannen. Stahl und eisen. 1998;118(12):103–9.

38.   Li G, Liu J, Jiang G, Liu H. Numerical simulation of temperature field and thermal stress field in the new type of ladle with the nanometer adiabatic material. Adv Mech Eng. 2015;(January):1–13.

39.   Lian TW, Kondo A, Akoshima M, Abe H, Ohmura T, Tuan WH, et al. Rapid thermal conductivity measurement of porous thermal insulation material by laser flash method. Adv Powder Technol. 2016;27(3):882–5.

40.   Tran Le AD, Maalouf C, Mendonça KC, Mai TH, Wurtz E. Study of moisture transfer in a double-layered wall with imperfect thermal and hydraulic contact resistances. J Build Perform Simul. 2009;2(4):251–66.

41.   Gopal V, Whiting MJ, Chew JW, Mills S. Thermal contact conductance and its dependence on load cycling. Int J Heat Mass Transf [Internet]. 2013;66:444–50. Available from: http://dx.doi.org/10.1016/j.ijheatmasstransfer.2013.06.061

42.   Glaser B. A Study on the Thermal State of Steelmaking Ladles. Royal institute of technology Stockholm; 2012.

43.   Glaser B. Thermal conductivity meassruements of ladle slag using transient hot wite method. Metall Mater Trans B-PROCESS Metall Mater Process Sci. 2013;44(February):1–4.

44.   Fbg T. High Temperature FBG sensing. 2015;(2):3.

45.   Steps N. Fundamentals of Fiber Bragg Grating (FBG) Optical Sensing. 2016;(1):2–5.

46.   Gruner K-D. Principles of Non-contact Temperature Measurement. J Sol Energy Eng [Internet]. 2003;3(February):1–32. Available from: http://www.journals.cambridge.org/abstract_S0263034612001103%5Cnhttp://scitation.aip.org/content/aip/journal/rsi/70/6/10.1063/1.1149835%5Cnhttp://scholar.google.com/scholar?hl=en&btnG=Search&q=intitle:Principles+of+Non-Contact+Temperature+Measurement#0%5C

47. Schiewe C. The influence of the emissivity on the non-contact temperature measurement. DIAS Infared Syst. 2014;1–3.

48. Honnerová P, Martan J, Kučera M, Honner M, Hameury J. New experimental device for high-temperature normal spectral emissivity measurements of coatings. Meas Sci Technol. 2014;25(9).

49. Bauer W, Steinhardt R. Emissionsgrade feuerfester baustoffe. GASW?RME Int. 1990;39(9):388–91.

50. Bauer W, Funke T. Veranderung der Emissionsgrade feuerfester baustoffe in schutzgas-atmospharen und vakuum. GASW?RME Int. 1999;48(4):296–9.

51. Jain I, Singh RK, Mazumdar D. Measurements of Some Thermal Properties of Steel-Refractory Systems and Heat Losses from Steelmaking Furnaces. Trans Indian Inst Met. 2015;68(3):383–92.

52. Wall RN, Basch DR, Jacobson DL. High-temperature spectral emissivity of several refractory elements and alloys. J Mater Eng Perform. 1992;1(5):679–84.

53. Rulison AJ, Rhim WK. A noncontact measurement technique for the specific heat and total hemispherical emissivity of undercooled refractory materials. Rev Sci Instrum. 1994;65(3):695–700.

54. Elich JJP, Wieringa JA. Temperature effects influencing the spectral and total emissivity of refractories. Exp Therm Fluid Sci. 1995;10(3):318–26.

55. Otsuka A, Hosono K, Tanaka R, Kitagawa K, Arai N. A survey of hemispherical total emissivity of the refractory metals in practical use. In: Energy. 2005. p. 535–43.

56. Ohlhorst CW, Vaughn WL, Daryabeigi K, Lewis RK, Rodriguez AC, Milhoan JD, et al. Emissivity Results On High Temperature Coating for Refractory Composite Materials. 29th Int Therm Conduct Conf 17th Int Expans Symp [Internet]. 2007;15. Available from: https://ntrs.nasa.gov/search.jsp?R=20070031768

57. Wiecek M, Strakowski R, Wiecek B, Olbrycht R, Swiatczak T, Wittchen W, et al. Estimation of steel slag parameters using thermal imaging and neural

networks classification. In: International Conference on Quantitative InfraRed Thermography. 2010. p. 1–5.

58. Mourão AAC, Vivaldini DO, Salvini VR, Pandolfelli VC. Fundamentos e análise de tintas refratárias de alta emissividade (Fundamentals and analysis of high emissivity refractory coatings). Ceramica. 2015;61(357).

59. FLIR. ThermaCAM ® P65 data sheet.

60. Digital P, Thermometer R. Model : IR-AHS • ,IR-AHU • ,IR-AHT •.

61. Zhu C, Hobbs MJ, Masters RC, Rodenburg C, Willmott JR. A Novel Emissivity Measurement Instrument with Low Uncertainty and Controlled Atmospheric Conditions. 2019;

62. Damhof F. Numerical-experimental analysis of thermal shock damage in refractory materials. 2010. 153 p.

63. Cotter RJ. Ultrasonic Temperature Measurements Device. US 8,801,277 B2, 2014. p. 8–15.

64. Lillygreen D. FEA of Teeming Ladle for installation of Thermocouples TheМещерякова, Л М. 2017.

65. Beurden P Van. Rapport Onderwerp : Thermisch procesmodel van de OSF2 staalpan Inleiding Modelopbouw Modelvalidatie en bepaling van de randvoorwaarden Toepassingen van het model Conclusies Referenties Appendix : Technische tekening B34371. 2015;31(0).

66. Rahm C, Kirschen M, Kronthaler A. Energy savings through appropriate ladle Energy Savings Through Appropriate Ladle Lining Concepts. 2015;(March 2008).

67. Kestin J, Imaishi N. Thermal conductivity of sulfur hexafluoride. Int J Thermophys. 1985;6(2):107–18.

68. Promat. MICROTHERM ® PANEL Technical data sheet.

69. Wahl FM, Grim RE, Graf RB. Phase Transformations in Silica as Exmined by Continuous X-Ray Diffraction. Am Mineral. 1961;46:196–208.

70. Kivi N, Moore A, Dyar K, Haaf S. Devitrification Rates of Fused Silica in the

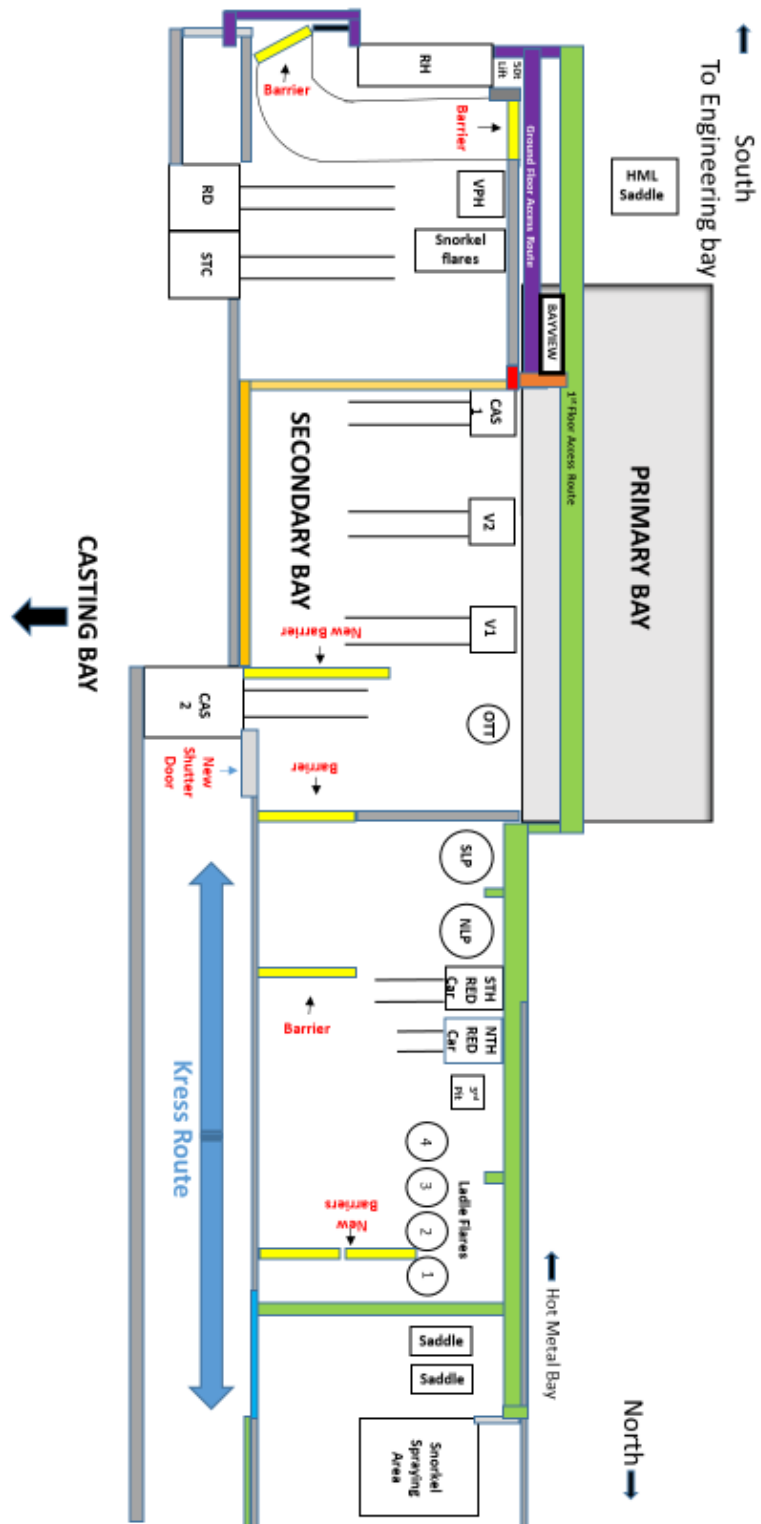Presence of Trace Impurities. 2016.

71. Chen B, Feng J, Zhai Y, Sun Z, Liu H, Jiang Y, et al. Effect of oxide particles on microstructure and mechanical properties of the 45 carbon structural steel. Materials (Basel). 2020;13(5).

72. KLUG FJ, PROCHAZKA S, DOREMUS RH. Alumina-Silica Phase Diagram in the Mollite Region. J Am Ceram Soc. 1987;70(10):750–9.

73. HARRISON DE, HUMMEL FA. Reactions in the System TiO2-P2O5. J Am Ceram Soc. 1959;42(10):487–90.

74. Sakka S, Bouaziz J, Ben Ayed F. Sintering and mechanical properties of the alumina-tricalcium phosphate-titania composites. Mater Sci Eng C [Internet]. 2014;40:92–101. Available from: http://dx.doi.org/10.1016/j.msec.2014.03.036

75. Kivi N, Moore A, Dyar K, Haaf S. Devitrification Rates of Fused Silica in the Presence of Trace Impurities. 2016.

76. Sohlberg K, Nie X, Zhuo S, Maeng G. Doping of TiO2 polymorphs for altered optical and photocatalytic properties. Int J Photoenergy. 2009;2009(November 2009).

77. Silica: Amorphous. Van Nostrand's Sci Encycl. 2007;

78. Horbach J, Kob W, Binder K. Specific heat of amorphous silica within the harmonic approximation. J Phys Chem B. 1999;103(20):4104–8.

79. BS EN ISO 22007-4 : 2017 BSI Standards Publication Plastics - Determination of thermal conductivity and thermal diffusivity. 2019;

80. NETZSCH. NETZSCH-LFA Help. NETZSCH-Ger€atebau GmbH, Selb, Ger. 2000;(215):3.

81. NETZSCH. Key Technical Data. NETZSCH-Ger€atebau GmbH, Selb, Ger [Internet]. 2000;449. Available from: https://www.netzsch-thermal-analysis.com/media/thermal-analysis/Data-Sheets/Key_Technical_Data_en_DSC_404_F1_F3_Pegasus.pdf

82. Smith DS, Alzina A, Bourret J, Nait-Ali B, Pennec F, Tessier-Doyen N, et al.

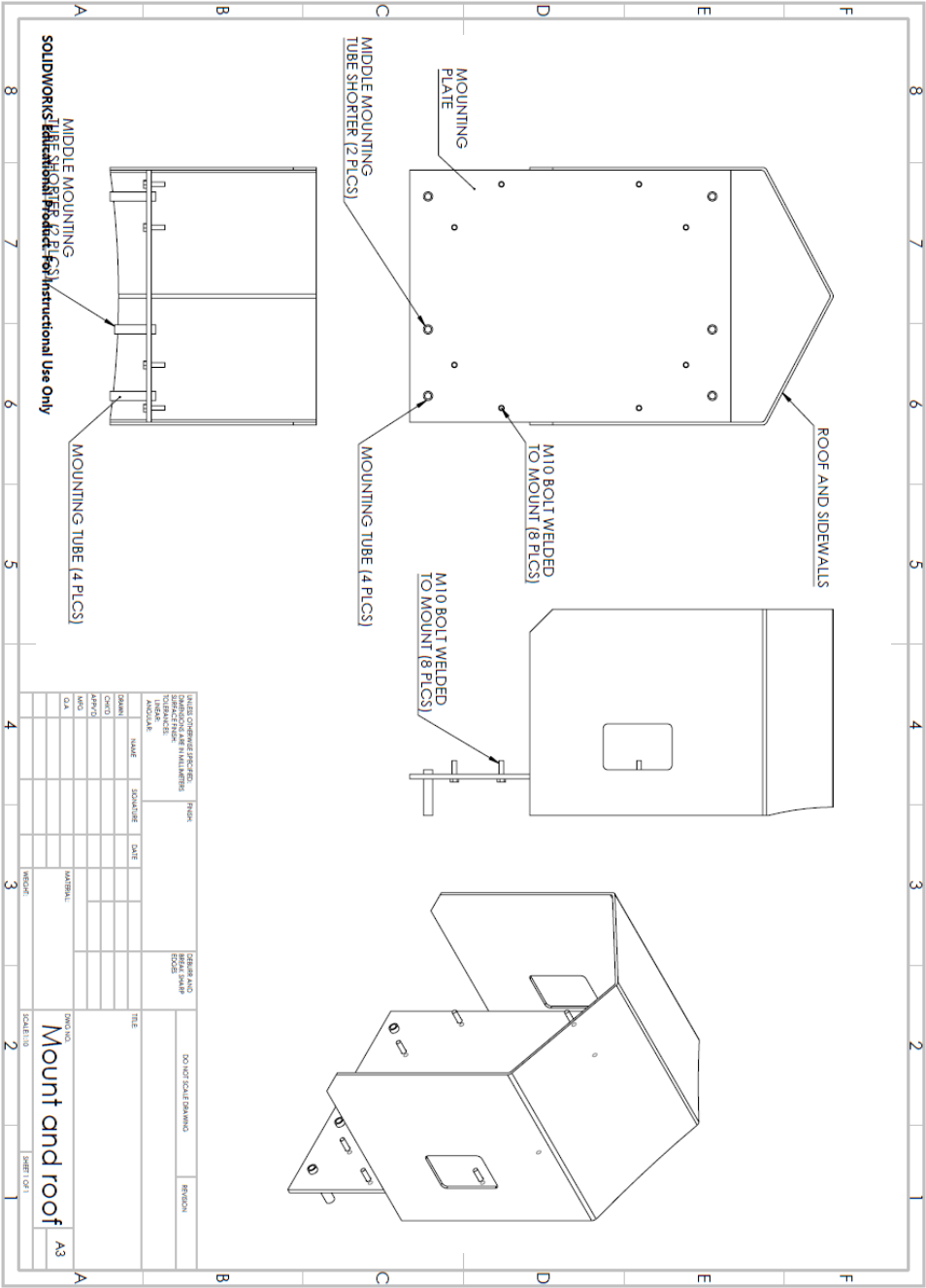Thermal conductivity of porous materials. J Mater Res. 2013;28(17):2260–72.

83.   Wilkes TC, Stanger LR, Willmott JR, Pering TD, McGonigle AJS, England RA. The development of a low-cost, near infrared, high-temperature thermal imaging system and its application to the retrieval of accurate lava lake temperatures at Masaya volcano, Nicaragua. Remote Sens. 2018;10(3).

Appendices

11.1 BOS plant layout

11.2 Engineering drawing of insulation box mount

11.3 Insulation box engineering drawing
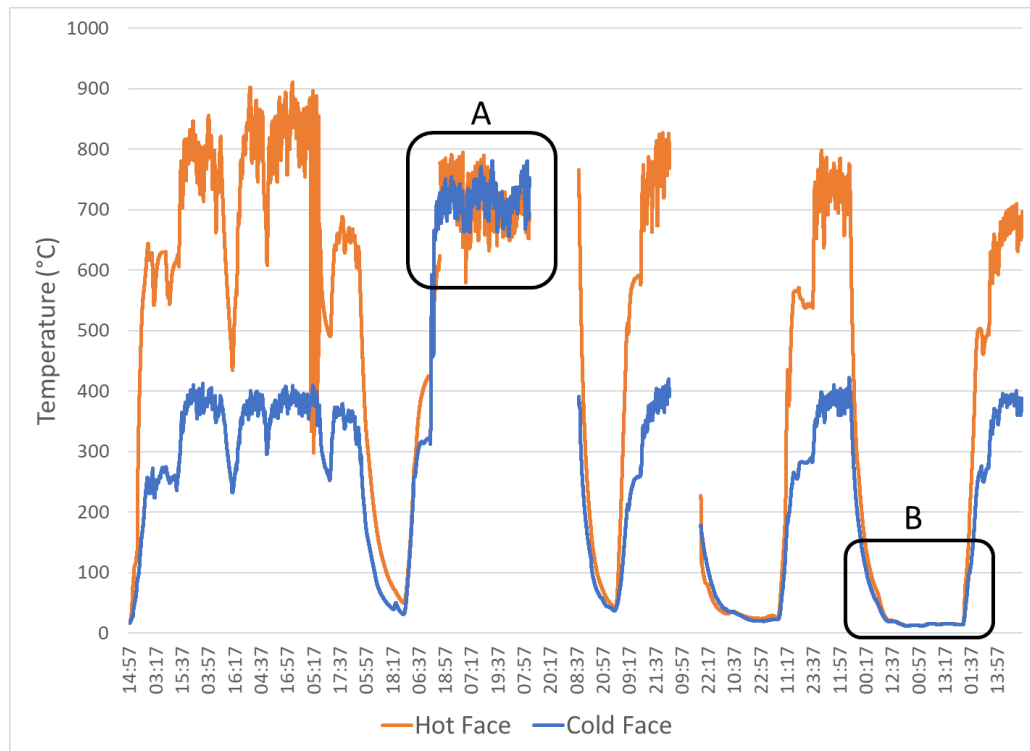
11.4 Thermocouples installed 1.6m high in barrel from thermocouple trial #2 section
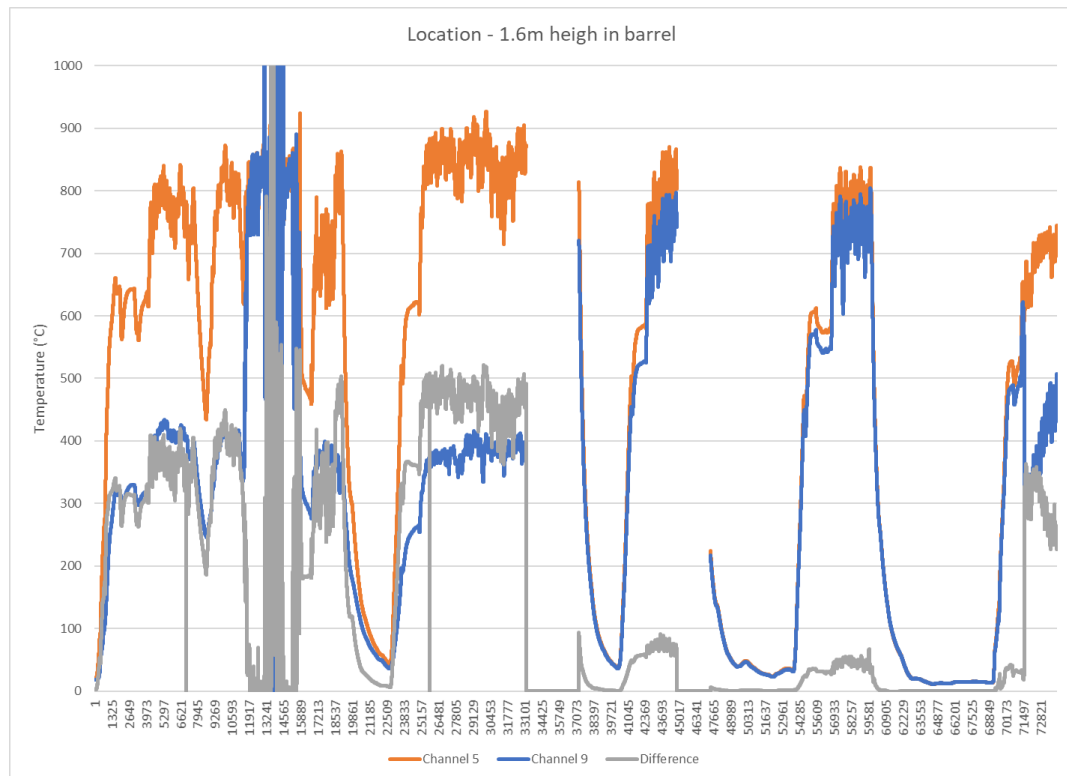
11.5 Thermocouples installed 1.1m high in barrel from thermocouple trial #2 section
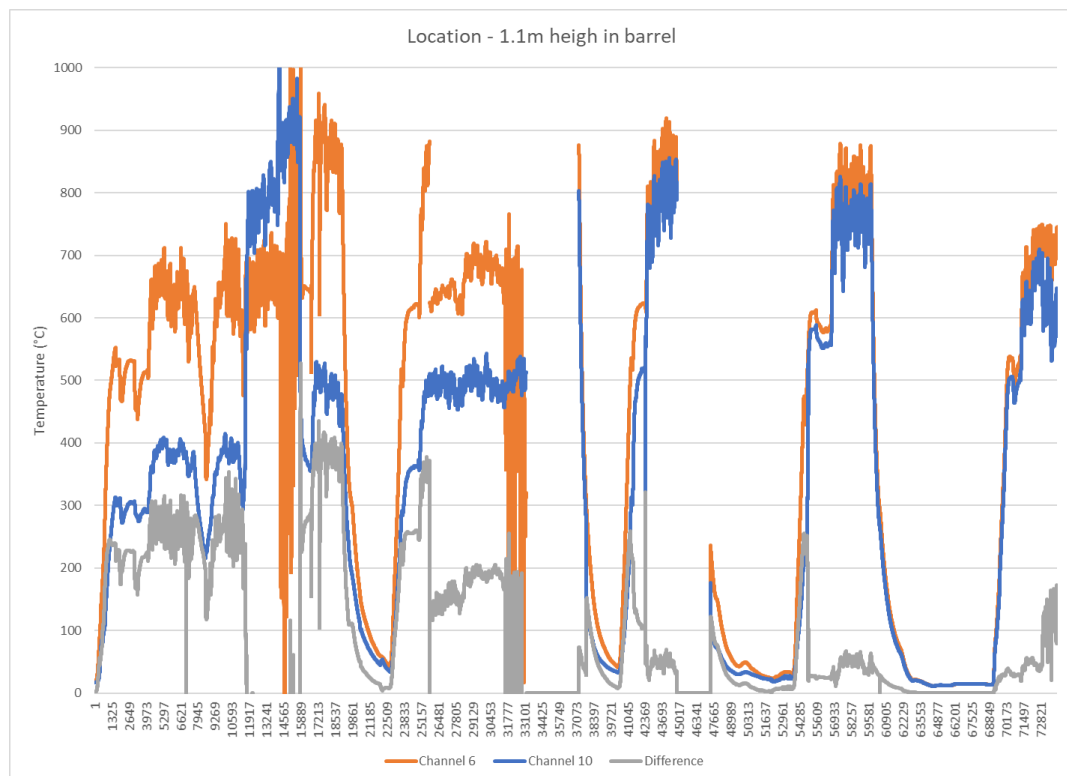
11.6 Thermocouples installed 0.8m high in barrel from thermocouple trial #2 section

11.7 Thermocouples installed 0.3m high in barrel from thermocouple trial #2 section